Deciphering the mechanism of action of armeniaspirol: A polyketide Gram-positive antibiotic

Puneet Labana

A thesis submitted in partial fulfillment

of the requirements for the

Doctorate in Philosophy degree in

Chemistry

Department of Chemistry and Biomolecular Sciences

Faculty of Science

University of Ottawa

March 2021

Abstract

Antibiotics are an important resource in modern medicine used to treat serious infections and enable a wide array of vital medical interventions including surgery and cancer chemotherapy. However, due to the increasing prevalence of antibiotic resistant pathogens, many clinically useful antibiotics are being rendered ineffective with too few new antibiotics in development to combat them. With highly diverse chemistry and bioactivity exquisitely shaped by evolution, natural products provide an unrivaled source of antibiotic compounds that is impossible to reproduce instinctively in the laboratory. The armeniaspirols are polyketide natural products with a unique spiro-[4.4]non-8-ene core that were isolated from *Streptomyces armeniacus* and were shown to be active against drug-resistant Gram-positive bacteria. Promisingly, *in vitro* resistant *Staphylococcus aureus* strains could not be readily obtained even after thirty serial passages under sub-lethal doses. Herein, we decipher the mechanism of action for this structurally unprecedented natural product antibiotic in the Gram-positive model organism *Bacillus subtilis*.

Through chemical proteomics with an armeniaspirol-inspired activity-based probe, quantitative proteomics, biochemical assays, and microscopy, we show that armeniaspirol is a competitive inhibitor of the AAA+ proteases ClpXP and ClpYQ. Armeniaspirol represents the first known natural product inhibitor of ClpP, a highly coveted target due to its prominent role in bacterial virulence. Using overlapping proteomic fingerprints of armeniaspirol-treatment with *ΔclpQ* and *ΔclpP* deletions in *B. subtilis*, inhibition or deletion of these proteases appears to dysregulate key proteins involved in cell division, including FtsZ, DivIVA, and MreB. The dual ClpXP and ClpYQ inhibition is responsible for armeniaspirol's potent antibiotic activity and this unique pharmacology makes it a promising candidate for antibiotic development. Several

armeniaspirol-inspired analogs were generated as part of a medicinal chemistry study and evaluated for antibiotic activity towards a panel of clinically relevant Gram-positive pathogens. As a result, we identify three exciting armeniaspirol analogs with improved antibiotic activity.

Lastly, the foundation for elucidating the ClpYQ degradome is developed. Our proteomic fingerprint of the *B. subtilis ΔclpQ* deletion strain generated some of the first insights into potential substrates of the ClpYQ protease. As a largely uncharacterized AAA+ protease implicated in the mechanism of action of armeniaspirol, we pursued a previously established acyl-intermediate covalent trapping strategy to characterize the ClpYQ-substrate complexes in *B. subtilis* cell lysate. Through unnatural amino acid incorporation using an evolved tRNA/aminoacyl-tRNA synthetase pair, the N-terminal active site serine of ClpQ is substituted with a photocleavable precursor that generates 2,3-diaminopropionic acid. While we were successful in synthesizing the photocleavable precursor, initial experiments to incorporate this unnatural amino acid in ClpQ expression proved unsuccessful, leading us to outline necessary control experiments for future endeavours. Ultimately, the covalently trapped substrates will be identified by LC-MS/MS, where we expect to identify key divisome and elongasome proteins in corroboration with the armeniaspirol mechanism of action study.

Table of Contents

List of Figures

List of Tables

List of Schemes

List of Symbols, Abbreviations and Nomenclature

°C	degrees Celsius
Å	Ångström
AAA+	ATPase associated with diverse cellular activities
aaRS	aminoacyl-tRNA synthetase
ABC	ammonium bicarbonate
ABP	activity-based probe
ABPP	activity-based protein profiling
ADEP	acyldepsipeptide
ADP	adenosine diphosphate
AMC	amido-4-methylcoumarin
Amp^R	ampicillin resistance
API	analytical profile index
Asp	aspartic acid
ATP	adenosine triphosphate
Cbz	carbobenzoxy
CID	collision-induced dissociation
CuAAC	copper(I)-catalyzed azide-alkyne cycloaddition
Da	dalton
DAP	2,3-diaminopropionic acid
DAPI	4′,6-diamidino-2-phenylindole
DIPEA	N,N-diisopropylethylamine
DMSO	dimethylsulfoxide
DNA	deoxyribonucleic acid

DSC	N,N-disuccinimidyl carbonate
DTT	dithiothreitol
E	enzyme
EDTA	ethylenediaminetetraacetic acid
Em.	emission
eq.	equation
Ex.	excitation
FDR	false discovery rate
FIC	fractional inhibitory concentration
GFP	green fluorescent protein
Glu	glutamic acid
Gly	glycine
h	hour
His	histidine
HIV	human immunodeficiency virus
HPLC	high-performance liquid chromatography
hν	UV light
I	inhibitor
IC_{50}	inhibitor concentration for 50% enzyme activity
IPTG	isopropyl-1-thio-β-D-galactopyranoside
J	coupling constant
k_{cat}	enzyme turnover number
k_{inact}	inactivation rate constant
K_i	reversible inhibitor inhibition constant

K_M	Michaelis-Menten constant
Kan^R	kanamycin resistance
kDa	kilodaltons
kg	kilograms
LB	Luria-Bertani
LC	liquid chromatography
Leu	meucine
Lys	mysine
M	molar
m	multiplet
MBC	minimum bactericidal concentration
mg	milligrams
MIC	minimum inhibitory concentration
min	minute
mL	milliliter
mM	millimolar
mm	millimeter
mol	mole
MOPS	3-(*N*-morpholino)propanesulfonic acid
mRNA	messenger RNA
MRSA	methicillin-resistant *Staphylococcus aureus*
MS	mass spectrometry
MSSA	methicillin-sensitive *Staphylococcus aureus*
Mtb	*Mycobacterium tuberculosis*

m/z	mass to charge ratio
n.d.	not detected
nm	nanometer
NMR	nuclear magnetic resonance
o/n	overnight
OD_{600}	optical density measured at a wavelength of 600 nm
P	product
PAGE	polyacrylamide gel electrophoresis
PBS	phosphate buffer saline
PCR	polymerase chain reaction
PDB	Protein Data Bank
PEG	polyethylene glycol
pH	negative logarithm of the hydronium concentration
Phe	phenylalanine
Pro	proline
PRSP	penicillin-resistant *Streptococcus pneumoniae*
q	quadruplet
Rf	retention factor
RFU	relative fluorescent units
RNA	ribonucleic acid
rpm	revolutions per minute
S	substrate
s	singlet
SAR	structure-activity relationship

SDS	sodium dodecylsulfate
t	triplet
TBTA	tris[(1-benzyl-1H-1,2,3-triazol-4-yl)methyl]amine
TCEP	tris(2-carboxyethyl)phosphine
TEAB	triethylammonium bicarbonate
TEV	tobacco etch virus
TFA	trifluoroacetic acid
THF	tetrahydrofuran
Thr	threonine
TLC	thin layer chromatography
tmRNA	transfer-messenger RNA
Tris	tris(hydroxymethyl)aminomethane
Tyr	tyrosine
UV	ultraviolet
v	rate
V	volts
v_0	initial rate in the absence of inhibitor
v_{max}	maximum rate
VRE	vancomycin-resistant *Enterococcus faecium*
α	substrate competition factor ($\alpha=1+[S]/K_M$)
δ	chemical shift
µg	microgram
µM	micromolar
µm	micrometer

CHAPTER ONE: **Introduction**

1.1 Natural product antibiotics: important prospects in the resistance era

1.1.1 Secondary metabolism in microorganisms

Secondary metabolism in microbes produce natural products that do not play explicit roles in growth, yet still serve important functions in survivability and fitness[1]. These naturally occurring compounds permit access to highly complex and diverse chemistry and possess important biological activities that have coincidentally provided us with an indispensable resource for modern medicine as antimicrobial and even anti-tumour agents[2]. While the biological functions of many secondary metabolites are relatively unknown, it is postulated that microorganisms would only retain these energetically expensive pathways if it served some evolutionary advantage to do so[3]. The most cited example attributed to secondary metabolism is in the production of natural product antibiotics in microorganisms as a means for inhibiting competing species[4] – a biological interaction known as antibiosis. This has generated immense interest in secondary metabolism with the specific intent to combat infectious disease. However, secondary metabolites serve multi-purpose roles that extend beyond antibiosis. The dynamic conditions of the natural environment demands constant acclimation by a microbial species, and secondary metabolite production at sub-inhibitory concentrations have been shown to enhance biological fitness through a range of other processes including cell signaling, colonization, motility, stress responses, and/or biofilm production[5,6].

1.1.2 Natural product antibiotic discovery and limitations

The natural product secondary metabolites produced by microbes to inhibit a competitive species are fittingly termed antibiotics. The bacterial warfare that promotes antibiotic production has been exploited for human benefit as a means for treating infectious disease, with the world's

first antibiotic accredited to Alexander Fleming in 1928 and the serendipitous discovery of penicillin G from the fungus *Penicillium notatum*[7,8]. This ignited a flurry of ensuing research emphasizing natural product antibiotics in the mid-twentieth century, a time now regarded as the "golden age" of antibiotic discovery[9,10] (**Figure 1.1**). It was during this time that approximately half of the antibiotics commonly in use today were discovered[11], with synthetic derivatives produced in the years following aimed at improving their clinical efficacy. Accordingly, these natural product discoveries have played a prominent role in improving quality of life, by both enabling and revolutionizing modern medicine. In addition to treating serious infections, antibiotics have permitted therapies that otherwise pose significant risk of infection such as cancer chemotherapy, surgery, and transplantation[9,12]. However, the innately complex and evolution-driven chemistry of natural products makes proposing clinically viable synthetic antibiotic compounds *de novo* essentially impossible[13]. Even more complicated is the fact that natural products, including antibiotics and antifungals, tend not to conform to Lipinski's rules which makes their compound design substantially less intuitive[14]. Thus, this limitation suggests – as evidenced by an extended discovery gap – that developing antibiotics is almost entirely dependent on our ability to continuously discover new natural products.

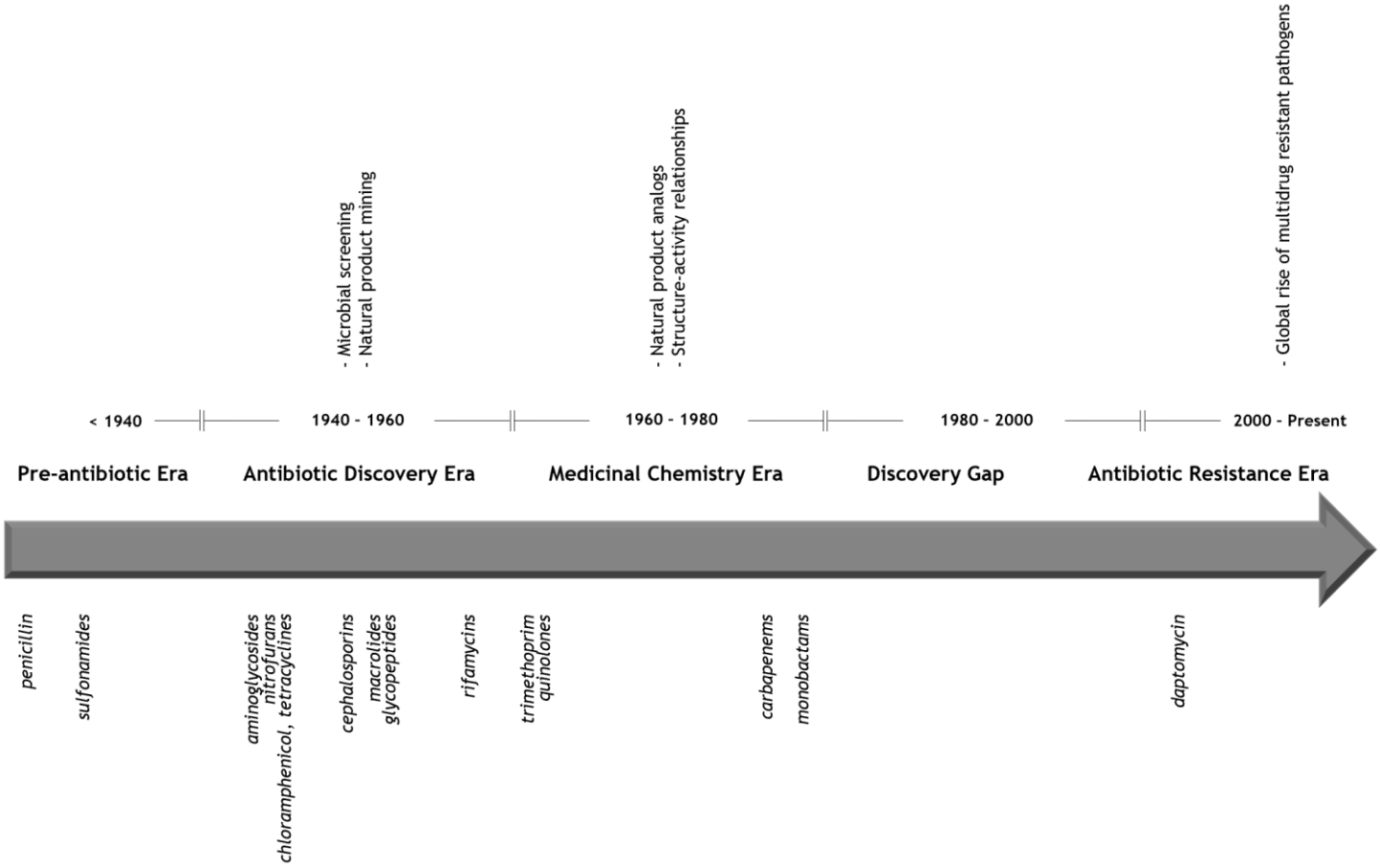

Figure 1.1. Timeline examining the evolution of antibiotic discovery. Most antibiotics were discovered in the mid-twentieth century, regarded as the "golden age" of antibiotic discovery. The current rate of discovery of new antibiotics has propelled the world into an antibiotic resistance era with an alarming rise in multidrug resistant pathogens.

Many of the current antibiotics were discovered through wide-spread research into marine and soil microbial species. Initially, the commencement of soil investigation in the late nineteenth century was undertaken in an effort to identify bacterial agents of infectious disease; it was reasoned that over the course of existence of organic life, pathogens eventually all end up in the soil either through excrement or the remains of the deceased[15]. However, the discovery that soil harboured few pathogens led to the hypothesis that native soil-inhabiting microbes might instead be responsible for the demise of these pathogens in the environment[15]. Thus, serious considerations were given to the screening methods of environmental samples in an effort to

identify microbes antagonistic to pathogens[16]. The antagonistic action of soil microorganisms to certain pathogens was first demonstrated by Louis Pasteur and Jules Francois Joubert in 1877, but the term "antibiotic" was coined by Selman A. Waksman in 1941[17,18]. Considered a pioneer in the isolation of antibiotics from soil microflora, Waksman first isolated actinomycin from *Actinomyces antibioticus* in 1940[19].

This early approach for screening natural products was highly successful for discovering the first and most prevalent natural product antibiotic classes during the mid-twentieth century. However, the vast majority of screens eventually started to produce natural product antibiotics that had already been discovered[20]. The standard workflow of cultivation, extraction, and structural elucidation now too often results in natural product re-discovery[21]. Additionally, many microbial species are uncultivatable outside of their native environments, leaving much to be desired in accessing the full potential of microbial diversity in nature. Phylogenetic markers such as 16S RNA gene sequences from environmental DNA samples reveal a plethora of hidden microbial populations not recoverable under standard laboratory conditions[22]. Another commonly confronted challenge is the activation of secondary metabolite biosynthetic pathways. For example, the *Streptomyces* genus possesses the genetic potential to harbour upwards of thirty secondary metabolites, yet many of the products of these cryptic biosynthetic gene clusters have dodged cultivation and extraction methods[23]. Given these limitations, it is clear there is still a great deal of potentially bioactive natural products yet to be discovered. While positive strides are being made to access biosynthetic pathways and elucidate novel natural products through innovative screening strategies[24], the current lack of antibiotic development in conjunction with the global escalation of multidrug-resistant pathogens now threatens to upend the modern era of antibiotics[9].

1.1.3 Antibiotic mechanisms of action and resistance development

The molecular pharmacology of clinically approved antibiotics function through disruption of some critical bacterial cellular process. The majority of clinical antibiotics inhibits only a small number of cellular targets including the cell wall, ribosome, DNA replication, RNA transcription, or folate biosynthesis[9,25] (**Table 1.1**).

Table 1.1. Antibiotic classes sorted by mechanism of action. Most clinical antibiotics are derived from natural products and target either the bacterial cell wall, ribosomes, and DNA, RNA or folate biosynthesis.

Mechanism	Chemical Class	Spectrum of Activity
Cell wall	β-lactams	Gram-positive and Gram-negative
Ribosome	Aminoglycosides	Gram-negative
	Tetracyclines	Gram-positive and Gram-negative
	Macrolides	Gram-positive
	Chloramphenicol	Gram-positive and Gram-negative
	Oxazolidinones	Gram-positive
DNA replication	Fluoroquinolones	Gram-positive and Gram-negative
RNA transcription	Rifamycins	Gram-positive
Folate biosynthesis	Sulfonamides	Gram-positive and Gram-negative
	Trimethoprim	Gram-positive

The small subset of mechanistic targets has enabled the development of high-level antibiotic resistance mechanisms that are readily transferred between bacteria. There are four strategies by which bacteria demonstrate antibiotic resistance: (1) enzymatic inactivation of the antibiotic, (2) modification of the antibiotic target, (3) upregulation of efflux pumps, and (4) impaired penetration (**Figure 1.2**). Notably, the impermeability of antibiotics through the bacterial cell wall is an exclusively intrinsic resistance mechanism and a significant defense strategy especially in Gram-negative bacteria. The presence of the outer membrane in Gram-

negative bacteria provides a significant barrier that renders many antibiotics ineffective. Alternatively, antibiotic inactivation, target modification, and efflux pumps are resistance mechanisms induced in response to antibiotic exposure and can be intrinsic to the bacteria or acquired by gene transfer[27]. The mobilization of these resistance elements through horizontal or vertical gene transfer is a major contributor to the increasing prevalence of antimicrobial-resistant pathogens and diminishing antibiotic efficacy.

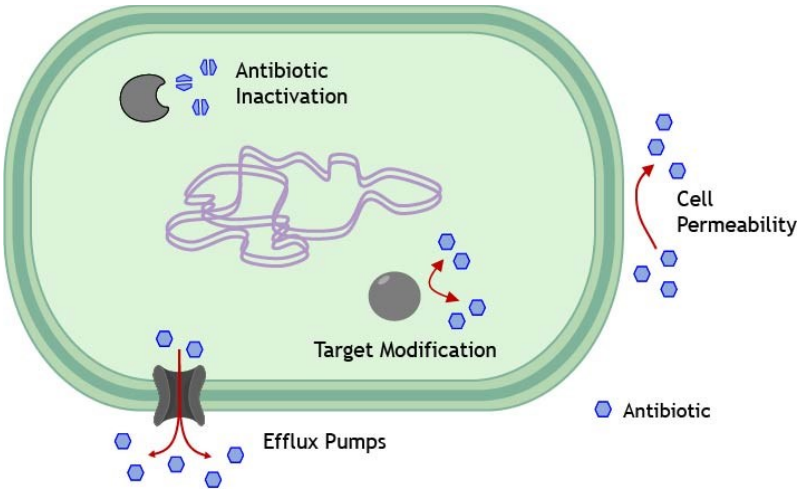

Figure 1.2. Intrinsic and acquired resistance mechanisms in bacteria. Antibiotic inactivation, target modification, efflux pumps, and cell permeability are commonly featured bacterial resistance mechanisms that counteract antibiotics, rendering them ineffective.

Chemical tailoring has produced second- and third-generation antibiotics with renewed efficacy and improved pharmacological properties to aid in temporarily outpacing evolved resistance mechanisms to first-generation antibiotics. However, since these subsequent iterations depend on the same fundamental mechanism of action, these antibiotics remain prone to rapid resistance development[28]. Thus, given the rise in antibiotic resistant bacteria and the limited breadth of antibiotic targets, there is a clear and dire need for the discovery of antibiotics that function through novel mechanisms of action to combat multi-drug resistant bacteria.

1.1.4 The antibiotic crisis

Multi-drug resistant bacteria, or superbugs, are internationally recognized as a significant emerging threat to human health[29]. Methicillin-resistant *Staphylococcus aureus* (MRSA) is one of the most prevalent causes of health-care associated infections in Canada and poses significant risk with a 25% fatality rate in those who develop a bloodstream infection[30]. Disturbingly, cases of MRSA resistant to the principal treatment of vancomycin have been documented in the United States and United Kingdom[31]. Several causes have led to the present crisis state of antibiotic resistant bacteria. According to the Public Health Agency of Canada, the overuse and abuse of antibiotics in humans and animals are leading contributors of antibiotic resistance[32]. The misuse of antibiotics in situations where they are not required only enables opportunity for bacteria to evolve resistance mechanisms.

To make matters worse, the pharmaceutical industry has vacated the field of antibiotic discovery in favour of research investments that produce greater economic returns[11]. Spending on the conversion of a chemical prospect to antibiotic is principally determined by cost versus profit assessment; the aversion towards antibiotic discovery stems in part from the technically challenging and time-intensive research to the unfavourable returns on investment[33]. From this perspective, development of drugs that treat chronic conditions such as diabetes and cancer are significantly more profitable than single-use antibiotics that end up being low-profit, short-lived, or both. Major biopharmaceutical companies such as Novartis, AstraZeneca, Sanofi, and Allergan have abandoned the sector all together, leaving only Merck & Co., Roche, GlaxoSmithKline and Pfizer with active antibiotic programs[34]. Additionally, companies entirely dedicated to the development of antimicrobials have seen their initially large capitals dry up, including Melinta Therapeutics, which was founded by Nobel Prize in Chemistry recipient

Thomas A. Steitz. Furthermore, Achaogen, a start-up entirely dedicated to the development of antimicrobials, declared bankruptcy despite hitting instrumental success with ZEMDRI (plazomicin), a United States Food and Drug Administration approved antibiotic for treatment of urinary tract infections caused by multidrug-resistant *Enterobacteriaceae*. Clearly, without government intervention or substantial market incentive, new solutions towards combating antimicrobial resistance falls largely on members of academia challenged with less funds and fewer resources.

1.2 AAA+ proteases: promising antimicrobial targets

1.2.1 Structure and function of AAA+ proteases

The AAA+ (**A**TPase **A**ssociated with cellular **A**ctivities) proteases are functionally diverse, multimeric complexes that couple ATP hydrolysis and proteolysis activities to degrade protein substrates. The AAA+ proteases in bacteria include the caseinolytic proteases ClpAP, ClpCP, ClpXP and ClpYQ (also called HslVU), as well as the Lon protease and FtsH[35]. In human cells, the mitochondrial AAA+ proteases include the Lon protease (LonP1) and ClpXP, both of which are implicated in various carcinomas[36,37]. The focus herein is on the role of the bacterial AAA+ proteases and their implications in bacterial pathogenesis. These complexes function through an *ATPase domain* responsible for recognizing and unfolding a protein substrate that is subsequently translocated into the proteolytic chamber of a *protease domain* for degradation into small peptide fragments of 5 to 25 amino acids[35,38] (**Figure 1.3**).

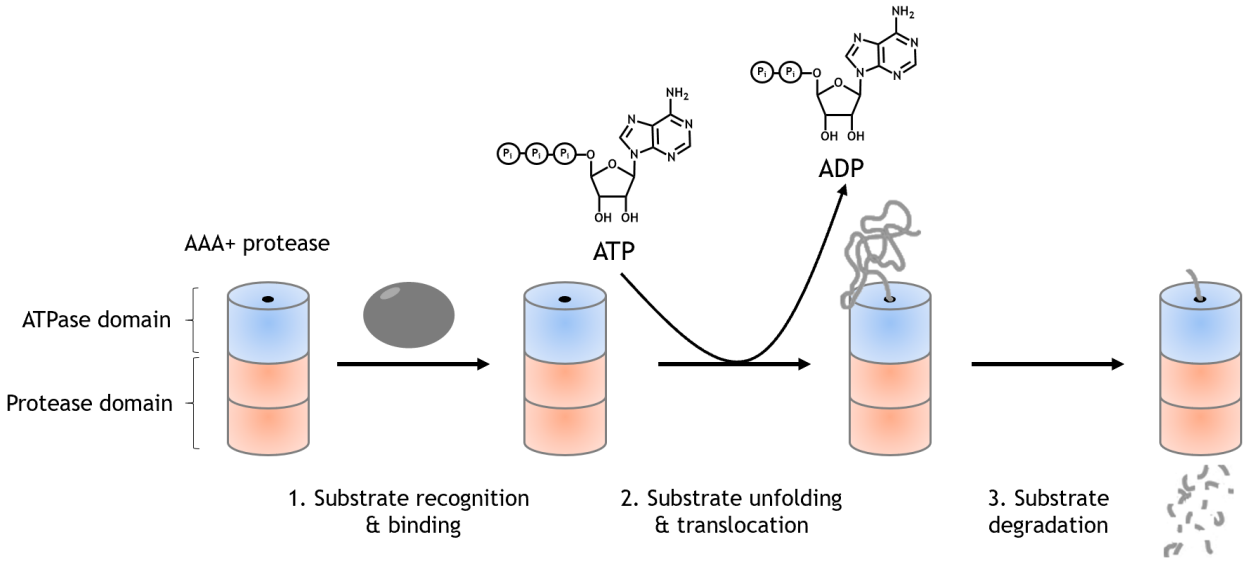

Figure 1.3. Mechanism of the AAA+ proteases in substrate degradation. The ATPase domain is responsible for binding and unfolding protein substrates which are transferred into the protease domain for degradation. Substrate unfolding and translocation is an energetically expensive, ATP-dependent process.

The ClpAP, ClpCP, ClpXP, and ClpYQ proteases are large multimeric complexes, with the ATPase domains (ClpA, ClpC, ClpX, and ClpY) and protease domains (ClpP and ClpQ) encoded on separate genes[35]. Each ATPase domain forms a cylindrical hexamer that stack with its protease domain[39]. The ClpP protease domain forms a stacked dimer of cylindrical heptameric multimers, resulting in a tetradecamer[40], that interacts with its respective hexameric ATPase. In contrast, the ClpQ protease domain forms a stacked dimer of cylindrical hexameric multimers, resulting in a dodecamer[41], that interacts with hexameric ClpY ATPase (**Figure 1.4**). In contrast, the Lon and FtsH proteases are encoded on a single polypeptide containing both the ATPase and protease domains[35]. Both Lon and FtsH form a similar cylindrical complex composed of six identical subunits[38] (**Figure 1.4**).

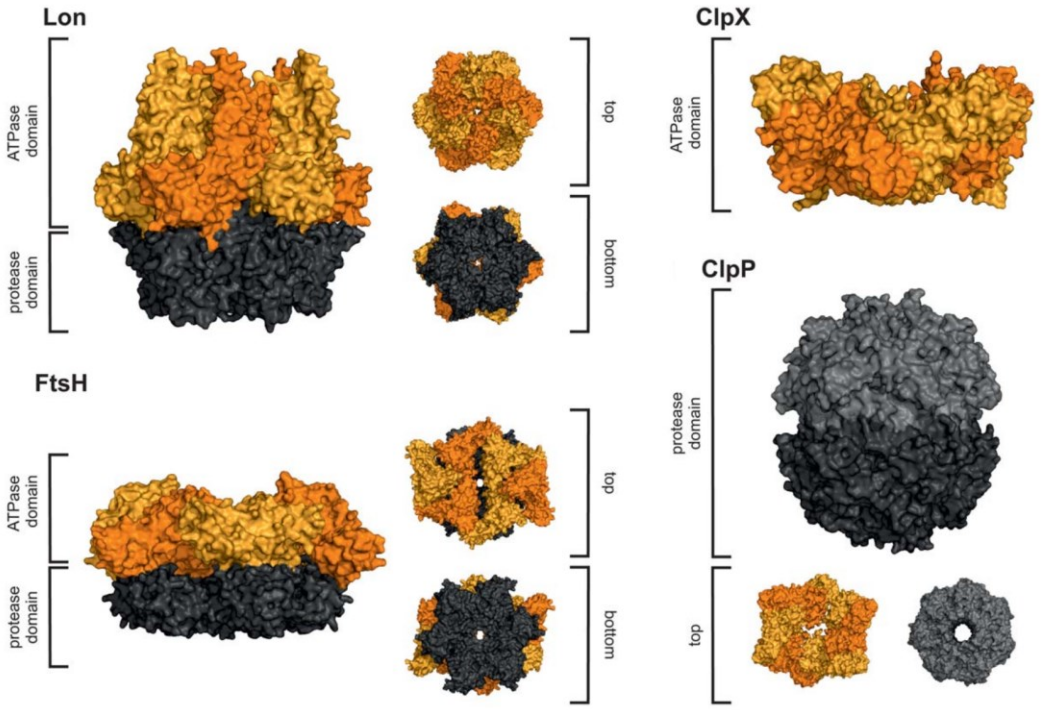

Figure 1.4. Structures of the multimeric AAA+ protease complexes. Lon (PDB: 3K1J) and FtsH (PDB: 2CE7) form hexameric complexes, with the ATPase and protease domains encoded on a single polypeptide. ClpXP is composed of hexameric ClpX (PDB: 3HWS) ATPase subunits and a dimer of heptameric ClpP (PDB: 3MT6) protease subunits. ClpYQ (not shown) is composed of hexameric ClpY ATPase subunits and a dimer of hexameric ClpQ protease subunits. Reproduced (adapted) with permission from Bittner, L. M. et al. *Biopolymers.* 2016, 105 (8), 505–517. Copyright 2016 John Wiley and Sons.

The ATP-dependent process of unfolding and translocation of a substrate is mechanistically conserved across the ATPase domains. Several cycles of ATP hydrolysis resulting in release of ADP and inorganic phosphate facilitate conformational changes within the ATPase domains that lead to unfolding of stable protein substrates[35,42]. Overall this step is an energetically expensive process requiring anywhere from less than 20 ATP molecules to upwards of 500 ATP molecules in the degradation of a single protein[42]. Alternatively, the catalytic mechanisms for proteolysis are distinct across all protease domains of ClpP, ClpQ, Lon, and FtsH. The ClpP protease functions through a Ser-His-Asp catalytic triad[43] which generates peptide products of 6-8 amino acids in *E. coli*[44]. The ClpQ protease functions through an N-terminal serine in *B. subtilis*[45] (or N-terminal threonine in *E. coli*[46]), which is allosterically

activated by a C-terminal sequence of the ATPase domain in response to ATP-binding[47,48]. The Lon protease functions through a Ser-Lys catalytic dyad[49], and finally, FtsH is a metalloprotease that consists of a catalytic zinc ion bound by a histidine HEXXH motif[50].

1.2.2 Quality control roles of the bacterial AAA+ proteases

Combined, the AAA+ proteases are responsible for maintaining protein quality control in bacteria. They are intimately involved in the regulation of various biological processes, and in some cases possess overlapping roles. ClpXP is one of the best characterized AAA+ proteases in both Gram-positive and Gram-negative bacteria. It recognizes specific peptide sequences called degrons that target a protein for degradation[51]. In *B. subtilis* and *E. coli*, a degron of eleven amino acids known as the ssrA tag is appended to the C-terminus of nascent proteins at stalled ribosomes[52–54]. This tag is added co-translationally to a nascent polypeptide chain through expression of a transfer-messenger RNA (tmRNA) encoded by the *ssrA* gene[52]. ClpXP recognizes this degron and targets the unstructured proteins for degradation, thereby rescuing the ribosome and allowing translation to recover. Additionally, significant upregulation of *clpP* transcription was observed in *B. subtilis* in response to conditions such as heat shock and exposure to excess salt or ethanol, suggesting ClpP plays a prominent role in mediating protein degradation under stress conditions[55]. These quality control mechanisms are crucial in maintaining proteostasis in the cell by preventing accumulation of abnormal or unfinished protein products. In comparison, the quality control responsibilities of the ClpYQ protease are much less understood.

In *E. coli*, the Lon protease plays a significant role in the degradation of misfolded proteins primarily by recognizing exposed hydrophobic peptide sequences that are otherwise inaccessible at the core of natively folded proteins[56]. This generic recognition results in its

promiscuous substrate specificity that allows for degradation of approximately 50% of the denatured proteins in *E. coli*[57]. In contrast, the two Lon proteases in *B. subtilis*, LonA and LonB, have only been observed to play a minor role in protein degradation[58]. While ClpXP is responsible for the degradation of over 90% of ssrA-tagged proteins, both Lon and FtsH contribute minor roles in degradation of these cytosolic proteins in *E. coli*[59,60]. The essential membrane-bound FtsH maintains protein quality control of both cytosolic and membrane proteins[61]. However, FtsH primarily mediates degradation of membrane-bound proteins by recognizing a cytosolic segment of a non-specific twenty amino acid residue tail at the N- or C-terminus of its substrate[62,63].

1.2.3 ClpP and bacterial virulence

A specific emphasis has recently been placed on the role of the ClpP protease given its implications in bacterial virulence, making it an intriguing anti-virulent and antibiotic target for both Gram-positive and Gram-negative pathogens, including *Staphylococcus aureus* and *Salmonella typhimurium.* A signature-tagged mutagenesis strategy was implemented in these pathogenic bacteria to identify genes required for virulence in a bacteraemia murine model[64]. In this original approach[65,66], a transposon insertion library of mutants of a bacterial strain is constructed, where each transposon carries a unique DNA sequence (signature tag or bar code) flanked by invariant DNA sequences to allow for all mutants to be amplified but also differentiated from each other. The mutant strains are combined, inoculated in mice, and recovered after a set period. The signature tags of inoculated strains and recovered strains are amplified, radiolabelled, and hybridized to the initial transposon library. A signature tag that is detected from the inoculated strains but not from the recovered strains represent mutants with attenuated virulence. This strategy identified virulence genes *clpP* in the Gram-negative *S.*

typhimurium[65] and *clpX* in the Gram-positive *S. aureus*[64], providing the first evidence connecting ClpXP to bacterial virulence.

This led to additional studies corroborating these results in murine infection models. ClpX and ClpP were both shown to be required for *S. aureus* virulence in a murine skin abscess model. Infection of mice with *S. aureus ΔclpX* or *ΔclpP* strains resulted in significantly less bacterial recovery from skin lesions compared to infection with wild-type *S. aureus*[67]. Similarly, a *Streptococcus pneumoniae ΔclpP* strain failed to colonize the lungs in a murine lung infection model and did not result in mortality[68]. In stark contrast, a wild-type *S. pneumoniae* lung infection model resulted in 100% mortality after 48 hours[68]. Finally, in yet another example using the pathogenic Gram-negative *S. typhimurium*, *ΔclpX* and *ΔclpP* strains lost the ability to cause systemic infection in mice, resulting in survival beyond five days as opposed to mice infected with the wild-type strain of which none survived beyond five days[69].

Attenuating virulence represents a viable approach to treating infection. Virulence factors are produced by bacterial pathogens to either damage the host and/or evade the host immune system[70]. As antibiotic resistance becomes more prevalent, targeting proteins that hamper virulence mechanisms offers a unique strategy for treating infection by disabling targets essential for infection and allowing for bacterial elimination by the host immune response[71,72]. Antibiotics that typically target essential pathways impose severe selection pressures that favour resistance mechanisms by *de novo* mutation that is consequently spread among bacteria with high frequency[73]. It has been argued that anti-virulence strategies would apply a reduced selective pressure since most virulence traits are not essential for survival, reducing resistance development and increasing clinical lifespan[74]. As a result, there has been a significant increase in the discovery and publication of novel synthetic small molecule anti-virulence compounds

over the past decade showing promising results for treating infectious disease[70,74]. Thus, identifying compounds that inhibit virulence factors (such as ClpP) provide a new arsenal of drugs and drug targets worth exploring.

1.2.4 Natural products targeting ClpP

Given the direct relationship between ClpP and bacterial virulence in various Gram-positive and Gram-negative bacteria, ClpP provides an interesting target for inhibiting bacterial pathogens. Synthetic compound libraries were successful in identifying a group of β-lactones and phenyl esters as potent ClpP inhibitors *in vitro,* but poor pharmacokinetics and selectivity has limited further clinical development[75,76]. Instead, we direct our attention towards the natural products targeting ClpP as more promising anti-virulence or antibiotic agents. To date, only a few natural products modulating ClpP activity – through interaction with the ATPase or protease domain – have been discovered (**Figure 1.5**). The natural products cyclomarin A, sclerotiamide, and the acyldepsipeptides lead to over-activation of ClpP and uncontrolled proteolysis, whereas lassomycin and ecumicin lead to inhibition of proteolysis.

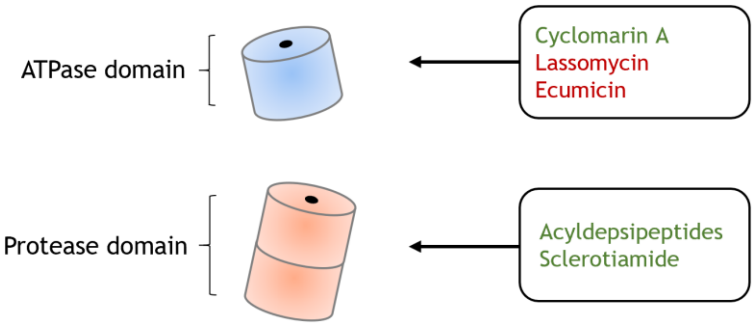

Figure 1.5. Natural products targeting the Clp AAA+ proteases. Few natural products have been discovered that target the ATPase or protease domains of the Clp AAA+ proteases. The resulting mode of action is either inhibition (red) or over-activation (green) of overall proteolytic activity.

The natural products cyclomarin A, lassomycin, and ecumicin are large cyclic peptides that disrupt the ClpC1/ClpP1P2 interaction in *Mycobacterium tuberculosis* (*Mtb*), leading to

antibiotic activity (**Figure 1.7**). *Mtb* is the causative agent of tuberculosis, a top ten cause of death worldwide and leading cause of death from a single infectious agent according to the World Health Organization (2020 Global Tuberculosis Report)[77]. *Mtb* differs from most other bacteria by encoding a ClpC homolog, ClpC1, and two closely related ClpP homologs, ClpP1 and ClpP2, which assemble to form the proteolytic complex ClpP1P2[78]. Cyclomarin A was discovered through a natural product whole-cell screen[79], and determined to bind the N-terminal domain of *Mtb* ClpC1[80]. This binding interaction creates a large pore opening in the Clp complex for proteins to enter and undergo uncontrolled proteolysis[80]. Lassomycin and ecumicin were both discovered from actinomycete extracts that were screened against *Mtb*. Both bind the ClpC1 domain leading to an increase in ATP hydrolysis, but as opposed to cyclomarin A, result in proteolytic inhibition[81,82]. Interestingly, all of these compounds display no antibiotic activity towards other Gram-positive or Gram-negative bacteria[79], suggesting its activity is due to a combination of the essential function of ClpP1P2 in *Mtb* and also differences between ClpC domains[83].

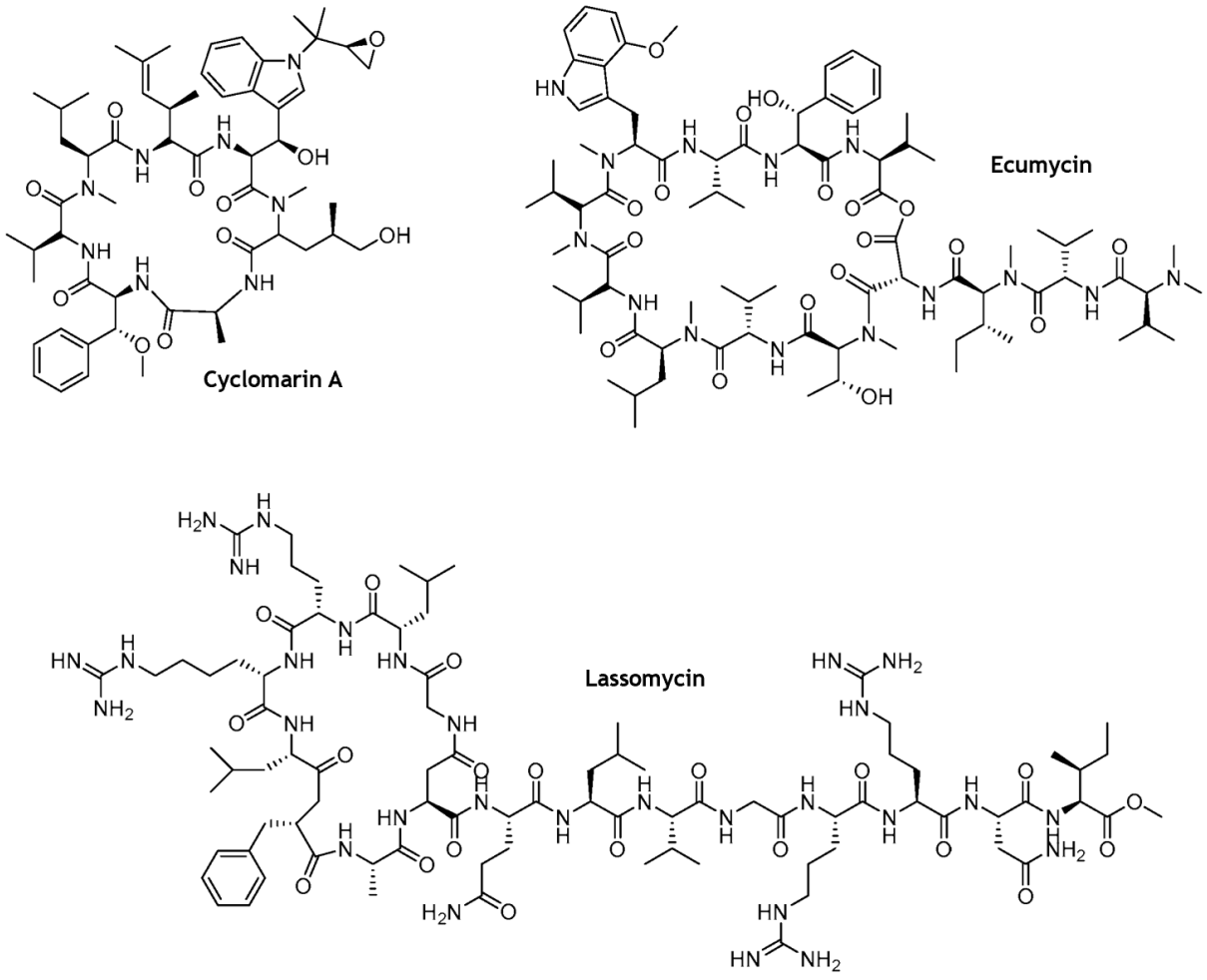

Figure 1.6. ClpC1-targeting natural products.

Additionally, the acyldepsipeptide (ADEP) natural products and sclerotiamide are ClpP-binding activators of proteolysis (**Figure 1.7**). The ADEPs display antibiotic activity towards a broad range of Gram-positive bacteria[84]. The ADEP structures and mechanism of action were elucidated by the Brötz-Oesterhelt group[84] following isolation of eight uncharacterized factors with potent antibiotic activity from fermentation broth of *Streptomyces hawaiiensis* by Eli Lilly and Company[85]. The ADEPs bind to sites on ClpP that compete with and displace the ATPase domain[86]. Thus, even in the absence of ATP hydrolysis, the result is a conformational change in the ClpP tetradecameric complex that forces it to adopt an active state in which proteins can non-

selectively enter the proteolytic chamber and be degraded[87,88]. Additionally, a high-throughput screen of a large bacterial and fungal secondary metabolite library resulted in the discovery of another ClpP-activating natural product called sclerotiamide[89]. While sclerotiamide results in uncontrolled proteolysis of the *E. coli* ClpP activity in *in vitro* biochemical assays, no appreciable antibiotic activity was observed with this compound[89].

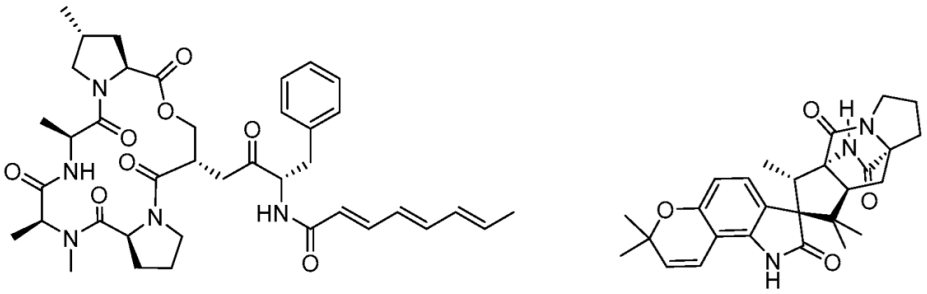

Figure 1.7. ClpP-targeting natural products.

1.3 Degradomics: characterizing protease-substrate interactions

1.3.1 Defining the degradome

Aside from maintaining overall protein quality control in the cell by a general degradation of aberrant and unfolded proteins, proteases are responsible for degrading specific substrates under certain conditions. These conditional substrates provide an in-depth understanding of the biological processes regulated by a given protease. The term "degradome" has been proposed as a subset of the proteome referring to the complete natural substrate repertoire of a specific protease in a cell, tissue, or organism[90]. At a molecular level, specific protease-substrate interactions can provide insights into a mechanistic action that can be used to develop therapeutics or be taken advantage of as biological tools. For example, the discovery of the unique nature of the Phe-Pro, Phe-Leu, and Phe-Thr scissile bonds in substrates of the human

immunodeficiency virus (HIV) protease enabled development of peptidomimetic protease inhibitors such as ritonavir[91]. Additionally, proteases such as the Tobacco Etch Virus (TEV) protease has become a staple in molecular biology with a defined recognition sequence that can be used to cleave fusion tags from recombinantly expressed proteins[92]. On a cellular level, the characterization of the degradomes of proteases enables a more global understanding into their biologically relevant regulatory roles, including in pathology and virulence in bacteria or various carcinomas in human cells[93]. Thus, insights into protease function and their interacting substrates may unlock new pharmaceutical targets for treating disease. This section will focus primarily on the degradomes of the bacterial AAA+ proteases.

1.3.2 Strategies for characterizing the degradome of AAA+ proteases

Two innovative trapping strategies have been implemented in order to identify the direct substrates of AAA+ proteases in bacteria. The first strategy involves mutational alterations to the Walker motifs on the ATPase domains, which prevents the substrate from being unfolded and translocated into the proteolytic chamber (**Figure 1.8A**). The second strategy involves mutational alterations to the active site of the protease domain, which disables its catalytic mechanism (**Figure 1.8B**). Thus, in both strategies the protease substrates are capable of associating with the AAA+ protease but are unable to be degraded. By deleting the corresponding wild-type protease and overexpressing these variants in a bacterial strain instead, the protease-substrate complexes can be recovered and identified by mass spectrometry (MS) based proteomics.

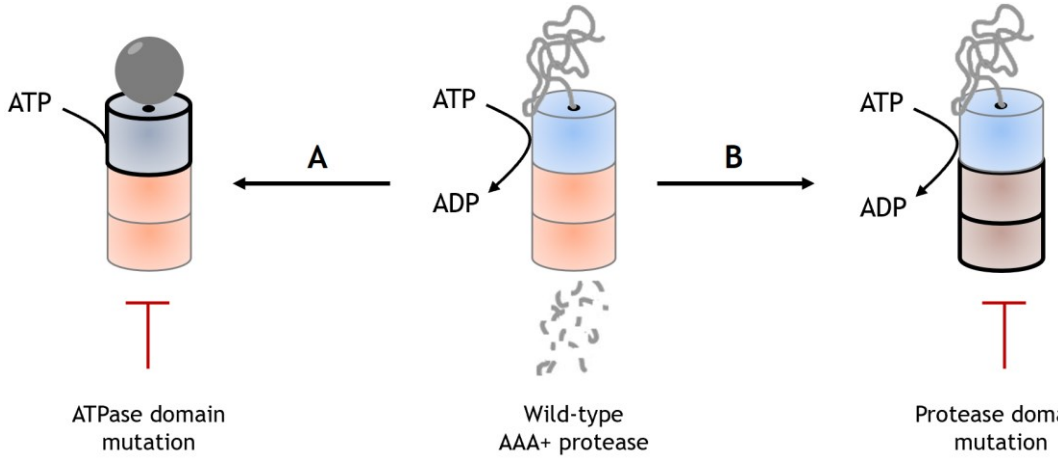

Figure 1.8. Strategies for characterizing direct substrates of AAA+ proteases. Two strategies have been successfully implemented for characterizing protease-substrate interactions. The first involves mutation of the ATPase Walker motifs to prevent ATP hydrolysis maintaining transient interaction with native substrate (A). The second strategy involves mutation of the protease active site allowing substrates to be unfolded and translocated into the proteolytic chamber, but unable to be degraded (B). In both strategies, the protease-substrate complexes can be purified and identified.

The Walker A and B motifs in the ATPase domains are responsible for facilitating ATP binding and hydrolysis, respectively[35]. By introducing mutations to the Walker B motifs, ATP binds to the ATPase domain but is unable to be hydrolyzed, resulting in ATPase-substrate complexes. This strategy was successfully applied to the ClpB ATPase in *E. coli*[94], which does not interact with a protease partner but instead coordinates with the DnaK chaperone system to solubilize and refold aggregated proteins[95]. Introducing mutations Glu279Ala and Glu678Ala in the Walker B motifs of ClpB resulted in the first characterization of the direct interactions of ClpB with protein aggregates[94]. A similar strategy was applied to the AAA+ protease ClpCP in *S. aureus* in which a ClpC variant, called ClpC^{TRAP}, possessing mutations Glu280Ala and Glu618Ala in the Walker B motifs was used to identify the direct substrates of ClpC[96].

The principles of introducing mutations to inactivate the ATPase domains can similarly be applied to the active site of the protease domains of AAA+ proteases. In this strategy, unfolded and translocated proteins mediated by the ATPase are held in the proteolytic chamber

of the inactivated protease. An advantage to this strategy is that the resulting protease-substrate complex is more effectively purified together as compared to the more transient interaction formed between the ATPase-substrate complex[35]. Thus, this has been the method of choice in characterizing substrates for the AAA+ proteases, including for ClpP, Lon, and FtsH. Several studies to determine substrates of ClpP proteases utilize an active site variant called ClpP^{TRAP} in which the active site serine residues are mutated to alanine. This strategy has proven successful for characterizing ClpP substrates in the Gram-positive *S. aureus*[97] and Gram-negative *E. coli*[98] and *Caulobacter crescentus*[99]. This trapping strategy has also been implemented in the one-component AAA+ proteases, Lon and FtsH. Since the Lon protease also possesses an active site serine, a Lon^{TRAP} variant substituting the serine for an alanine was successfully constructed and implemented to identify substrates in *E. coli*[100]. The FtsH protease is a zinc-dependent metalloprotease, in which a catalytic zinc ion is bound by the histidine residues of a C-terminal HEXXH peptide motif in conjunction with an aspartic acid residue located further away[50]. Thus, a FtsH^{TRAP} variant was constructed with a His417Tyr mutation of the first histidine residue in the HEXXH zinc binding motif, leading to an ATPase-active but proteolytically-inactive complex to identify substrates[101]. Combined, these strategies have uncovered many substrates of the AAA+ proteases in the effort to elucidate the degradomes for each of these proteases.

1.3.3 Substrates of the AAA+ proteases

Several substrates have been characterized that enable insights into the cellular roles of AAA+ proteases such as in competence development, motility, various stress responses, sporulation, and biofilm formation[61], with many of the proteases having overlapping substrates. Both the Lon and FtsH AAA+ proteases are implicated in various stress response mechanisms, such as the SOS and heat shock responses in *E. coli*[102–104]. While the Lon protease displays a

high level of promiscuity in protein degradation, the Lon^{TRAP} variant demonstrated it is responsible for degradation of SulA, a cell division inhibitor and a regulatory protein induced during the SOS response[100]. As would be expected, the FtsH^{TRAP} variant demonstrated it is largely responsible for the degradation of several membrane proteins in *E. coli* including FdoH, DadA, and YfgM, as well as LpxC and KdtA which are both involved in lipopolysaccharide biosynthesis[101]. Approximately 70 proteins were identified in a ClpP^{TRAP} variant in *E. coli* with a diverse array of functions; these include proteins involved in transcription regulation, translation (ribosomal proteins, Rpl), cell motility, metabolism, and cell division (FtsZ)[98]. A ClpP^{TRAP} variant instituted in *S. aureus* also yielded many of the same cellular substrates, including transcriptional regulators CtsR and Spx, and the cell division protein FtsZ[97]. The ClpQ protease, whose degradome has yet to be characterized through this variant approach, has only been implicated in degradation of cell division related proteins SulA in *E. coli*[105] and EzrA in *B. subtilis*[106].

1.4 Thesis overview and goals

The primary objective of this thesis is to elucidate the mechanism of action of the novel polyketide Gram-positive antibiotic, armeniaspirol. In Chapter Two the direct biochemical protein targets of armeniaspirol in *Bacillus subtilis* cell lysate are identified, while Chapter Three discusses how inhibition of these targets lead to armeniaspirol's observed antibiotic activity. A diverse array of experimental techniques including chemical proteomics, quantitative proteomics, microscopy and biochemical assays are implemented to ultimately accomplish these goals. Using armeniaspirol as a lead structure, a medicinal chemistry evaluation of armeniaspirol analogs is examined in Chapter Four for the purposes of identifying optimized antibiotic candidates suitable for preclinical drug development. Lastly, expanding on the armeniaspirol mechanism of action

study is a second project aimed at clarifying the degradome of the largely uncharacterized AAA+ protease ClpYQ (HslVU).

CHAPTER TWO:
Armeniaspirol Inhibits AAA+ Proteases ClpXP and ClpYQ

2.1 Introduction

2.1.1 Armeniaspirols are a structurally unique class of antibiotic

Armeniaspirols A-C are polyketide natural products that were first isolated from the bacteria *Streptomyces armeniacus* in 2012[107–109] (**Figure 2.1**). A combination of NMR spectroscopy and X-ray crystallography were implemented to elucidate their structures, identifying a unique spiro-[4.4]non-8-ene core scaffold[110]. Additionally, the armeniaspirols share a resemblance to the pyrrole-containing natural products pyrrolomycins[111], marinopyrroles[112], and chlorizidine[113], all of which possess five membered nitrogen-containing heterocycles and display potent bioactivities as antimicrobial and anti-tumour agents. Specifically, armeniaspirol A was shown to be active against multidrug resistant Gram-positive bacteria including methicillin-resistant *S. aureus* (MRSA), vancomycin-resistant *Enterococcus* (VRE) and penicillin-resistant *S. pneumoniae* (PRSP) at low micromolar concentrations[107,110] (**Table S1** in **Appendix I**). Promisingly, intravenous administration of armeniaspirol A translated to a 67% survival rate in a MRSA-induced murine sepsis model[110]. The unique structure of armeniaspirol increases the prospect of a novel mechanism of action and also decreases the likelihood of existing resistance mechanisms as demonstrated by the inability to acquire resistance in *S. aureus* after 30 serial passages at sub-inhibitory concentrations[110]. However, the target and mechanism of action of these compounds was entirely unknown and is uncovered herein. Notably, native armeniaspirol was inaccessible by organic synthesis; instead, a synthesis resulting in the chlorination of the phenol ring yielding 5-chloro-armeniaspirol[107], **1**, was used instead for our mechanism of action studies (**Figure 2.1**).

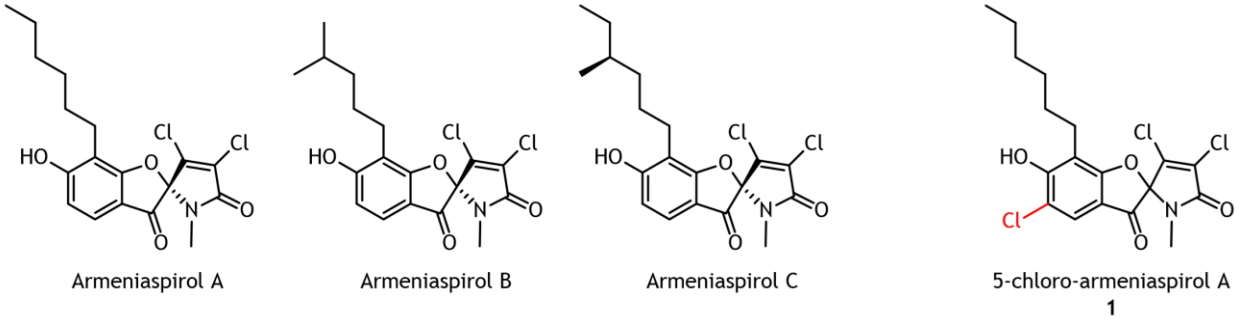

Figure 2.1. Structures of armeniaspirols A-C. Armeniaspirols were isolated from *Streptomyces armeniacus* DSM19369 and possess a unique spiro-[4.4]non-8-ene scaffold. A synthetic route to armeniaspirol A generated a racemic mixture of the chlorinated derivative 5-chloro-armeniaspirol A, **1**.

2.1.2 Armeniaspirol inhibits drug-resistant Gram-positive bacteria

A minimum inhibitory concentration (MIC) assay was implemented to screen activity of **1** towards Gram-positive and Gram-negative bacteria (**Table 2.1**; **Figure S1** in **Appendix I**). A MIC assay measures the lowest concentration at which bacterial growth is inhibited upon two-fold serial dilutions of test compound, in this case **1**. Although **1** is ineffective against Gram-negative bacteria *Escherichia coli* and *Pseudomonas aeruginosa* (MIC >32 μg/ml), its potency towards drug-resistant Gram-positive bacteria such as MRSA (MIC 4 μg/mL) and VRE (8 μg/mL) is intriguing as an antibiotic candidate. Despite the addition of a chlorine atom to the phenol ring, the antibiotic activity of **1** is retained at appreciable concentrations. In addition to the MIC, the minimum bactericidal concentration (MBC) is a complementary assay that identifies the lowest concentration of **1** that results in complete microbial death, represented by a 3-log reduction (99.9%) of the MIC microbial subcultures re-streaked on non-antibiotic containing agar plates[114]. A compound is considered bactericidal if it has a MBC less than 4X the MIC[115]. The high MBCs indicate that **1** is a bacteriostatic antibiotic of the Gram-positive pathogenic bacteria (**Table 2.1**). For example, subcultures of MRSA USA300 are recovered at concentrations as high as 8X the MIC (32 μg/mL) (**Figure S2** in **Appendix I**). Thus, the unique

scaffold and potent antibiotic activity of armeniaspirol fully warrants investigation into its unknown mechanism of action.

Table 2.1. Minimum inhibitory/bactericidal concentration (MIC/MBC) assays. MIC/MBC (μg/mL) profiles with **1** indicate bacteriostatic antibiotic activity towards Gram-positive bacteria, including clinically relevant MRSA and VRE strains. Each MIC was performed in triplicate (n = 3).

Gram-Positive Bacteria	MIC **1** (μg/mL)	MBC **1** (μg/mL)
Staphylococcus aureus IA116-USA100 (MRSA)	4	32
Staphylococcus aureus MN8-USA200 (MSSA)	4	>32
Staphylococcus aureus LAC-Fitz-USA300 (MRSA)	4	>32
Staphylococcus aureus MW2-USA400 (MRSA)	4	>32
Enterococcus faecalis NJ-3 ATCC 51299 (VRE)	8	>32
Bacillus subtilis 168	2	4
Gram-Negative Bacteria	MIC **1** (μg/mL)	MBC **1** (μg/mL)
Escherichia coli BW25113	>32	>32
Pseudomonas aeruginosa PA01	>32	>32

Bacillus subtilis was used to determine the mechanism of action for the antibiotic activity of **1**. *B. subtilis* is a Gram-positive bacteria that has been used extensively as a model organism to study pathogenic Gram-positive bacteria such as *Bacillus anthracis*, *Listeria monocytogenes,* and *Staphylococcus aureus*[116]. Access to a comprehensive *B. subtilis* genomic directory[117], deletion library repository[118], and rigorous characterization of essential genes[119] together justify the use of *B. subtilis* as a model system. *B. subtilis* 168 is inhibited by **1** at a MIC of 2 μg/mL (**Figure S1** in **Appendix I**). Additionally, the MBC of **1** is 4 μg/mL, making it a bactericidal antibiotic towards the non-pathogenic *B. subtilis.*

2.2 Identifying direct biochemical targets of armeniaspirol in *B. subtilis*

2.2.1 Activity-based protein profiling

Activity-based protein profiling (ABPP) is an indispensable chemical proteomic approach that utilizes a functionalized small molecule, or activity-based probe (ABP), to investigate enzyme targets[120]. These probes interact with enzymes in the proteome which are subsequently characterized through downstream gel- or LC-MS-based methods. ABPP has been instrumental for a variety of applications such as elucidating uncharacterized enzymes, discovering selective inhibitors of enzyme classes, and capturing targets of bioactive small molecules including natural products[120–122]. ABPs are constructed with three basic components: a reactive group, a linker region, and a reporter tag. The reactive group is typically an electrophilic center that participates in an enzyme's catalytic mechanism to mediate protein-probe binding[120]. Thus, conserved active sites of a targeted family of enzymes, such as serine hydrolases or cysteine proteases, can be exploited to enhance probe selectivity and minimize promiscuity throughout the proteome[123]. The linker region separates the reactive group from the reporter tag and consists of either extended alkyl or polyethylene glycol (PEG) units. The functional purpose of the linker region can be two-fold depending on the protein of interest: to minimize overall steric hinderance of the ABP or to modulate solubility[121]. Finally, the diverse utility of ABPP is a direct result of the reporter tags that can be appended on to the probes. Two examples of common reporter tags include fluorophores, such as rhodamine, or affinity labels, such as biotin, for visual detection or pull-down assays, respectively[124]. While fluorescent probes can be used for rapid visualization of proteins and with high sensitivity, the use of biotin as an affinity label is more commonly used because it allows for the combination of image-based visualization by

Western blot immunoassays as well as LC-MS-based identification of targeted proteins through recovery with streptavidin-agarose beads[124].

Additionally, an ABP can be functionalized with a bio-orthogonal handle to mediate the bioconjugation of a reporter tag subsequent to the protein-probe interaction. This ingenious strategy was famously coined "click chemistry" by K. Barry Sharpless in 2001[125]. This added flexibility helped overcome limitations of having an ABP possess a bulky reporter group that may otherwise hinder cellular uptake for *in vivo* labeling[126,127]. The most widely used click chemistry reaction is the copper(I)-catalyzed azide-alkyne cycloaddition (CuAAC), which utilizes reactivity between a probe appended with a terminal alkyne and a reporter tag appended with an azide, or vice versa, to generate a 1,4-disubstituted 1,2,3-triazole[126,128] (**Figure 2.2**). Using this strategy, we set out to elucidate the direct biochemical targets of armeniaspirol by employing ABPP to the cell lysate of *B. subtilis*.

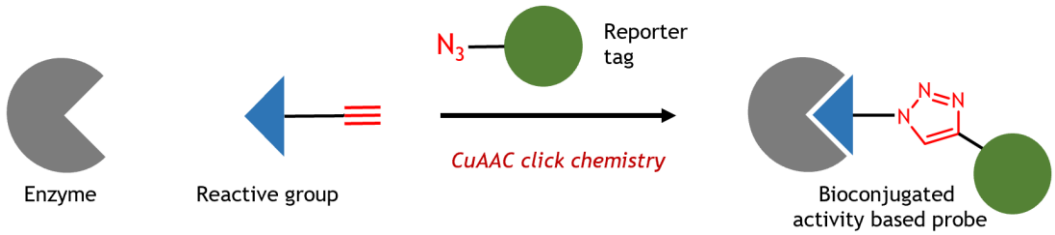

Figure 2.2. CuAAC-mediated activity-based protein profiling. Click chemistry-based approaches utilize bio-orthogonal handles to facilitate the attachment of a reactive group to a reporter tag. The most widely used click chemistry reaction is copper(I)-catalyzed azide-alkyne cycloaddition that results in formation of a 1,4-disubstituted 1,2,3-triazole.

2.2.2 Development of an armeniaspirol-based capture probe

Several derivatives of **1** were synthesized in a structure-activity relationship (SAR) study to design a functionalized armeniaspirol probe. Importantly, the ability to sustain antibiotic activity was evaluated by MIC against *B. subtilis* (**Figure 2.3A**). Both the aromatic alcohol and the alkyl chain on the nitrogen were targeted as possible sites for modification. Our SAR

indicated that (1) the free phenol is essential as demonstrated by the abolished antibiotic activity upon replacement of the aromatic alcohol with a methoxy group, and (2) extending the N-alkyl chain maintains modest antibiotic activity (**Figure 2.3B**). Based on these results, a capture probe harbouring an alkyne in place of the N-methyl was synthesized, resulting in probe **2** (**Figure 2.3C**). Gratifyingly, **2** displayed antibiotic activity with an MIC of 8 µg/ml against *B. subtilis*. Retaining comparable biological activity is an essential prerequisite in order to ensure the interaction that determines antibiotic activity is still able to occur with our modified probe.

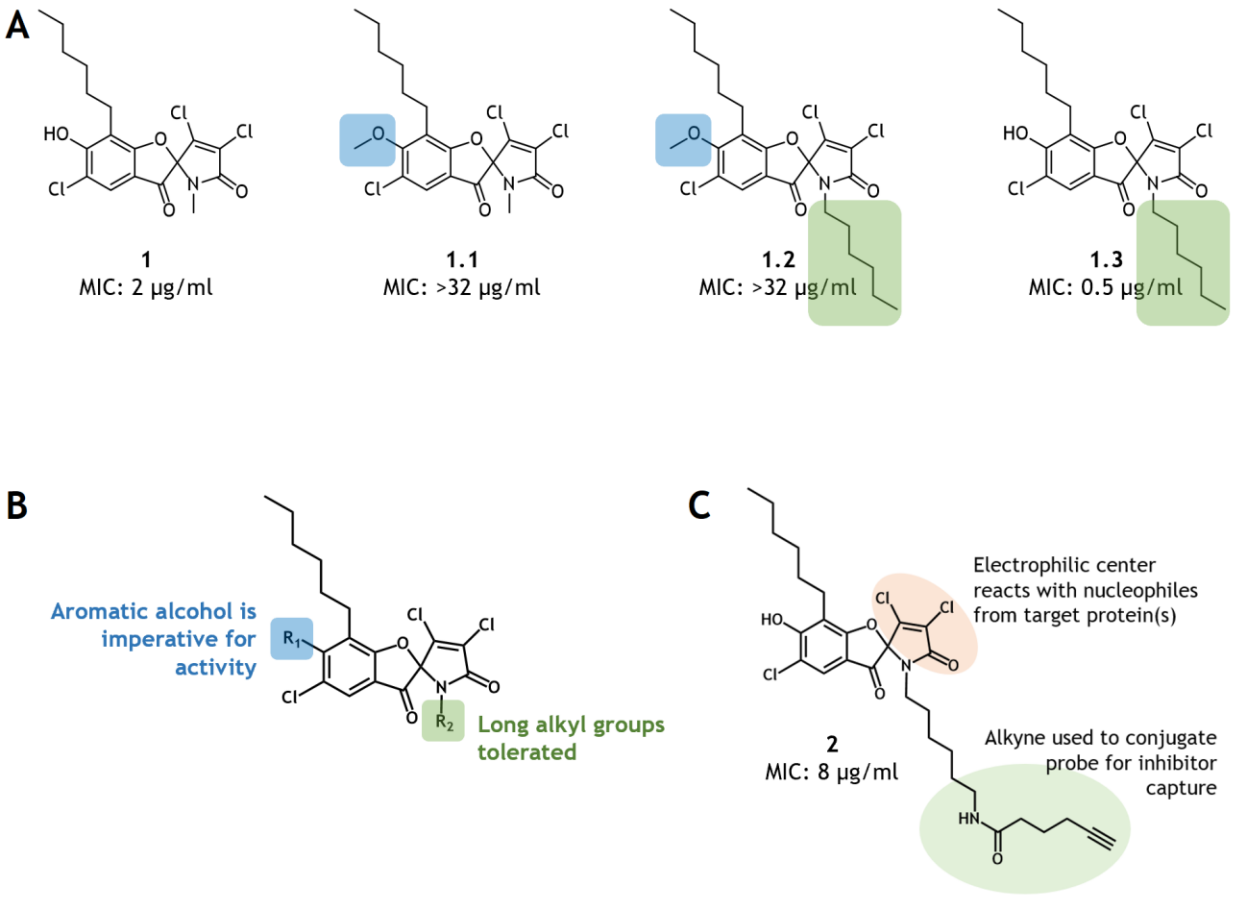

Figure 2.3. Structure-activity relationship of armeniaspirol. (A) Derivatives of armeniaspirol evaluated against *B. subtilis*. (B) Results of the SAR indicate that the aromatic alcohol is required for antibiotic activity, while extending the alkyl chain on the nitrogen does not diminish its inhibitory effect. (C) Construct of the armeniaspirol-derived capture probe, **2**, functionalized with an alkyne for activity-based protein profiling.

2.2.3 Target capture using activity-based protein profiling

A standard ABPP strategy was employed to capture protein candidates with probe **2** in *B. subtilis* cell lysate[129] (**Figure 2.4A**). The alkyne installed on probe **2** was bioconjugated to biotin-azide through CuAAC click chemistry. The protein-probe complexes were recovered following binding to streptavidin agarose beads. On-bead trypsin digestion followed by LC-MS/MS analysis provided relative abundances of all identified proteins. Only proteins with a high confidence, 1% false discovery rate (FDR), and with at least two detected peptides were included in the data analysis. Of these, only proteins that were detected in three of four replicates were used for the analysis. Ideally, this strict analysis would allow for only the most likely of candidates to be represented.

However, non-specific protein-probe interactions are one of the main limitations of ABPP[122,130]. Thus, in a parallel experiment a competitive ABPP approach was performed with **1** in order to discern actual protein targets from false positives[122] (**Figure 2.4A**). The cell lysate was pre-treated with an excess concentration of **1** to block available binding sites of the protein targets, and subsequently treated with **2** to capture remaining proteins with accessible binding sites. This competition should result in the capture of mostly non-specific false positive protein targets which are screened against the proteins obtained from **2** alone. Thus, significant increases in protein abundance captured with **2** alone versus the competition-based non-specific capture deconvolute the actual protein targets. In total, twelve proteins showed a statistically significant (p-value <0.05) and biologically relevant (fold-change >2) increase in abundance with **2** versus the sample pre-treated with **1** as shown by a volcano plot distribution (**Figure 2.4B**; **Table S2** in **Appendix I**).

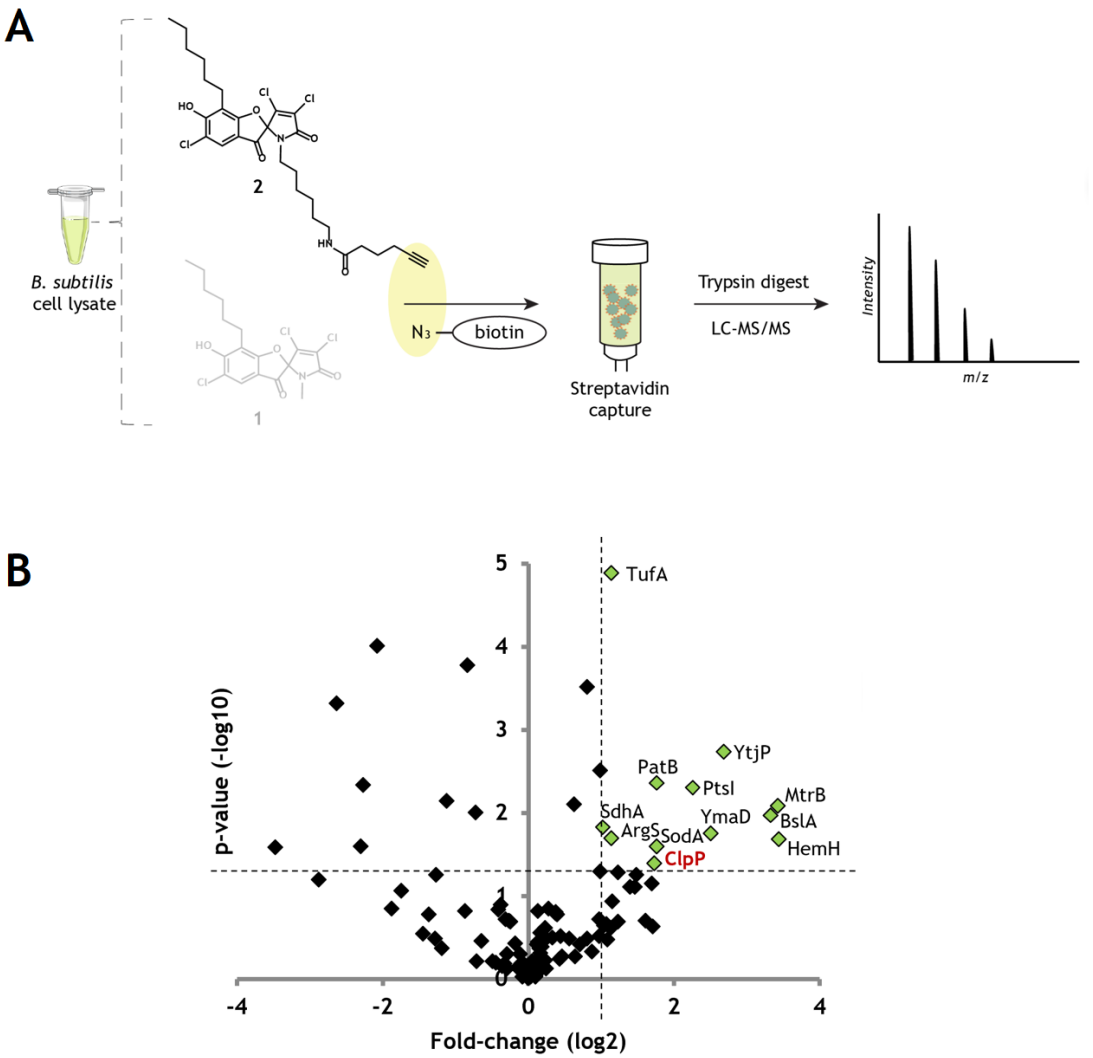

Figure 2.4. Inhibitor capture strategy to determine biochemical targets of armeniaspirol. (A) Experimental workflow for profiling armeniaspirol protein targets. The electrophilic center binds to the protein of interest in *B. subtilis* cell lysate. The free alkyne is conjugated to biotin-azide and captured on streptavidin beads. Captured proteins are subjected to digestion and LC-MS/MS for identification. A competition assay with **1** is included to clarify targets. (B) Volcano plot of inhibitor covalent capture, resulting in 12 biologically and statistically significant hits. Biological and statistical significance is defined as fold-change >2 and p-value <0.05, respectively.

Interestingly, ClpP showed a 3.3-fold increase in abundance in the probe-only capture versus the competition-based capture. As previously discussed in Chapter One (Section 1.2), ClpP is the proteolytic component of the ClpXP AAA+ bacterial protease and represents an attractive antibiotic and antivirulent target. Thus, the capture of ClpP warrants further investigation and excitement as a direct biochemical target of armeniaspirol. Moreover, ClpQ, was also detected at high abundance in our probe-only inhibitor capture experiment, though in only one of the four replicates. The decreased sensitivity of LC-MS/MS detection of ClpQ across replicates may be explained by the much lower cellular abundance of ClpYQ compared to ClpXP in *B. subtilis*[131]. Nevertheless, the single detection of ClpQ lends support to the hypothesis that the Clp proteases may be targets of armeniaspirol. Thus, we sought to determine if **1** inhibits the ClpXP and ClpYQ proteases *in vitro* in biochemical assays. A further comprehensive analysis of the other apparent biologically and statistically significant biochemical targets of armeniaspirol is discussed in Chapter Three (Section 3.4.4).

2.3 Kinetic characterizations of ClpXP and ClpYQ AAA+ proteases

2.3.1 Michaelis-Menten kinetics

A continuous biochemical assay to monitor proteolytic activity of the ClpXP protease from the Gram-negative *E. coli* has been extensively developed[132]. In the presence of active protease, the commercially available fluorogenic peptide substrate, N-Succinyl-Leu-Tyr-7-amido-4-methylcoumarin, is cleaved to release amido-4-methylcoumarin (AMC) which is measured in relative fluorescent units (RFU) (**Figure 2.5**). Thus, we used this established ClpXP assay as a foundation to construct our biochemical assays and characterize Michaelis-Menten kinetics. This provides us with a quantitative reference for understanding an enzyme's affinity

for a substrate (K_M) and its catalytic efficiency ($\frac{k_{cat}}{K_M}$) under given experimental conditions. Analyzing how these parameters are affected in the presence of **1** provides valuable insight into characterizing its mode of action.

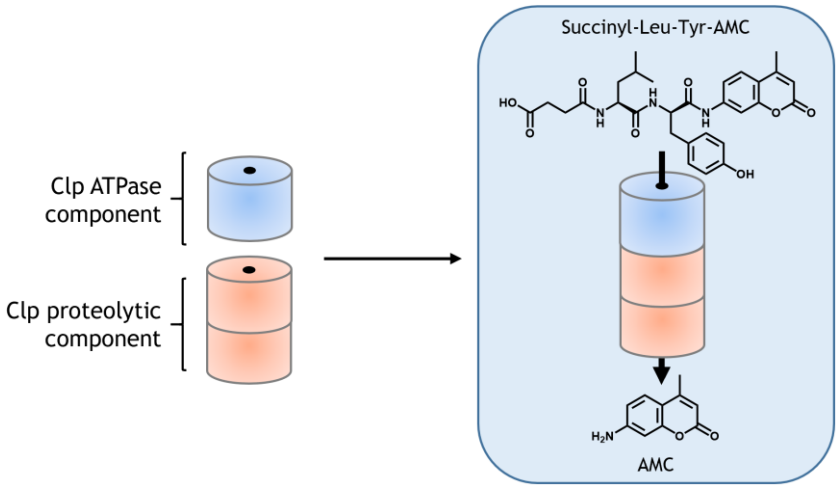

Figure 2.5. General schematic for assaying Clp proteolysis *in vitro*. The degradation of fluorogenic peptide, Succinyl-Leu-Tyr-AMC, leads to the release of AMC that can be detected at an excitation and emission of 355 nm and 460 nm, respectively.

While we were able to heterologously express and purify the *B. subtilis* ClpX and ClpP proteins in *E. coli* BL21(DE3), we could only achieve single turnover of the peptide substrate despite the many assay conditions tested (data not shown). Thus, we chose instead to characterize the proteolytic activity of the homologous *E. coli* ClpXP (ecClpXP) complex, using this as a model for ClpXP inhibition kinetics with **1**. Both ClpX and ClpP were readily expressed and purified (**Figure S3A** in **Appendix I**). We obtained a Michaelis-Menten curve for the ecClpXP complex, yielding a K_M of (365.4 ± 25.5) x 10^{-6} M and k_{cat} of 0.0512 ± 0.0038 s^{-1} (**Figure 2.6A**; **Figure S4** in **Appendix I**). Furthermore, since ClpP is known to possess modest peptidase activity in the absence of ClpX[133], we obtained a Michaelis-Menten curve for ecClpP alone (**Figure 2.6A**). Similarly, a biochemical assay for *B. subtilis* ClpYQ (bsClpYQ) has also

been developed using an alternative AMC fluorogenic peptide substrate, carbobenzoxy-Gly-Gly-Leu-7-amido-4-methylcoumarin[45,134]. Upon successful expression and purification of bsClpQ and bsClpY, we kinetically characterized its proteolytic activity (**Figure 2.6B**; **Figure S3B** in **Appendix I**). In contrast with ecClpP, we observed no peptidase activity for ClpQ in the absence of ATP or the ATPase component ClpY in accordance with the literature[45] (**Figure S5** in **Appendix I**).

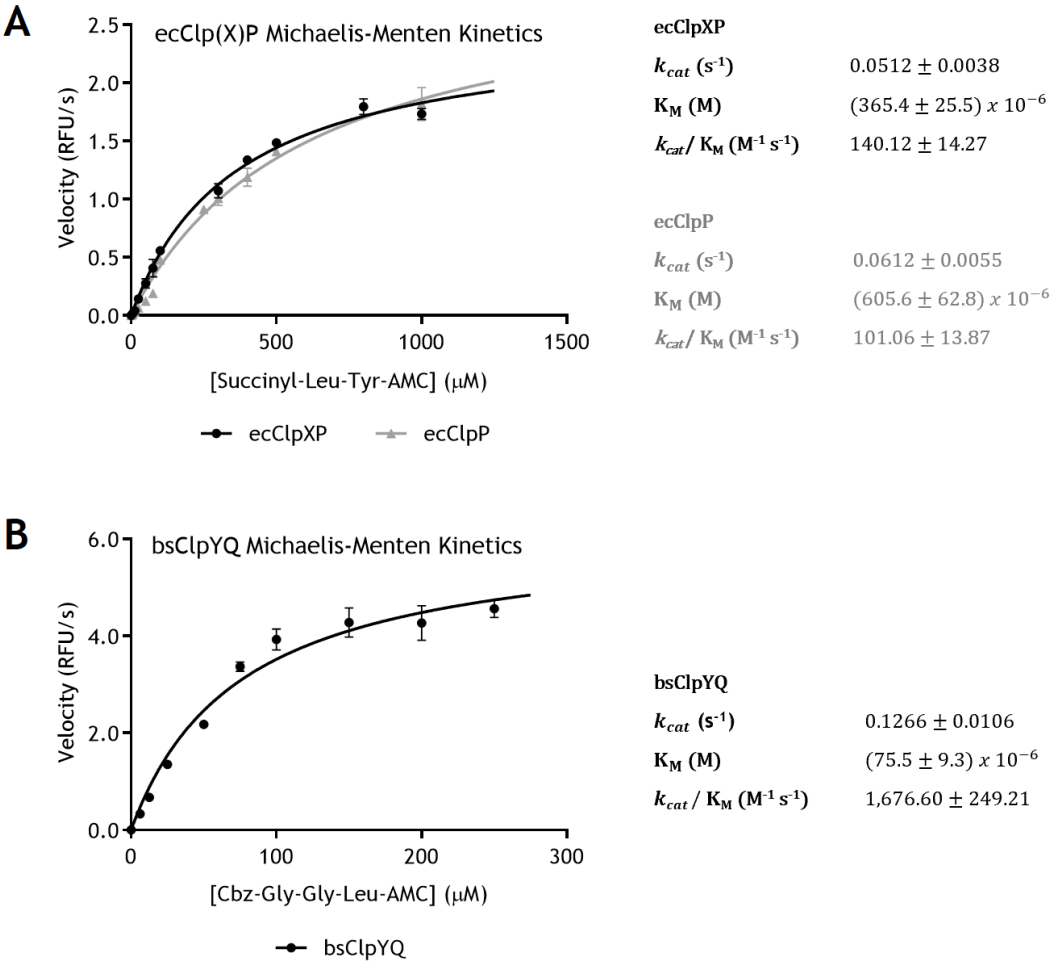

Figure 2.6. Michaelis-Menten kinetics for ecClp(X)P and ecClpYQ proteolysis activity. (A) Michaelis-Menten curve of ecClpP and ecClpXP proteolysis. (B) Michaelis-Menten curve of bsClpYQ proteolysis. Experimentally, Michaelis-Menten curves are produced by plotting initial velocities of peptide hydrolysis at varied substrate concentrations. The k_{cat}, K_M, and $\frac{k_{cat}}{K_M}$ Michaelis-Menten parameters are displayed. Each data point was collected in triplicate (n = 3).

2.3.2 Armeniaspirol inhibition kinetics

In the presence of increasing concentrations of **1**, we observed a clear dose response towards the proteolytic activities of both the ClpYQ and ClpXP complexes. We characterized protease inhibition by IC_{50}. Addition of **1** showed protease inhibition for ecClpP and ecClpXP with an IC_{50} of 61.0 ± 1.0 μM and 48.6 ± 1.0 μM, respectively (**Figure 2.7A**), whereas **1** inhibited protease activity of bsClpYQ with an IC_{50} of 15.2 ± 1.0 μM (**Figure 2.7B**).

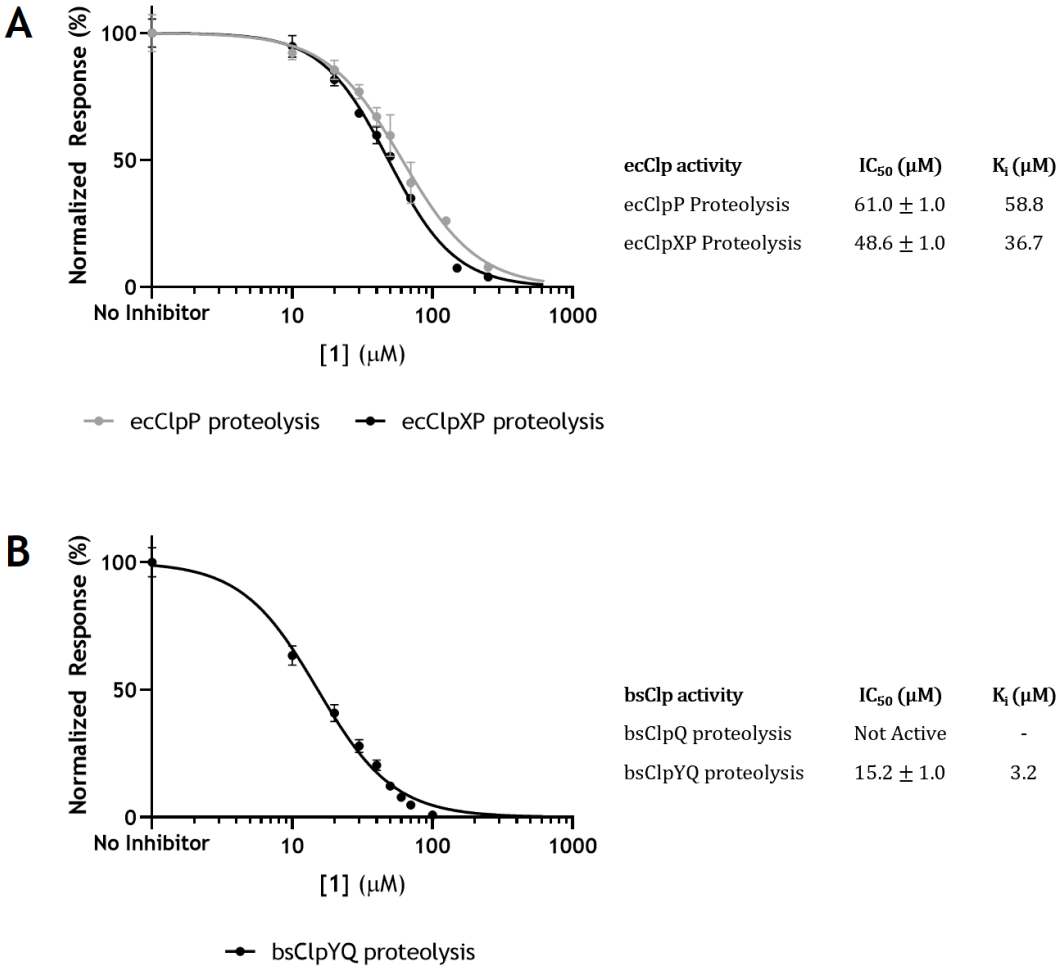

ecClp activity	IC_{50} (μM)	K_i (μM)
ecClpP Proteolysis	61.0 ± 1.0	58.8
ecClpXP Proteolysis	48.6 ± 1.0	36.7

bsClp activity	IC_{50} (μM)	K_i (μM)
bsClpQ proteolysis	Not Active	-
bsClpYQ proteolysis	15.2 ± 1.0	3.2

Figure 2.7. IC_{50} curves of ecClpXP and bsClpYQ proteolysis activity. (A) **1** inhibits ecClpXP and ecClpP with an IC_{50} of 48.6 μM and 61.0 μM with 0.1 mM succinyl-Leu-Tyr-AMC, respectively. (B) **1** inhibits bsClpYQ with an IC_{50} of 15.2 μM with 0.1 mM Cbz-Gly-Gly-Leu-AMC.

Surprisingly, we did not observe irreversible inhibition in our biochemical assays despite obtaining ClpP and ClpQ using a covalent ABPP chemical proteomic strategy[122]. This was tested by incubating ClpYQ with an excess concentration of **1** for 4 hours, diluting the incubation mixture to an inhibitor concentration well below the IC_{50}, and evaluating proteolysis activity (**Figure 2.8**).

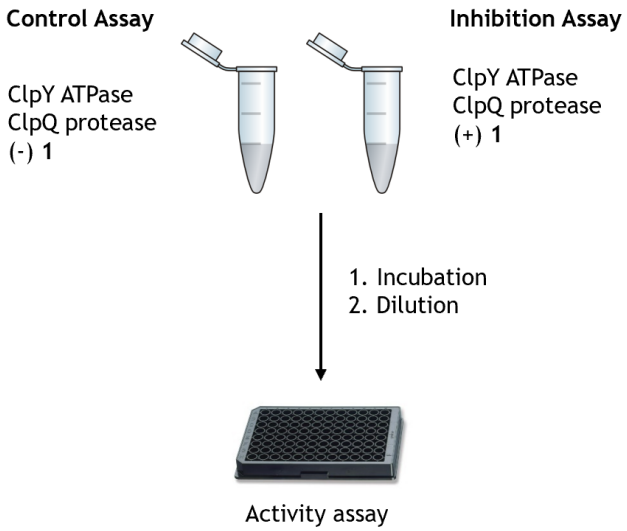

Figure 2.8. Enzyme inhibition assay to evaluate reversibility. Irreversible versus reversible enzyme inhibition was tested by incubating an excess of **1** with ClpYQ. Following a substantial incubation period, the mixture was diluted to yield a concentration of **1** below the IC_{50}. Irreversibly bound inhibitor should result in no proteolysis activity, while reversibly bound inhibitor should recover significant proteolysis activity.

For irreversible inhibition, enzyme activity will remain fully inhibited even upon large dilution of inhibitor, whereas enzyme activity will recover for a reversible inhibitor. Following a dilution of **1**, ClpYQ proteolysis activity was recovered at 78% of the control without **1**. One possible explanation for this irregularity is that a very slow inactivation rate (k_{inact}) may enable formation of covalent enzyme-inhibitor complex for capture, but insufficient covalent modification to be able to exhibit detectable irreversible inhibition. In order to further characterize the mode of inhibition by **1**, we monitored changes in K_M and v_{max} values of the *B. subtilis* ClpYQ proteolytic activity at a range of inhibitor concentrations under classical steady-state conditions. We

observed an increase in K_M and stable v_{max} in the presence of increasing inhibitor concentrations, demonstrating that **1** functions as a competitive inhibitor of the Clp proteases[135] (**Figure S6** in **Appendix I**). In the competitive inhibition model, substrate and inhibitor contend for the same active site of an enzyme leading to a reversible enzyme-inhibitor complex. Thus, binding of inhibitor to free enzyme prevents binding of substrate and vice versa (**Scheme 2.1**).

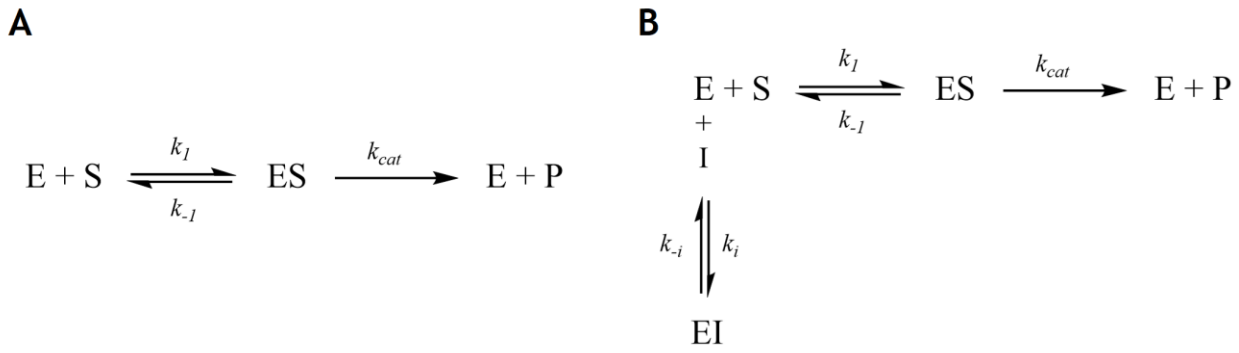

Scheme 2.1. Enzyme kinetics reaction schematics. (A) Michaelis-Menten enzyme reaction schematic. Enzyme binds substrate to produce product. (B) Competitive inhibition enzyme reaction schematic. Enzyme binds substrate or inhibitor to produce product or enzyme-inhibitor complex, respectively. Enzyme (E), Substrate (S), Inhibitor (I), Enzyme-substrate complex (ES), Enzyme-inhibitor complex (EI), Product (P).

The inhibition constant for reversible inhibition, K_i, measures the dissociation of the enzyme-inhibitor complex and is given by the following equation:

$$K_i = \frac{k_{-i}}{k_i} \qquad \textbf{[eq. 2.1]}$$

Under conditions of competitive inhibition, the Cheng-Prusoff equation allows for the conversion of IC_{50} values to obtain K_i[136]. The Cheng-Prusoff equation for competitive inhibitors is defined as follows:

$$IC_{50} = (1 + \frac{[S]}{K_M})K_i \qquad \textbf{[eq. 2.2]}$$

The K_i from this equation can be validated graphically using a modified Dixon plot represented by $\frac{1}{v}$ versus $\frac{[I]}{1+\frac{[S]}{K_M}}$, where the x-intercept of the trendline represents -K_i (**Figure S7** in **Appendix**

I). The K_i constants for bsClpYQ and ecClpXP were determined to be 3.21 μM and 36.68 μM, respectively. Surprisingly, the K_i for ecClpXP is significantly greater than both the K_i of bsClpYQ and the MIC of **1** (4.8 μM in *B. subtilis*). While it is possible that **1** possesses a lower affinity towards the Gram-negative ClpXP complex, the inaccessibility to a functional Gram-positive ClpXP complex makes it difficult to substantiate this claim. However, in conjunction with the inhibitor capture, these data still coincide with ClpXP and ClpYQ as direct biochemical targets of armeniaspirol.

In order to fully understand the impact of **1** on the AAA+ proteases, ATPase activity was also investigated *in vitro*. A discontinuous colorimetric malachite green assay was used to monitor free inorganic phosphate release following ATP hydrolysis at an absorbance wavelength of 650 nm[137] (**Figure 2.9**).

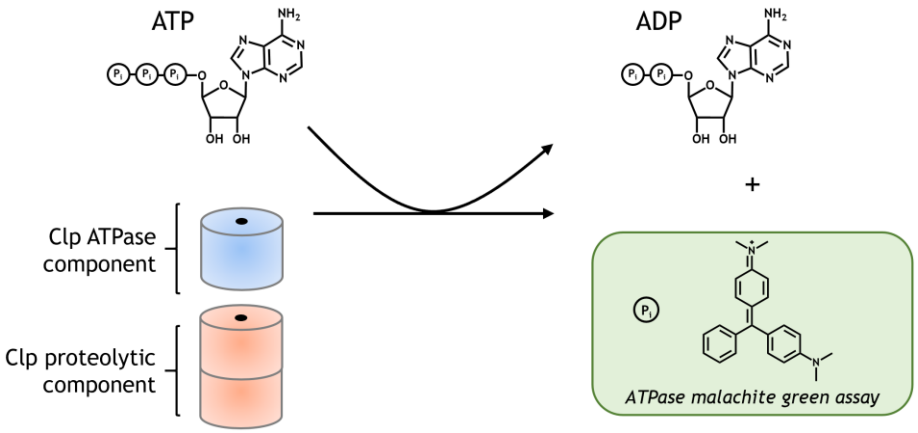

Figure 2.9. General schematic for assaying Clp ATP hydrolysis *in vitro*. ATP hydrolysis is monitored through interaction of free phosphate with malachite green dye and measured at an absorbance of 650 nm.

The ATPase activities of the ecClpXP and bsClpYQ complexes, as well as the individual components ecClpX and bsClpY, were inhibited by **1**. The IC_{50} of bsClpXP and ecClpX ATP hydrolysis is 54.4 ± 1.1 μM and 42.2 ± 1.0 μM, respectively (**Figure 2.10A**). Additionally, the

IC_{50} of bsClpYQ and bsClpY ATP hydrolysis is 96.9 ± 1.0 μM and 107.9 ± 1.0 μM, respectively (**Figure 2.10B**).

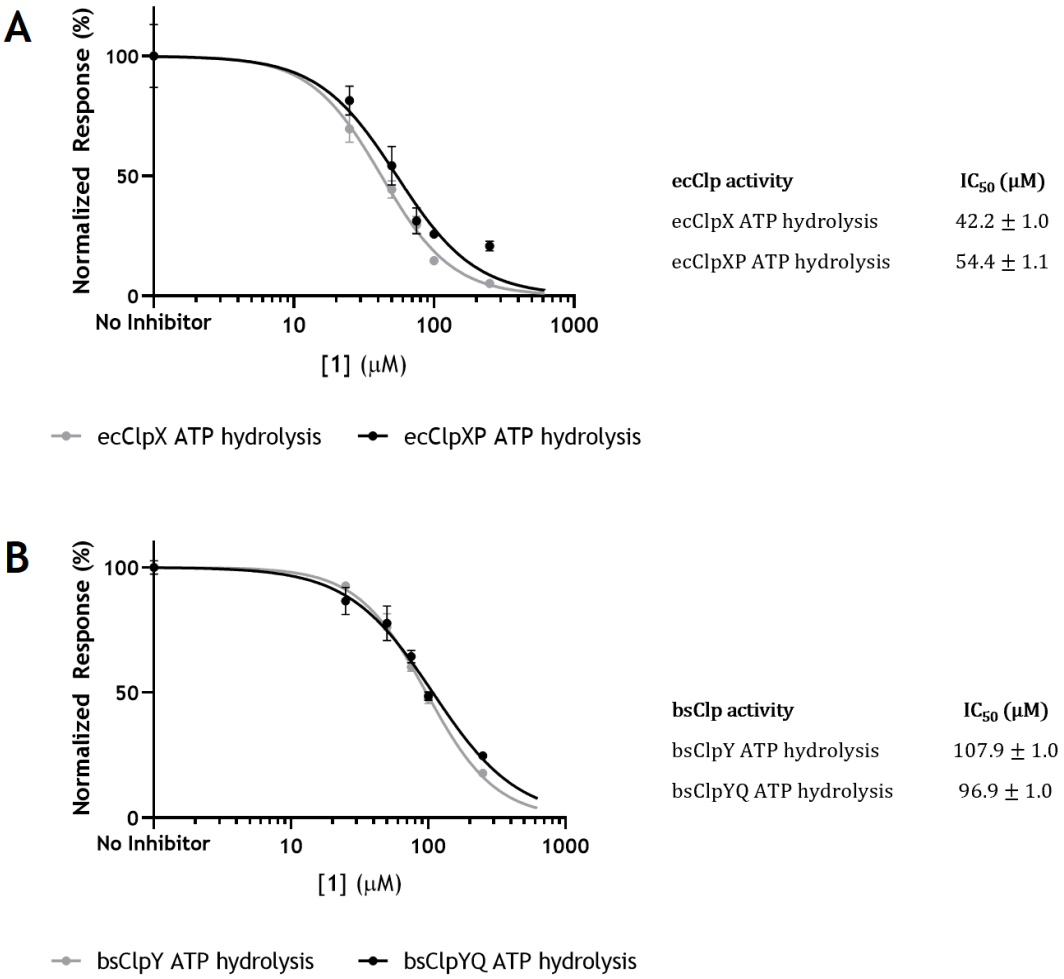

Figure 2.10. IC_{50} curves of ecClpXP and bsClpYQ ATPase activity. (A) **1** inhibits ecClpXP and ecClpX with IC_{50}s of 54.4 μM and 42.2 μM with 1 mM ATP, respectively. (B) **1** inhibits bsClpYQ and bsClpY with IC_{50}s of 96.9 μM and 107.9 μM with 1 mM ATP, respectively.

2.4 Conclusions

2.4.1 Armeniaspirol inhibitor kinetics suggest a complex molecular interaction

Interestingly, armeniaspirol inhibits both the protease and ATPase activities of the ecClpXP and bsClpYQ complexes. The AAA+ ATPases group into class I and class II chaperones depending on the presence of one or two nucleotide-binding domains. ClpC and

ClpE are class I chaperones with two nucleotide-binding domains, while ClpY and ClpX are class II chaperones with one nucleotide binding domain[138]. The amino acid sequences of ClpY and ClpX show close homology to each other relative to ClpC and ClpE[139]. Thus, while it would be reasonable to propose a mechanism for armeniaspirol that targets these ATPases leading to protease inhibition, this would be inconsistent with the inhibitor capture of ClpP and the competitive mode of inhibition observed in our biochemical assays, including with the ClpP protease activity alone. A second possibility is that binding of **1** at the active site of either ClpP or ClpQ may lead to allosteric disruption of ATPase function. However, this would also be inconsistent with the inhibition of both ClpX and ClpY ATPase activities alone. Moreover, we could not discern any obvious disruptions to the multimeric aggregation of ClpYQ by non-denaturing polyacrylamide gel electrophoresis under *in vitro* assay conditions, even at high concentrations of **1** (**Figure S8** in **Appendix I**). Thus, the molecular interaction between armeniaspirol and these complexes remains uncharacterized and of particular interest moving forward.

2.4.2 Antibiotic implications of ClpXP and ClpYQ inhibition

Based on our chemical proteomics and *in vitro* biochemical assays, the antibiotic mechanism of action of armeniaspirol appears to be a consequence of inhibition of the ClpXP and ClpYQ AAA+ proteases. Interestingly, there is precedence to support that the combined activities of ClpQ and ClpP are essential in Gram-positive bacteria. For instance, while *clpP* and *clpQ* are non-essential genes, attempts to produce a Δ*clpQ* Δ*clpP* double mutant in *S. aureus* proved to be synthetically lethal[140]. Additionally, *clpP* is essential in the Gram-positive *Mycobacterium tuberculosis* which lacks *clpQ*[78,83]. Thus, we propose that abolishing both ClpXP and ClpYQ activities together is responsible for antibiotic activity, though we cannot explicitly

rule out the possibility of other biochemical targets, as is often the case with natural products[141]. In further support of this is that a mutation in either ClpXP or ClpYQ would likely lead to rapid resistance towards armeniaspirol, but inability to develop resistant strains suggests a more complicated mechanism is at work.

2.4.3 Armeniaspirol is the first known natural product inhibitor of ClpP

ClpP is a highly coveted antivirulence target for inhibiting pathogenic bacteria[67,142–144]. However, extensive compound library screens in search for clinically viable ClpP inhibitors have been met with limited success. Synthetic compounds including certain β-lactones and phenyl esters have been identified as selective inhibitors of ClpP with anti-virulence properties, but suffer from poor plasma stability and pharmacokinetics[75,76]. Alternatively, armeniaspirol represents the first natural product ClpP inhibitor and is inherently more likely to overcome these *in vivo* challenges given its naturally evolved scaffold[145] and efficacy in MRSA-induced septicemia models[110]. Armeniaspirol is also unique in displaying antibiotic activity, whereas the synthetic selective inhibitors of ClpP result in reduced virulence in the Gram-positive pathogens *S. aureus* and *Listeria monocytogenes* but exhibit no antibiotic activity[75,146].

The ADEPs represent the only other class of natural product antibiotics that target ClpP. In contrast to armeniaspirol, the ADEPs bind to ClpP and activate rather than inhibit proteolytic activity[147]. Although ADEP-activated ClpP is unable to degrade stably folded proteins, unstable proteins and newly emerging proteins from the ribosome are highly susceptible to degradation[86]. This uncontrolled and undiscriminating protein degradation leads to loss of cellular homeostasis and results in antibiotic activity. However, given that the ADEPs are single enzyme-targeting antibiotics, they are substantially more prone to rapid development of resistant phenotypes

rendering them ineffective[20,84,148]. As already noted, armeniaspirol does not appear to suffer from this clinical complication given the inability to generate resistant *S. aureus* strains[110].

2.5 Contributions

The syntheses of chloro-armeniaspirol **1**, analogs **1.1-1.3** for the structure-activity relationship study, and inhibitor capture probe **2** were performed by Mark H. Dornan, Ph.D., University of Ottawa. LC-MS/MS for inhibitor capture proteomics was performed by Zoran Minic, Ph.D., John L. Holmes Mass Spectrometry Facility, University of Ottawa. Plasmid constructs for expression and purification of *E. coli* ClpX (pProEx-Htb-ClpX) and *E. coli* ClpP (pET9a-ClpP) were provided by Prof. Walid A. Houry, University of Toronto.

CHAPTER THREE:

Armeniaspirol Leads to Cell Division Arrest in Gram-positive Bacteria

3.1 Introduction

3.1.1 Stable-isotope dimethyl labeling quantitative proteomics

Advances in mass spectrometry based analytical methods have increased our ability to identify and quantify proteins to obtain proteomic representations of a biological sample[149]. Quantitative proteomics strategies have been developed that allow for relative or absolute quantifications of protein levels in a cell or tissue and provide useful information in understanding how a proteome changes in response to an altered biochemical state[150]. Quantitative proteomics can be performed through diverse chemical label-based or label-free approaches. The chemical label-based approach allows for the incorporation of stable isotopes into peptides to quantify and compare multiple samples in one combined LC-MS/MS experiment.

Stable-isotope dimethyl labeling is an extensively used chemical label-based proteomics approach for quantifying relative protein levels between samples[151]. The labeling of peptides is dependent on a reductive alkylation reaction with formaldehyde and cyanoborohydride to methylate primary amine groups on the N-terminus or lysine side chains of peptides. This approach allows for up to a maximum of three proteomic samples to be analyzed simultaneously through addition of formaldehyde (light label) or deuterated formaldehyde (intermediate label) with cyanoborohydride, or deuterated ^{13}C-labeled formaldehyde with cyanoborodeuteride (heavy label) to label corresponding samples[151] (**Table 3.1**). The addition of the light, intermediate, and heavy labels create mass shifts of 28, 32, or 36 Daltons per primary amine, respectively[152]. Only the light and intermediate labels are typically used when comparing two samples, whereas all

labels are used when comparing three samples. The labeled samples are mixed in a 1:1 or 1:1:1 ratio accordingly and analyzed by LC-MS/MS.

Table 3.1. Light, intermediate, heavy stable isotope labels of dimethyl labeling. Dimethyl labeling quantitative proteomics tolerates a simultaneous analysis of up to three samples, which can be attained by addition of formaldehyde (light label), deuterated formaldehyde (intermediate label), or a combination of deuterated and ^{13}C-labeled formaldehyde (heavy label).

Structure:	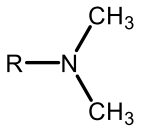	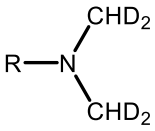	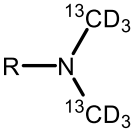
Reagents:	CH_2O $NaBH_3CN$	CD_2O $NaBH_3CN$	CD_2O $NaBD_3CN$
Label:	Light	Intermediate	Heavy
Mass shift:	+28 Da	+32 Da	+36 Da

Herein, we applied stable-isotope dimethyl labeling to quantitatively profile changes in the *B. subtilis* proteome following treatment of cultures with either a vehicle control (DMSO) or a sub-lethal dose of **1** (1 μg/mL – ½ the MIC) (**Figure 3.1A**). Proteome extracts of DMSO (untreated) and **1**-treated (treated) *B. subtilis* cultures were labeled with formaldehyde and deuterated formaldehyde, respectively, and quantified by LC-MS/MS (**Figure 3.1B**). Our high confidence (1% FDR) protein recovery across three replicates yielded a sufficiently broad coverage of the total *B. subtilis* proteome comparable to that seen in the literature[153] (**Figure 3.1C**). Of this coverage, only protein hits detected in at least two of three treated/untreated replicates were used for analysis, thus providing a stringent proteomic profile of *B. subtilis* in response to treatment with **1**. The resulting proteins were graphically distributed using a volcano plot to visualize the statistical and biological significance of each detected protein for further analysis (**Figure 3.1D**).

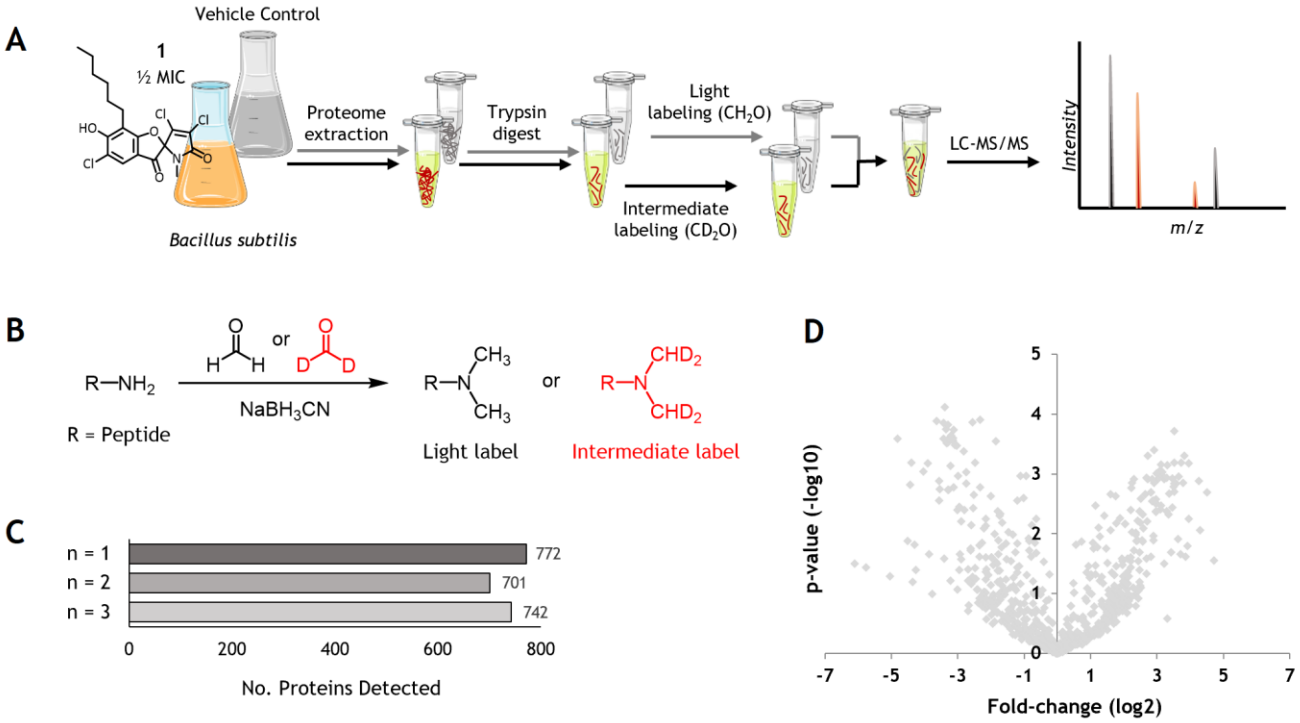

Figure 3.1. Dimethyl labeling and quantitative proteomics of the *B. subtilis* proteome. (A) Proteome extract of *B. subtilis* following DMSO- and **1**- treated growth are isotopically labeled with formaldehyde and deuterated formaldehyde, respectively, and quantified by LC-MS/MS. Experiments were carried out in biological triplicate. (B) Stable isotope dimethyl labeling by addition of formaldehyde at the N-terminus and ε-amino groups of lysine residues, followed by the immediate reduction with sodium cyanoborohydride. (C) Total protein recovery following dimethyl labelling for each replicate, n, is shown. (D) Volcano plot of high confidence treated/untreated *B. subtilis* proteins detected in at least two of three replicates.

3.2 Armeniaspirol has a distinct mechanism of action

3.2.1 Armeniaspirol-treatment displays a unique proteomic profile

The *B. subtilis* proteome has been extensively profiled in response to several antibiotics of various mechanisms including those that inhibit protein biosynthesis, fatty acid biosynthesis, cell wall biosynthesis, and DNA damaging agents[154–159]. Each of these antibiotic profiles display increases in abundance of specific protein biomarkers that are characteristic to its mechanism. Thus, overlaying our **1**-treated proteomic profile with each of these established antibiotic profiles will allow us to directly compare similarities in mechanisms. However, the increase in abundance of key proteins with these other antibiotics are not similarly observed with treatment

of **1**. Instead, most referenced proteins show a statistically and biologically insignificant change resulting in a unique proteomic profile (**Figure 3.2**; **Table S3** in **Appendix II**).

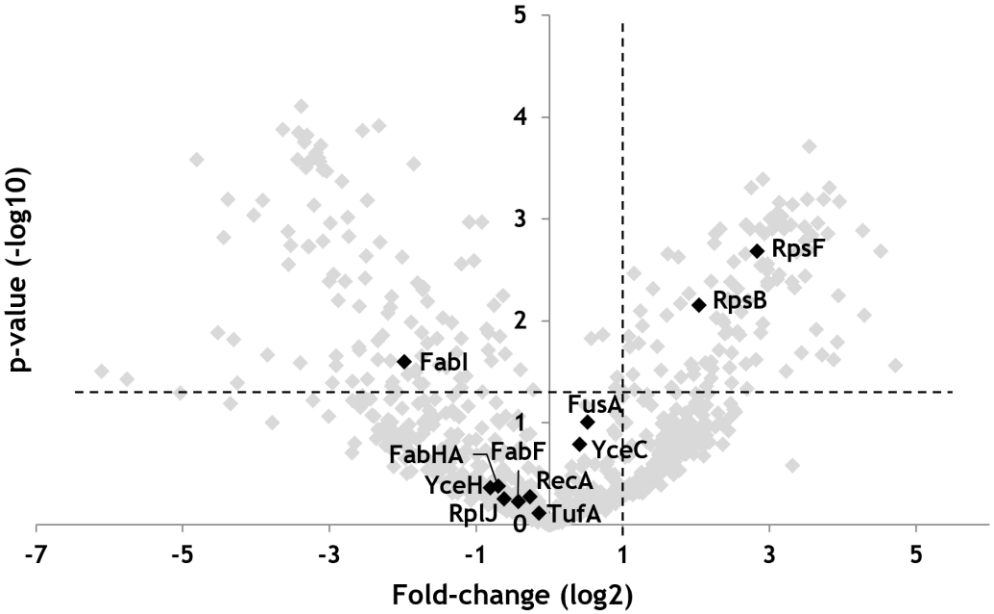

Figure 3.2. Antibiotic protein biomarker abundances in relation to 1-treatment. Protein fold-change and p-values are identified for specific proteins associated with certain antibiotic treatments. Each protein marker highlighted has been shown to have substantial enrichment with known antibiotic treatments. Biological and statistical significance is defined as fold-change >2 and p-value <0.05, respectively.

Treatment of *B. subtilis* with the protein biosynthesis inhibitors tetracycline and chelocardin show an increase in ribosomal proteins (RpsB, RpsF, RplJ) and translation elongation factors (TufA, FusA) by two-dimensional gel-based proteomics[155]. While our data shows **1** increases RpsB and RpsF, there is a less than two-fold change in RplJ, FusA, and TufA, suggesting it does not principally target protein biosynthesis. Likewise, the fatty acid biosynthesis inhibitors platencin, platensimycin, cerulenin and triclosan all cause a significant increase in FabHA, FabHB, FabF, and FabI levels[156]. Upon treatment with **1**, none of these proteins showed a greater than two-fold increase. The cell wall biosynthesis inhibitors merscadin, bacitracin, and vancomycin all show a significant increase in YceH and YceC

levels[157]. However, in only one replicate of our proteomics does YceC increase above two-fold when treated with **1**. Lastly, treatment of *B. subtilis* with DNA-damaging agents mitomycin, daunomycin, and adriamycin leads to significant increases in RecA and the SOS response, whereas treatment with **1** led to no change in RecA levels[154,159]. Thus, the distinction between the many characterized proteomic profiles of *B. subtilis* treated with a range of antibiotics versus treatment with **1** suggests a unique antibiotic mechanism.

3.2.2 Armeniaspirol is not synergistic with common antibiotics

Studying the synergistic interactions of two antibiotics on bacterial growth is another way to elucidate mechanisms of inhibition. Synergy is defined when a combination of antibiotics leads to an inhibitory response much greater than that expected from either individual antibiotic activity alone[160]. If one antibiotic displays synergy with another, it is highly likely that both function through a related mechanism. This is described as parallel pathway inhibition, which states that the combined inhibitory effect of two antibiotics that inhibit targets on parallel mechanisms is often more severe than either antibiotic's effect individually[161]. Synergy is determined experimentally through 96-well plate MIC checkerboard assays, where one antibiotic is serially diluted horizontally from left-to-right and the other vertically from top-to-bottom. A drastic decrease in the MIC in both dimensions of the 96-well plate is representative of synergy, while no change in the MIC in either dimension represents no interaction between antibiotic activities (**Figure 3.3A**). Thus, we sought to identify synergy of **1** with known antibiotics of various mechanisms such as the protein biosynthesis inhibitor tetracycline, DNA replication inhibitor ciprofloxacin, cell wall biosynthesis inhibitor penicillin, and the fatty acid biosynthesis inhibitor cerulenin in *B. subtilis* (**Figure 3.3B**).

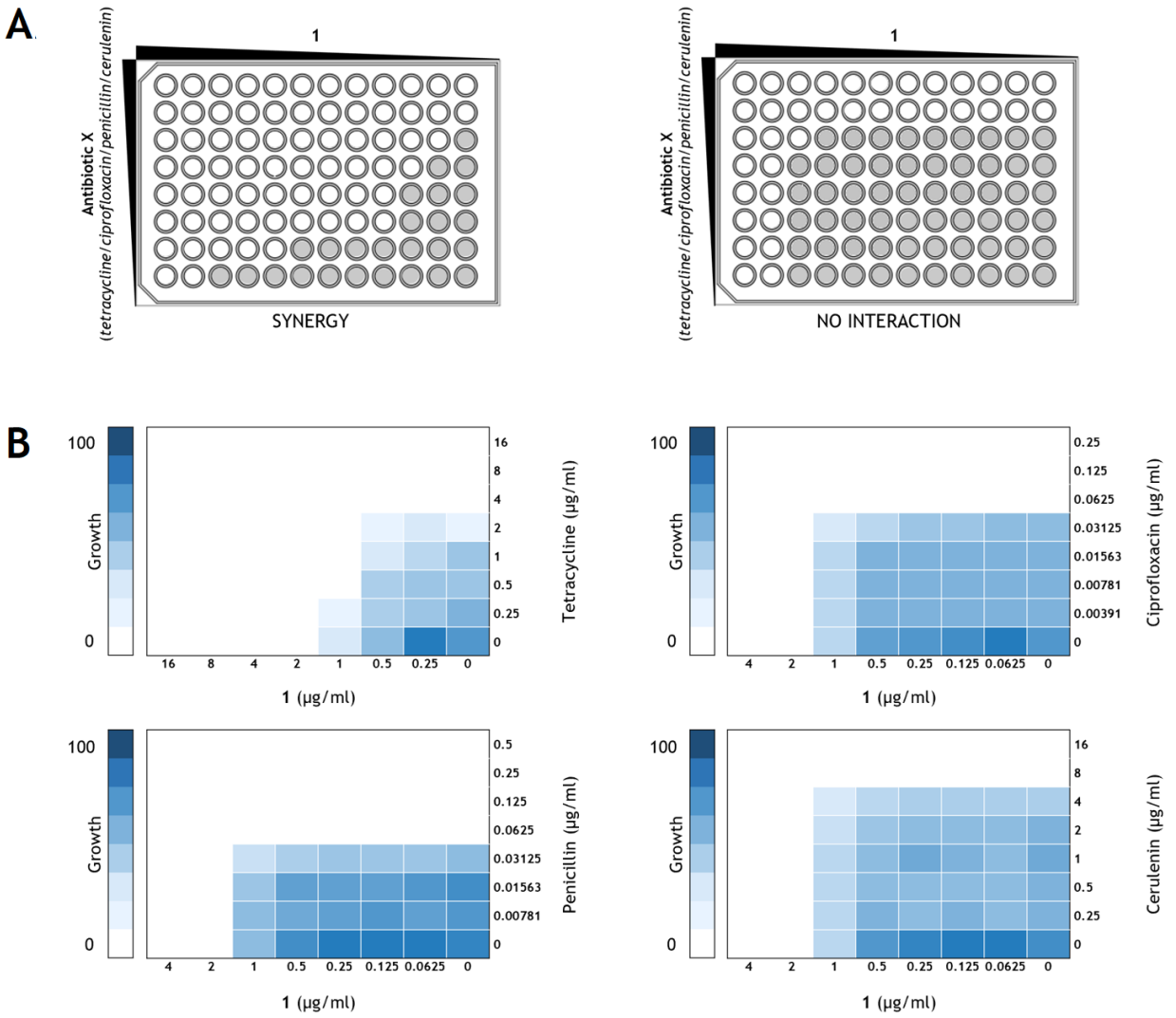

Figure 3.3. Checkerboard synergy assays with 1. (A) Depending on the extent of growth inhibition, a pair of antibiotics may be considered synergistic (left), antagonistic (not shown), or indifferent (right). (B) **1** is paired with Gram-positive antibiotics of varying mechanisms in *B. subtilis* to determine changes in MIC, including the protein biosynthesis inhibitor tetracycline, DNA replication inhibitor ciprofloxacin, cell wall biosynthesis inhibitor penicillin, and fatty acid biosynthesis inhibitor cerulenin. No synergy with **1** is observed.

Upon visual inspection, it was immediately obvious that **1** did not display synergy with any of the selected antibiotics. A fractional inhibitory concentration (FIC) index can additionally be calculated from these assays to quantitatively identify synergy[162]. The FIC index is calculated using the MICs of antibiotics in combination versus their MICs alone. The consensus follows that a FIC index ≤ 0.5 is defined as synergistic, while a FIC index > 4 is defined as

antagonistic[163]. A FIC index that falls between these two boundaries is considered to be indifferent, or have no interaction[163,164]. Our checkerboard synergy assays showed activity of **1** is independent of all tested antibiotics, as determined by their FIC indexes (**Table 3.2**). Thus, this data in conjunction with the proteomic profile in *B. subtilis* provides further evidence that **1** has a novel antibiotic mechanism.

$$FIC = \frac{MIC_{AC}}{MIC_A} + \frac{MIC_{XC}}{MIC_X} \qquad [\mathbf{eq.\ 3.1}]$$

Table 3.2 Fractional inhibitory concentration index of antibiotics paired with 1. The fractional inhibitory concentration (FIC) index was calculated according to the equation 3.1 above, where MIC_A represents the MIC of **1** alone, MIC_{AC} represents the MIC of **1** in combination with antibiotic X, MIC_X represents the MIC of antibiotic X alone, MIC_{XC} represents the MIC of antibiotic X in combination with **1**. Synergy is defined as FIC index ≤ 0.5. No synergy is observed with **1**.

Antibiotic X =	Tetracycline	Ciprofloxacin	Penicillin	Cerulenin
Mechanism of Action:	Protein biosynthesis	DNA replication	Cell wall biosynthesis	Fatty acid biosynthesis
		FIC index:		
5-chloro-armeniaspirol, **1**	0.625	≥ 1.000	≥ 1.000	≥ 1.000
Effect:	**Indifferent**	**Indifferent**	**Indifferent**	**Indifferent**

3.3 Implications of armeniaspirol in bacterial cell division

3.3.1 Profiling ΔclpP and ΔclpQ B. subtilis proteomes

Given that antibiotic activity is believed to be conferred through a combined mechanism inhibiting both ClpXP and ClpYQ proteases, we sought to characterize the proteomic profiles for *B. subtilis ΔclpP* and *B. subtilis ΔclpQ* deletion strains individually to compare to wild-type *B. subtilis* (**Table S8** in **Appendix V**). We expect the proteomic profiles of the *B. subtilis* deletion strains to share similarities with the proteomic profile of **1**-treated *B. subtilis.* Specifically, protease substrates for either ClpXP or ClpYQ are expected to significantly increase in abundance in their respective deletion strains, while the substrates for both proteases are

expected to significantly increase in abundance in **1**-treated *B. subtilis*. Thus, information from the enriched proteins of these proteomic profiles may be used to characterize the degradome and biological role of the ClpXP and ClpYQ proteases as well as infer a mechanism of action for armeniaspirol. As above, dimethyl isotopic labeling was used to quantitatively profile changes in each of the deletion strains with wild-type *B. subtilis* used as the control. Only proteins with a high confidence (1% FDR) and detection in two of three replicates were used for the analysis and represented in volcano plots (**Figure 3.4**). 109 proteins showed a biologically (fold-change >2) and statistically (p-value <0.05) significant enrichment in **1**-treated *B. subtilis*; the *ΔclpP* and *ΔclpQ B. subtilis* deletion strains displayed a significant enrichment of 264 and 191 proteins, respectively (**Figure 3.4**). 41 enriched proteins overlap between **1**-treatment and the *ΔclpP* deletion, while 21 enriched proteins overlap between **1**-treatment and the *ΔclpQ* deletion. The number of overlapping proteins is a statistically significant increase over the expected values from random as determined by the Chi square goodness of fit test ($P < 0.0001$). Thus, the significant overlap of enriched proteins between **1**-treated *B. subtilis* with each of the *ΔclpP* and *ΔclpQ B. subtilis* deletion strains strongly supports a mechanism of action relating to ClpXP and ClpYQ inhibition.

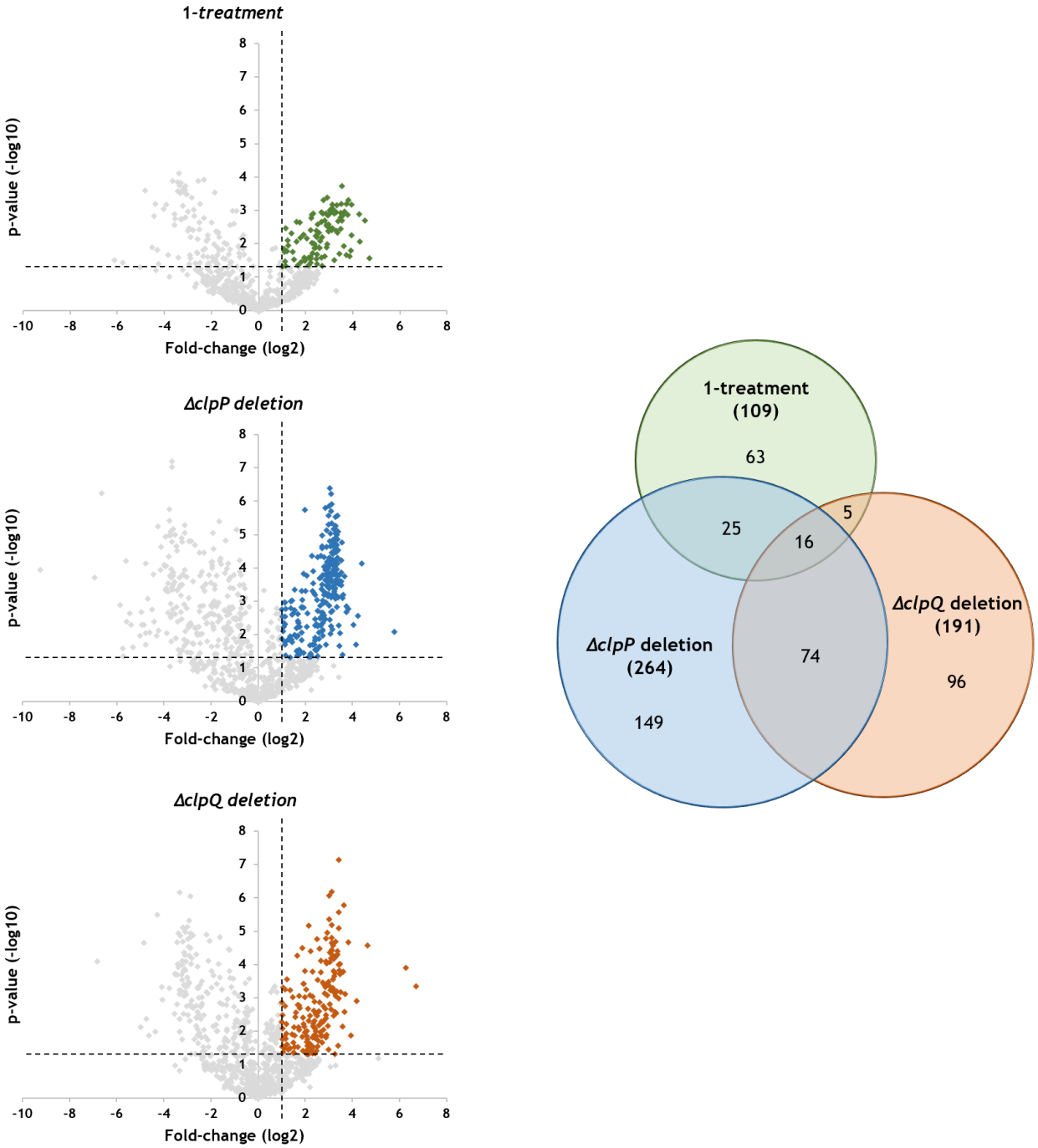

Figure 3.4. Proteomic profiles of 1-treated *B. subtilis* and *ΔclpP* and *ΔclpQ* deletion strains. Dimethyl labeling quantitative proteomics was performed on **1**-treated *B. subtilis*, a *ΔclpP* deletion strain, and a *ΔclpQ* deletion strain with wild-type *B. subtilis* used as the control. Proteomic profiles are represented as volcano plots of high confidence proteins detected in at least two of three replicates. The Venn diagram depicts upregulated proteins across treatments. Biological and statistical significance is defined as fold-change >2 and p-value <0.05, respectively. Upregulated proteins are proposed to include biological substrates of the ClpP and ClpQ proteases.

3.3.2 Divisome and elongasome proteomics

Interestingly, a systematic survey of the enriched proteins showed several divisome-related components increase in abundance across treatments (**Figure 3.5**; **Table S4** in **Appendix II**). The divisome complex plays a crucial role during cell division. In *B. subtilis*, cell division occurs at the mid-cell and is mediated by the formation of a ring-like structure (Z-ring) via polymerization of the essential divisome protein, FtsZ[165]. FtsZ and a number of chaperone proteins that scaffold with Z-ring formation to facilitate cell division – namely GroEL, DnaK, and Tig – increase significantly upon treatment with **1**[166–169]. These proteins are also observed to increase significantly in the *ΔclpP* deletion and are known substrates of the ClpXP protease[97,98,170,171].

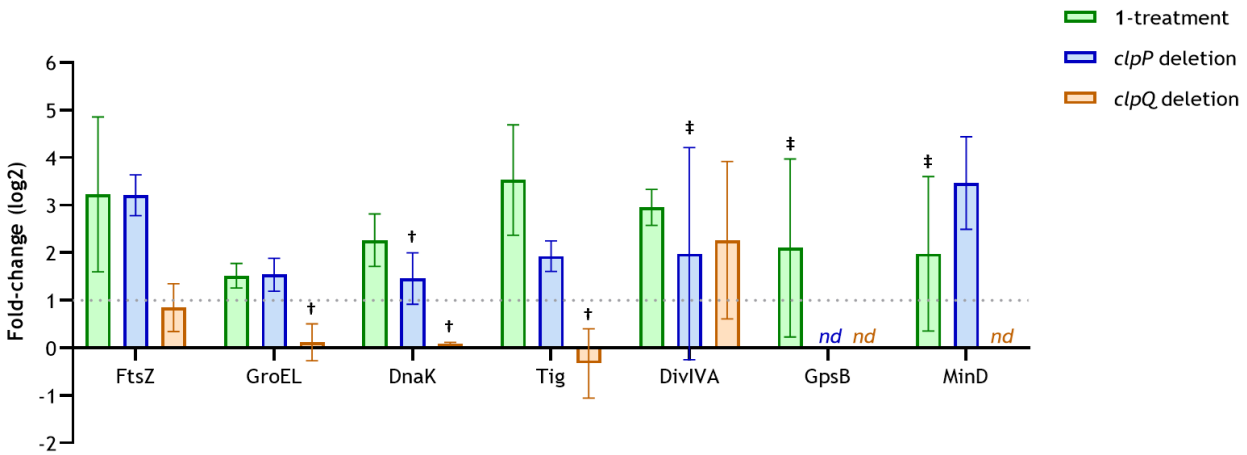

Figure 3.5. Divisome-related protein abundances. Effects on *B. subtilis* divisome protein abundances according to treatment versus wild-type. *nd,* not detected; †not significant; ‡not significant, detected in two of three replicates.

Additionally, several negative regulators of the divisome increase in abundance upon treatment with **1** including DivIVA, the DivIVA ortholog GpsB (detected in two of three replicates), and MinD (**Figure 3.5**; **Table S4** in **Appendix II**). DivIVA is recruited to sites of negative membrane curvature, including nascent cell division sites, where it complexes with

MinC and MinD to inhibit FtsZ polymerization[172–176]. While it is possible that DivIVA is a substrate for ClpXP given its increase in abundance in the *ΔclpP* deletion (detected in two of three replicates), DivIVA shows a significant increase in abundance in the *ΔclpQ* deletion. Notably, DivIVA is a proposed substrate of ClpXP in *Streptococcus mutans*, a Gram-positive bacteria that lacks ClpQ[177]. Thus, we propose DivIVA, and perhaps GpsB, are substrates of the ClpYQ protease in *B. subtilis*. Given that few targets of the ClpYQ protease are known[178], degradation of DivIVA would represent a significant new role for ClpYQ. MinD, also a negative regulator of the divisome Z-ring, is observed to significantly increase in abundance in the *ΔclpP* deletion and in two of three replicates upon treatment with **1**. As MinD is a known substrate of ClpXP in the Gram-negative *E. coli*[98,170], our proteomics would suggest MinD may similarly be a substrate of ClpXP in *B. subtilis*. Since both *divIVA* and the *min* operon are constitutively expressed with low transcript levels[179], their increases in abundance are likely due to decreased proteolysis as a result of the deletion or inhibition of ClpXP and ClpYQ. Additionally, the loss of regulation of each of these critical cell division proteins have been shown to have detrimental consequences in bacteria. The overexpression of FtsZ inhibits cell division in *E. coli*[180–183], the overexpression of DivIVA is not viable in *B. subtilis*[184], and elevated levels of MinD in the presence of MinC results in inhibition of cell division[175,185]. Given that each of these key cell division proteins are reportedly degraded by ClpXP, it follows suit that all increase in abundance upon treatment with **1** in *B. subtilis*.

In addition to the divisome, there appears to be dysregulation of the elongasome complex responsible for peptidoglycan hydrolysis and synthesis along the cell axis allowing for cylindrical growth in rod-shaped bacteria[186] (**Figure 3.6**; **Table S4** in **Appendix II**). Given that both the elongasome and divisome function through a complex of extracellular and integral

membrane proteins scaffolded to a cytosolic polymer to remodel peptidoglycan, they are thought to be evolutionarily related complexes[186]. Thus, both these complexes may share similar patterns of regulation.

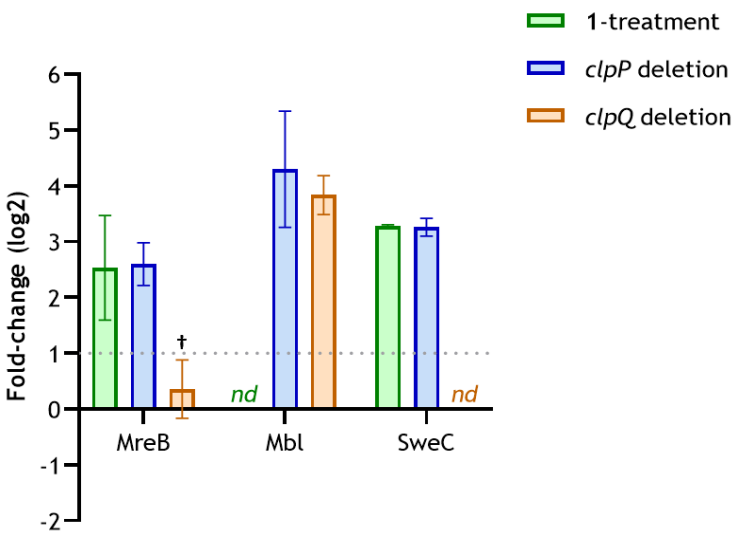

Figure 3.6. Elongasome-related protein abundances. Effects on *B. subtilis* elongasome protein abundances according to treatment versus wild-type. *nd,* not detected; †not significant; ‡not significant, detected in two of three replicates.

The cytosolic MreB polymer – and homologs Mbl and MreBH – scaffold the proteins of the elongasome complex[187–194]. MreB significantly increases in abundance upon treatment with **1** and in the *ΔclpP* deletion. Additionally, the *ΔclpP* deletion and the *ΔclpQ* deletion both show a significant increase in the MreB homolog, Mbl. These data suggest a new role for the ClpXP and ClpYQ proteases in the regulation of the elongasome. MreB is constitutively expressed suggesting the increase in abundance is due to decreased proteolysis[179]. Furthermore, the overexpression of MreB has been shown to be lethal in *B. subtilis*[194–197]. SweC is also observed to significantly increase in abundance upon treatment with **1** and in the *ΔclpP* deletion. SweC and SweD activate the extracellular peptidoglycan hydrolase, CwlO, which degrades the distal load bearing peptidoglycan layers[192,198]. The over-activation of CwlO due to SweC results in

weakening of peptidoglycan and ultimately cell lysis[199]. As an extracellular protein, CwlO likely evades detection in our proteomics due to limitations in the experimental setup which is biased to soluble cytosolic proteins. Thus, our proteomics data provides strong evidence that armeniaspirol arrests cell division through dysregulation of the divisome, but also weakens the cell wall through dysregulation of the elongasome. Both ClpXP and ClpYQ appear to have concerted roles in the regulation of the *B. subtilis* divisome and elongasome via proteolysis of, at minimum, principle proteins FtsZ from the divisome and MreB from the elongasome.

3.3.3 Microscopy evaluation of armeniaspirol-treated B. subtilis

We sought to examine phenotypic changes in *B. subtilis* at sub-inhibitory concentrations of **1** (½ MIC, 1 μg/mL) using confocal fluorescence microscopy. *B. subtilis* cells were stained with DAPI and FM 4-64FX to visualize the DNA and the membrane, respectively (**Figure 3.7A**). While we did not observe significant changes in cell length as might be expected with cell division inhibition, evaluation of **1**-treated *B. subtilis* compared to wild-type *B. subtilis* showed a clear and statistically significant change in nucleoid phenotype (**Figure 3.7B**). *B. subtilis* treated with **1** showed a statistically significant increase in the number of cells with separated nucleoids compared to untreated *B. subtilis*. The opposite was observed for single nucleoid containing cells in that most untreated cells appeared to display this phenotype. This data supports a mechanism involving negative regulation of cell division, whereby nucleoid replication can occur but without septation to produce daughter cells.

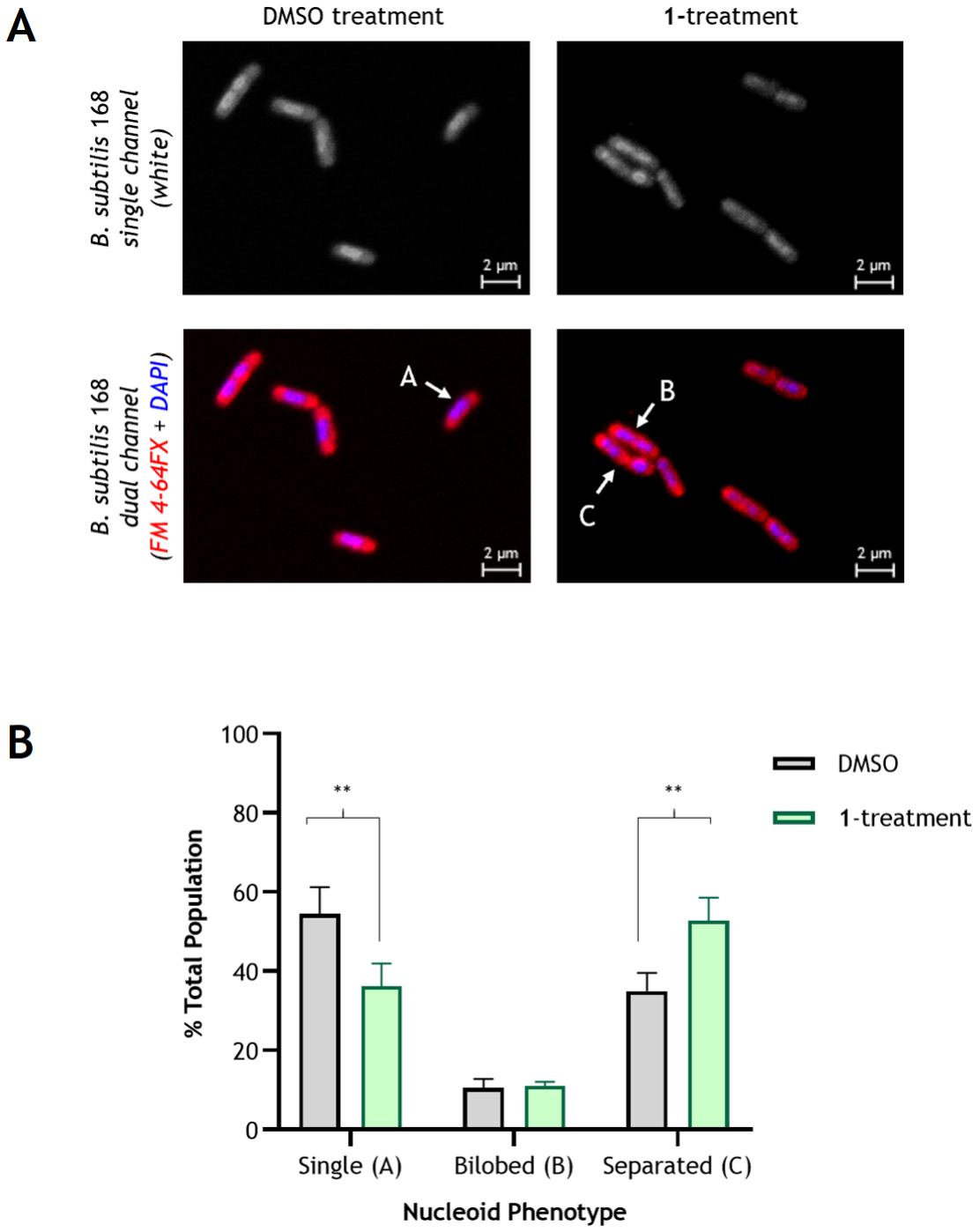

Figure 3.7. Confocal fluorescence microscopy of *B. subtilis*. (A) Micrographs of vehicle control versus **1**-treated (½ MIC, 1 µg/ml) *B. subtilis* stained with DAPI and FM 4-64FX showing representations of single nucleoids A, bilobed nucleoids B, and separated nucleoids C. (B) Septation defects were graphed according to nucleoid phenotype (biological triplicate; DMSO n=149, **1**-treatment n=157). **$p < 0.05$, statistical analysis was performed by 2-way ANOVA with Holm-Sidak's multiple comparison test.

3.4 Conclusions

3.4.1 Armeniaspirol does not appear to inhibit other AAA+ proteases

Our quantitative proteomics allows us to evaluate the selectivity of armeniaspirol towards two other bacterial AAA+ proteases, Lon and FtsH. A known substrate of the Lon protease in *B. subtilis* is SwrA, an activator of the *fla-che* operon[200,201]. Inhibition of Lon protease by **1** would lead to reduced proteolysis of SwrA and increased abundance of proteins encoded by the *fla-che* operon. Two of these detected proteins, CheA and CheC, are instead observed to decrease in abundance by 3.6- and 9.3-fold with p-values of 0.03 and 0.0007, respectively. FtsH is a membrane-bound metalloprotease that degrades EzrA, a negative regulator of cell division[202]. If FtsH were inhibited by **1**, there would be an increase in abundance of EzrA. Instead, our quantitative proteomics shows EzrA abundance decreased significantly (23-fold) with a p-value of 0.01. Thus, based on these results it does not appear as though armeniaspirol inhibits the other AAA+ proteases.

3.4.2 Armeniaspirol-treatment displays enrichment of known ClpXP substrates

We hypothesized initially that ClpXP inhibition by **1** should lead to several of its protein substrates to be enriched in the proteome due to decreased proteolysis. Fortunately, many of these proteins have been proposed or directly identified in the literature[97,98,170,171,203]. In support of our findings, examination of our **1**-treated *B. subtilis* quantitative proteomics showed a biologically and statistically significant enrichment (fold-change >2, p-value <0.05) of at least nine known or suspected protein substrates of ClpXP, including the aforementioned divisome-related proteins DnaK, FtsZ, GroEL, and Tig (**Figure 3.8**; **Table S5** in **Appendix II**). This overlap in proteomic profiles supports ClpXP as a target of **1**.

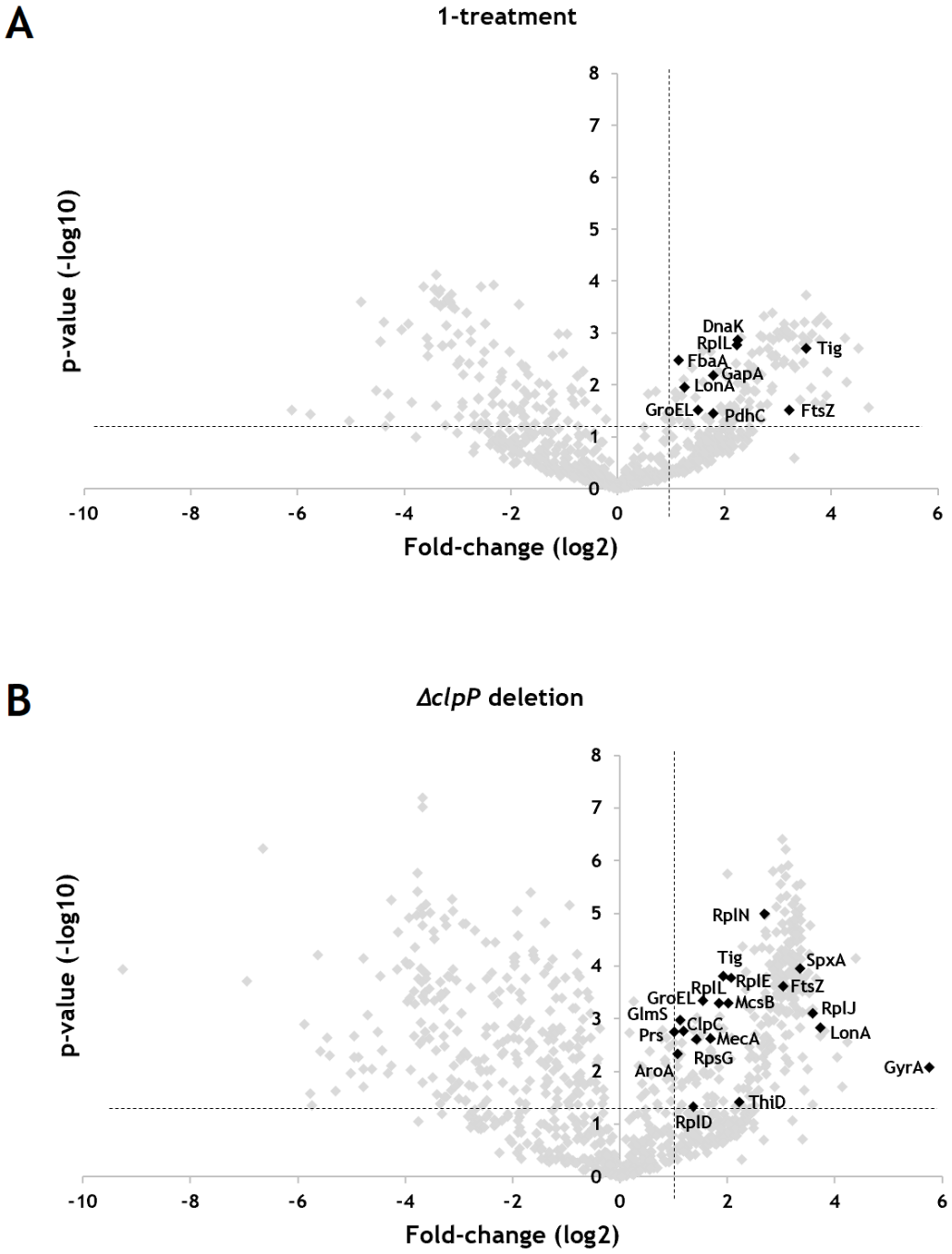

Figure 3.8. Enrichment of known ClpXP substrates. Several substrate proteins of ClpXP show a statistically and biologically significant increase in abundance in (A) **1**-treated and (B) *ΔclpP* deletion *B. subtilis*, supporting a mechanism involving inhibition of ClpXP. Biological and statistical significance is defined as fold-change >2 and p-value <0.05, respectively.

3.4.3 Discussion of other observed proteomic trends

Our quantitative proteomics showed a significant increase in abundance of translation-related proteins upon treatment with **1**. The increase in proteins of the large and small ribosome subunits L12, L13, S4, S11, and S13 suggest a disruption of ribosome assembly[204]. The ribosome checkpoint GTPases Obg and RgbA are also significantly increased in abundance, and in the presence of elevated guanosine pentaphosphate or tetraphosphate, (p)ppGpp, from the stringent response are known to inhibit ribosome assembly[205]. However, if ribosome assembly was directly perturbed by treatment with **1**, we would expect synergy with the protein biosynthesis inhibitor tetracycline. Instead, our data shows that **1** and tetracycline are indifferent with an FIC >0.5 (**Figure 3.3**; **Table 3.2**). We propose this is a general, indirect effect of protease inhibition. The stringent response, which is initiated by an increase in uncharged tRNA[206], presumably due to the decrease in proteolysis, is well known to inhibit protein synthesis until sufficient charged tRNAs are available[207]. Supporting a stringent response is the increase in abundance of several aminoacyl-tRNA synthetases, and the observation that many of the most abundant *B. subtilis* proteins show an increased abundance upon treatment with **1**, reducing the available amino acid pool. Thus, while several factors suggest a perturbation of translation by **1**, this is likely an indirect effect of inhibition of ClpXP and ClpYQ via the stringent response.

Our quantitative proteomics also show six iron transport proteins significantly increase in abundance in the **1**-treatment. The elemental iron transporter EfeO, the Fe-citrate transporter YfmC, and the siderophore transporters YclQ, FhuD, YfiY, FeuA are all increased. While upregulation of the genes encoding these proteins is typical of iron limitation[208], there is a high coincidence of gene regulation between iron limitation and the stringent response[209], suggesting that this may also be an indirect effect of **1**-treatment via the stringent response.

3.4.4 Revisiting captured biochemical targets

Our quantitative proteomics data allows us to re-examine and thoroughly evaluate the other captured biochemical targets obtained from ABPP in Chapter Two (**Figure 2.4**) as antibiotic candidates:

Firstly, ArgS and TufA, are the only essential proteins pulled down in the inhibitor capture[210] (**Table S2**). ArgS is an aminoacyl-tRNA synthetase that combines the amino acid arginine with its corresponding tRNA, while TufA is responsible for promoting the binding of aminoacyl-tRNAs to ribosomes[211,212]. Thus, both proteins are intimately associated with translation and protein biosynthesis. However, since **1** does not display synergy with the protein biosynthesis inhibitor tetracycline, we hypothesized that these are not key targets resulting in the antibiotic activity of armeniaspirol.

HemH, MtrB, and BslA each showed a significantly high abundance at around 10-fold enrichment (**Table S2**). However, none of these proteins encoded by non-essential genes appear to possess an obvious mechanism for antibiotic activity. HemH is a ferrochelatase whose mammalian ortholog has been observed as an off-target binder of small molecule kinase inhibitors in similar chemical proteomics experiments[213]. Thus, we expect this to be the case here as well. MtrB regulates *B. subtilis* expression of the tryptophan biosynthesis operon[214]. Inhibition of MtrB by the protein RtpA leads to higher levels of TrpE expression and activity[215]. If **1** were inhibiting MtrB, we would expect to see a similar response in our quantitative proteomics, yet we do not observe a statistically significant increase in TrpE. BslA is an extracellular hydrophobin protein that coats *B. subtilis* biofilms. The hydrophobic nature of BslA can potentially interact with our probe, resulting in non-covalent capture, and thus ruling it out as a true direct biochemical target[216].

Six proteins were enriched at slightly lower abundances: YtjP (6.4-fold), YmaD (5.7-fold), PtsI (4.7-fold), SodA (3.4-fold), PatB (3.4-fold), and SdhA (2.0-fold) (**Table S2**). YtjP is an uncharacterized metalloprotease[116]. A *S. aureus* ortholog with 42% identity contains an exposed cysteine residue that could potentially react with the electrophilic center of the probe[217]. Similarly, YmaD is a peroxiredoxin that has a hydrophobic binding cavity containing a nucleophilic cysteine residue[218]. SdhA is also a cysteine-rich protein that may result in capture by the probe. Additionally, PtsI and SodA are two of the most abundant proteins in the *B. subtilis* proteome which may lead to non-selective capture with the probe[131]. Lastly, PatB is a cystathionine-β-lyase involved in methionine biosynthesis and can be inhibited by cysteine alkylation with N-ethylmaleimide[219,220]. However, this inhibition is not implicated in any antibiotic activity[221]. Thus while these proteins can not be definitively eliminated as potential direct biochemical targets, they are all encoded by non-essential genes and do not provide a reasonable avenue to explain antibiotic activity.

3.4.5 Summarizing antibiotic potential

The importance of the divisome in bacterial cell division has made it a considerably attractive target for antibiotic development. Specifically, there has been increased focus on the discovery of compounds targeting the essential and highly conserved bacterial divisome protein, FtsZ, to achieve broad-spectrum antibiotic activity[222]. Several natural products and synthetic compounds have been identified that directly perturb the dynamics of FtsZ assembly and disassembly, modulate GTPase activity, or indirectly activate proteolysis[222,223]. However, while potent *in vitro* and *in vivo* inhibitors have been discovered, even the most pharmacologically promising compounds suffer from spontaneous amino acid mutations in FtsZ leading to rapid antibiotic resistance[223]. Given that laboratory selection efforts have failed to generate

armeniaspirol-resistant strains[110], the inhibition of AAA+ proteases ClpXP and ClpYQ to dysregulate the divisome and elongasome represents a potentially novel and promising mechanism to target bacterial cell division.

3.5 Contributions

LC-MS/MS for dimethyl labeling proteomics was performed by Zoran Minic, Ph.D. of the John L. Holmes Mass Spectrometry Facility, University of Ottawa.

CHAPTER FOUR:
Antibiotic Development of Armeniaspirol-inspired Synthetic Analogs

4.1 Introduction

4.1.1 Evaluating armeniaspirol as a drug development candidate

Natural products remain the greatest source for new and clinically valuable antibiotics. While synthetic compounds such as fluoroquinolones have been successful in treating infectious disease, large-scale synthetic screening campaigns have failed to yield fruitful candidates for antibiotic development[33,224]. Synthetic compounds tend to be poor representations of the complex chemical space of natural product antibiotics[225]. Instead, synthetic and semisynthetic approaches to modify existing natural product antibiotic scaffolds remains a widely used approach to improve antibiotic potency and pharmacology as well as temporarily outpace resistance mechanisms. For example, semisynthetic antibiotics such as the penicillin-derived ampicillin[226] and erythromycin-derived azithromycin[227] are of important clinical value.

The armeniaspirols represent a promising lead scaffold for antibiotic development given its novel mechanism of action and lack of detectable resistance. In fact, preliminary *in vivo* efficacy assessments of armeniaspirol A were previously performed in MRSA-induced septicemia mouse models. An intravenous dose of 15 mg/kg resulted in 4 out of 6 mice surviving infection[110]. However, complete eradication of infection could not be achieved and higher doses resulted in cardiac side-effects[110]. By comparison, a 20 mg/kg dose of vancomycin in the MRSA-induced septicemia mouse models resulted in 100% survival[110]. Thus, while armeniaspirol exhibits moderate *in vivo* efficacy, there is a need to pursue and evaluate derivatives with improved pharmacology before being considered clinically viable.

A semisynthetic chemical derivation program was originally initiated by Sanofi following their discovery of the armeniaspirols. Three derivatives, **4.1**, **4.2**, and **4.3**, were generated directly from armeniaspirol A with various nucleophilic substitutions (isopropyl amine, pyridine-4-yl-methylamine, and 2-diethylamino–ethanethiol) at the activated β-position of the unsaturated lactame[110] (**Figure 4.1**). None of these compounds displayed improved antibacterial activities compared to the parent compound, though exact data was not reported. Additionally, a fourth semisynthetic derivative, **4.4**, was generated through halogenation on the phenol ring[110] (**Figure 4.1**). Familiarly, this compound displayed improved antibacterial activity and served as inspiration for total synthesis of **1** for our mechanism of action study.

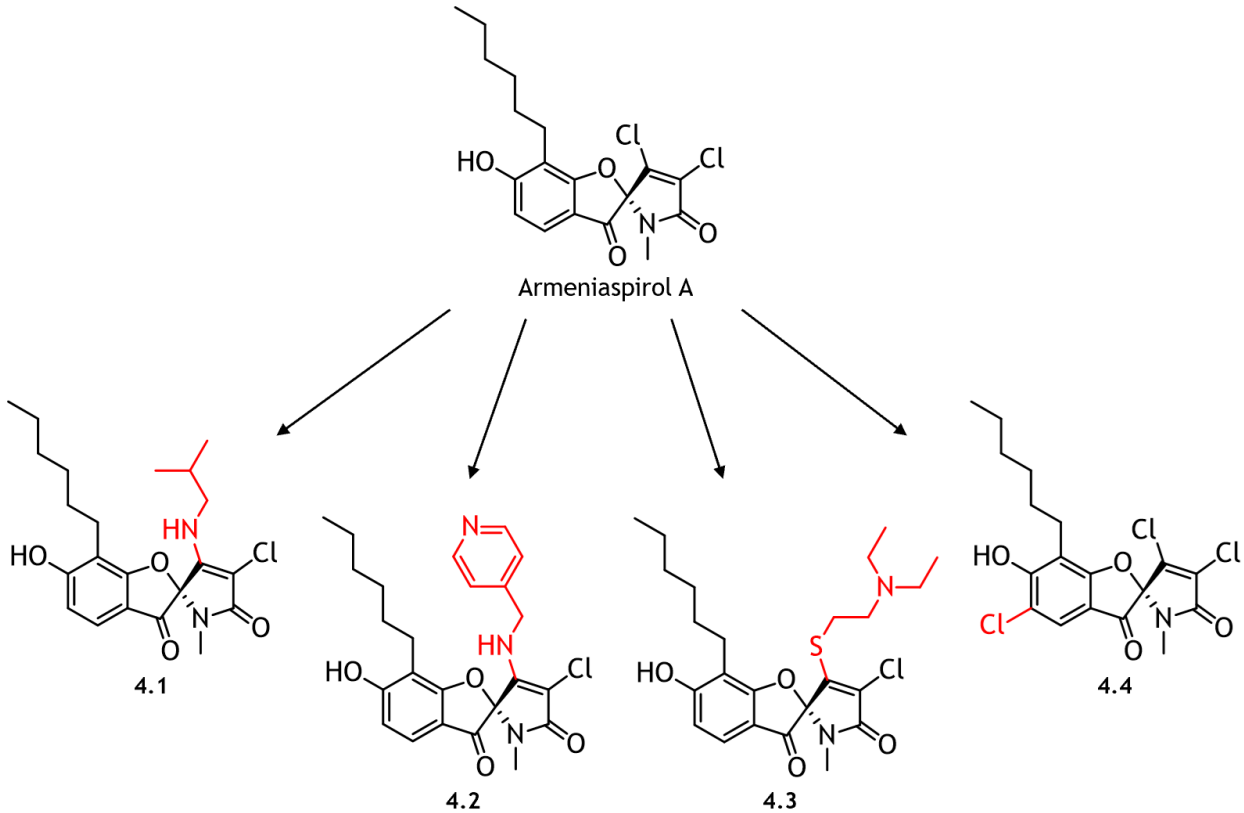

Figure 4.1. Armeniaspirol A semisynthetic derivatives. Three armeniaspirol A semisynthetic derivatives were generated by Sanofi with emphasis on substitution at the activated β-position of the unsaturated lactame. A fourth derivative with a chlorine substitution *ortho* to the phenolic alcohol, resulting in 5-chloro-armeniaspirol, was the only derivative to display antibacterial activity.

Our supplementary structure-activity relationship discussed in Section 2.2.2 revealed that modification to the N-methyl of armeniaspirol is well tolerated and retains antibiotic activity in *B. subtilis*. Importantly, our study also indicated that the aromatic alcohol is essential for antibiotic activity. Herein, we conduct initial studies of lead compound optimization of armeniaspirol in the early drug development process by modifying the alkyl-containing groups of armeniaspirol, R_1 and R_2 (**Figure 4.2**).

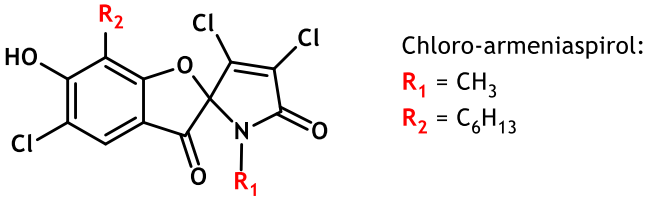

Figure 4.2. Sites of modification for synthesis of armeniaspirol analogs. First-generation analogs are exclusively focused to R_1 position, while second-generation analogs are constructed with additional modification to R_2.

4.1.2 First- and second-generation armeniaspirol analogs

First-generation analogs represent bioisosteres of armeniaspirol at the N-methyl position (**Figure 4.3**). **MD01** and **MD02** are extensions of the N-methyl group in armeniaspirol to hexyl and dodecyl alkyl chains, respectively. These two modifications introduce a non-polar side chain in addition to the hexyl group already present on the resorcinol ring of armeniaspirol. As seen with **1.3** (equivalent to **MD01**) from our SAR (Chapter Two), there is four-fold improved antibiotic activity in *B. subtilis* upon extension of this alkyl chain (MIC of 0.5 μg/mL for **1.3** versus MIC of 2 μg/mL for **1**). Thus, the primary aim of **MD02** is to investigate if extending the alkyl chain even further leads to a positive correlation with antibiotic activity. **MD03** is functionalized with a terminal alkene, a relatively simple functional group seen in some biologically active polyketides such as chrysomycin[228], curacin A[229], haliangicin[230], jamaicamide C[231], and tautomycetin[232,233]. Notably, the addition of a terminal alkene functional group in an

exhaustive SAR study to produce the synthetic epothilone analog sagopilone resulted in significant anti-cancer activity leading to clinical development[234,235]. Finally, **MD04** and **MD05** incorporate benzyl and benzyl-*p*-CF_3 on the nitrogen, respectively, in order to include electronic and steric diversity. In summary, the goal of the first-generation analogs is to identify modifications at the N-methyl that may provide improvements to the pharmacophore of armeniaspirol.

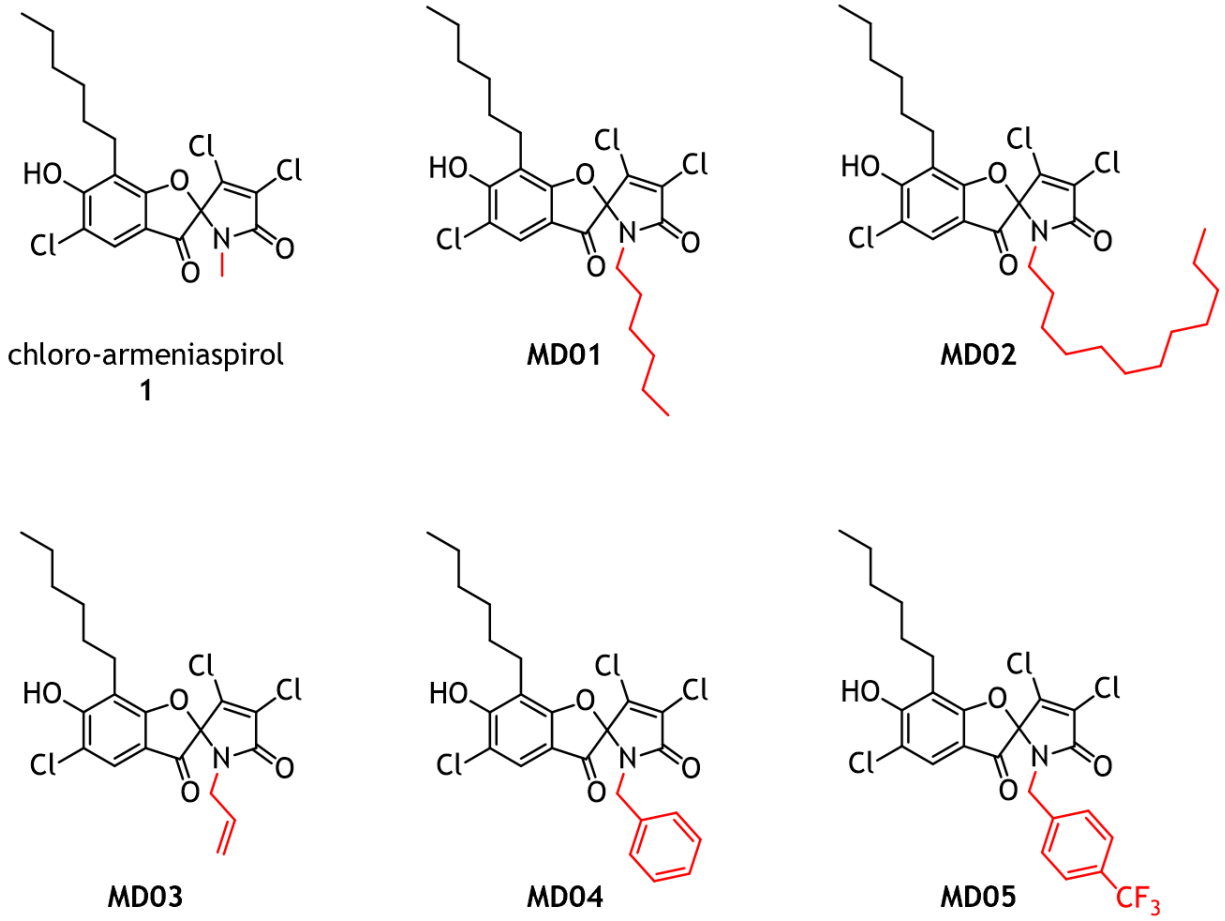

Figure 4.3. First-generation analogs of armeniaspirol. Analogs were designed exclusively with substitutions of the methyl group on the nitrogen of armeniaspirol, highlighted in red.

In addition to the spiro-[4.4]non-8-ene core scaffold of armeniaspirol, the hexyl side chain of the resorcinol ring is a unique feature of armeniaspirol biosynthesis[108]. Thus, to

determine if it plays a role in modulating antibiotic activity, we generated second-generation analogs with the hexyl chain shortened to a methyl. The same array of functional groups on the N-methyl selected in the first-generation analogs were included in the second-generation analogs (**Figure 4.4**). Thus, **MD06** retains the most similarity to armeniaspirol with a methyl group at R_1, while **MD07** represents a swap of the R_1 and R_2 alkyl chains found in native armeniaspirol.

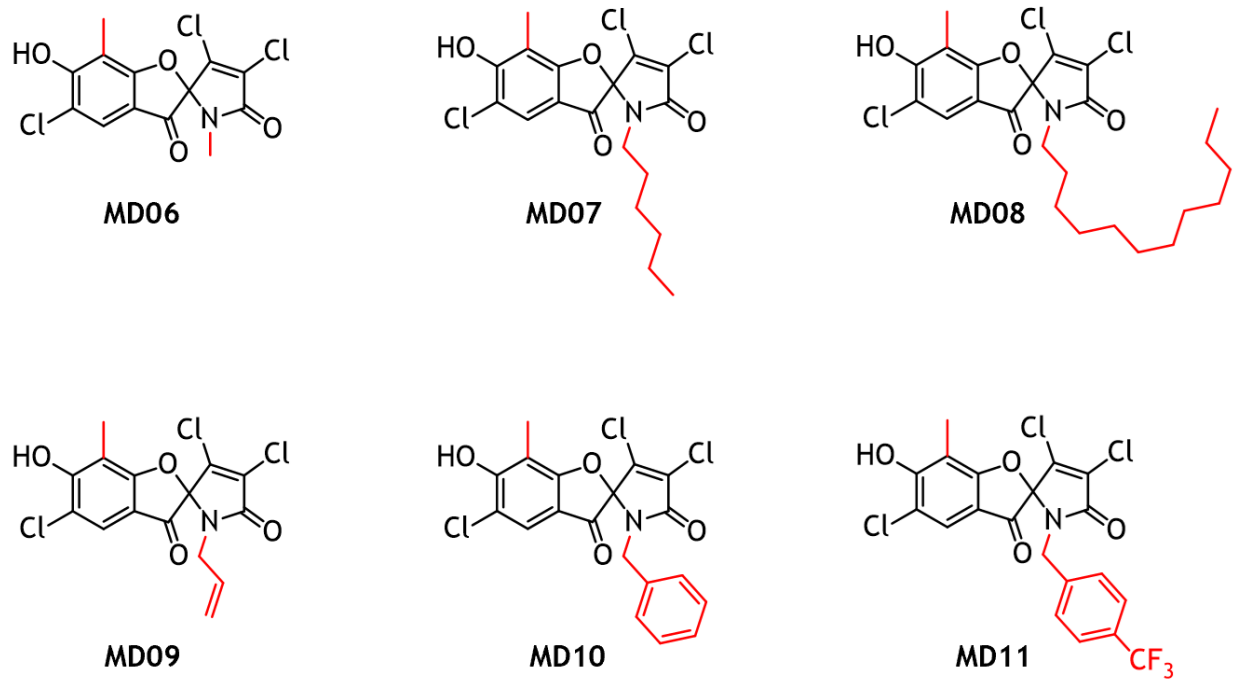

Figure 4.4. Second-generation analogs of armeniaspirol. Analogs were designed exclusively with substitutions of the methyl group on the nitrogen of armeniaspirol and a shortened alkyl chain on the resorcinol ring, highlighted in red.

4.2 Evaluation of armeniaspirol analogs

4.2.1 Minimum inhibitory concentration evaluation of analogs

The evaluation of antibiotic activity of armeniaspirol analogs was accomplished using MIC screens against a panel of clinically relevant Gram-positive pathogens including virulent MRSA strains predominantly responsible for hospital- and community-acquired infections[236], as well as the high-priority pathogen VRE (**Table 4.1**). MIC assays were also performed on a

Gram-negative pathogen, *P. aeruginosa*, to determine if any analogs resulted in broad spectrum antibiotic activity. However, none of the eleven analogs synthesized were active against *P. aeruginosa* (all MICs >32 μg/mL). Except for **MD02**, all first-generation analogs possess comparable or improved antibiotic activity towards the clinical isolates of MRSA. This may be a result of the very hydrophobic dodecyl chain of **MD02** impairing ability for the compound to penetrate the bacterial cell wall. Furthermore, **MD03** did not appear to play a role in altering antibiotic activity, displaying the same MIC as **1**. Interestingly, **MD04** and **MD05** both resulted in approximately four-fold improved antibiotic activity with MICs of 1 μg/mL. As observed with **1**, all first-generation analogs displayed bacteriostatic activity with minimum bactericidal concentrations greater than 4X the MIC (**Table S6** in **Appendix III**).

In contrast, the second-generation analogs exhibited mostly poor antibiotic activities. **MD06**, **MD09**, and **MD10** all displayed MICs ≥32 μg/mL. **MD07** and **MD08** displayed only comparable or marginally improved antibiotic activity compared to **1**. Like **MD02**, **MD08** also possesses a long hydrophobic dodecyl chain, yet unlike **MD02**, **MD08** exhibits decent antibiotic activity. Despite this extended hydrophobic alkyl chain, the shortened alkyl chain on the resorcinol ring likely reduces overall hydrophobic character and allows it to penetrate into the bacteria. Notably, these are the only two second-generation analogs of the six that retain any long alkyl chain functional group at all, suggesting it is a necessary feature for armeniaspirol antibiotic activity. Furthermore, **MD08** was observed to be bactericidal (**Table S6** in **Appendix III**), differentiating it from all other compounds and thus warranting further assessment along with **MD01** and **MD04**.

Table 4.1. MIC (μg/mL) evaluation of first and second armeniaspirol analogs. Analogs were screened for antibiotic activity against clinically relevant Gram-positive and Gram-negative pathogens. MICs were performed in triplicate (n = 3).

Compound	*S. aureus* IA116-USA100 (MRSA)	*S. aureus* MN8-USA200 (MSSA)	*S. aureus* LAC-Fitz-USA300 (MRSA)	*S. aureus* MW2-USA400 (MRSA)	*E. faecalis* NJ3 (VRE)	*P. aeruginosa* PA01
1	4	4	4	4	8	>32
MD01	1	1	1	1	2	>32
MD02	8	16	16	8	8	>32
MD03	4	4	4	4	8	>32
MD04	1	1	1	2	2	>32
MD05	2	2	2	2	2	>32
MD06	>32	>32	>32	>32	>32	>32
MD07	4	4	4	8	8	>32
MD08	2	2	1	2	0.5	>32
MD09	>32	>32	>32	>32	>32	>32
MD10	>32	>32	>32	32	>32	>32
MD11	16	16	16	16	32	>32

4.2.2 Preliminary ClpYQ inhibition and kinetic evaluation of analogs

The two most potent analogs determined by MIC assays, **MD01** and **MD04**, were selected for *in vitro* evaluation. Inhibition kinetics were performed on Gram-positive *B. subtilis* ClpYQ protease activity to determine if improved antibiotic activity was a direct consequence of improved protease inhibition. A clear dose response was observed with both compounds (**Figure 4.5**). Addition of **MD01** displayed protease inhibition for ClpYQ with an IC_{50} of 6.1 ± 1.0 μM, while **MD04** displayed protease inhibition for ClpYQ with an IC_{50} of 2.1 ± 1.0 μM. Under equivalent assay conditions, these are both improvements in inhibition of ClpYQ from **1** which has an IC_{50} of 13.6 ± 1.0 μM.

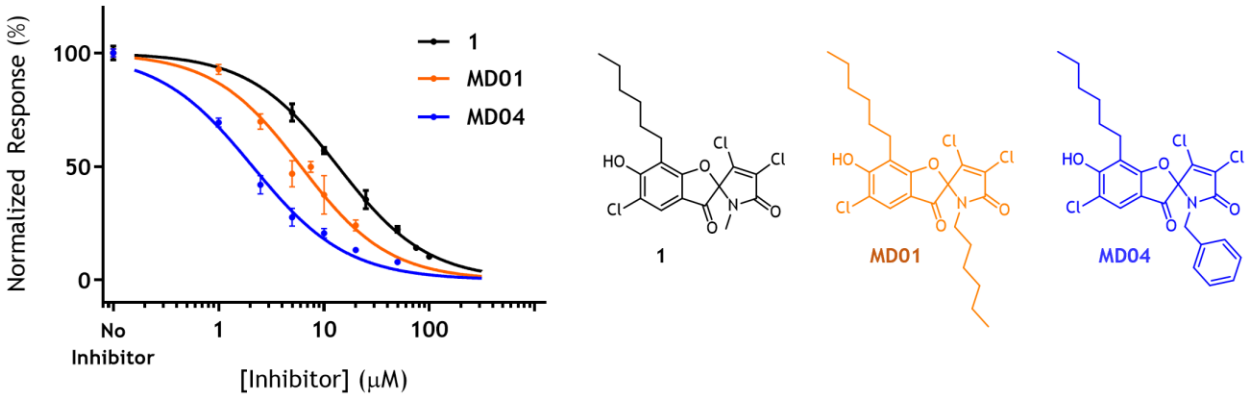

Figure 4.5. IC_{50} curves of ClpYQ proteolysis with MD01 and MD04. **1** inhibits ClpYQ with an IC_{50} of 13.6 μM with 0.1 mM Cbz-Gly-Gly-Leu-AMC, comparable to the IC_{50} determined in Section 2.3.2. **MD01** and **MD04** inhibit ClpYQ with an IC_{50} of 6.1 μM and 2.1 μM, respectively. Each data point is collected in triplicate (n = 3).

Given that the mode of action of armeniaspirol was previously determined (Chapter Two) to be competitive inhibitor of ClpYQ proteolysis activity, we applied the Cheng-Prusoff alteration to the Dixon plot to determine K_i values (**Figure S9** in **Appendix III**):

Compound	IC_{50} (μM)	Experimental K_i (μM)
1	13.6 ± 1.0	6.4
MD01	6.1 ± 1.0	2.6
MD04	2.1 ± 1.0	1.5

The K_i values for both **MD01** and **MD04** are lower than **1**, indicating a greater affinity for inhibitor towards the ClpYQ protease. Thus, these two compounds displaying improved antibiotic activity also observe greater inhibition of ClpYQ proteolysis *in vitro*, suggesting a direct correlation. We also selected **MD08** for *in vitro* evaluation given its improved antibiotic activity and surprising bactericidal activity (**Figure 4.6**). **MD08** appears to inhibit ClpYQ protease activity with an IC_{50} of 11.0 ± 1.0 μM, though we observe an unexpectedly steep dose-response curve with a Hill coefficient of -4.5.

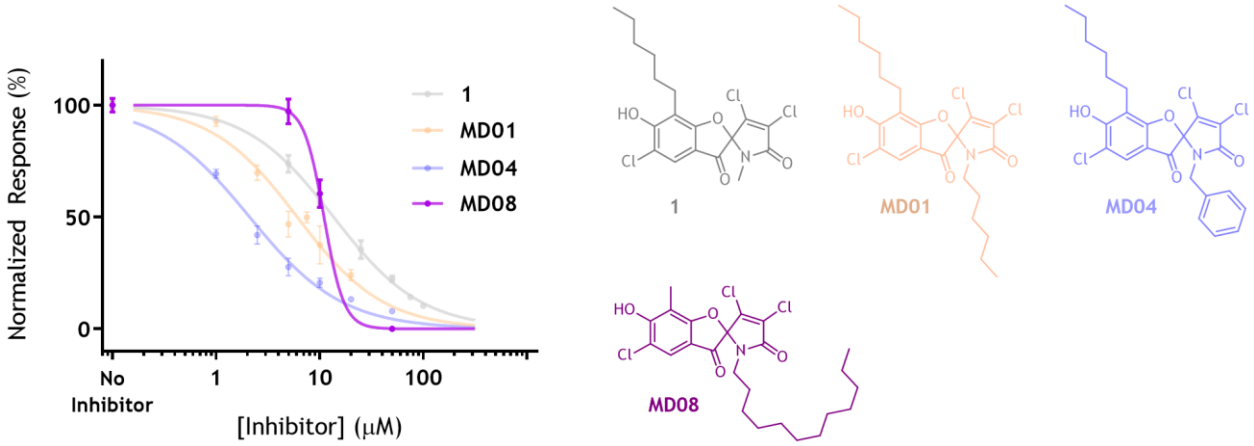

Figure 4.6. IC_{50} curve of ClpYQ proteolysis with MD08. **1** inhibits ClpYQ with an IC_{50} of 13.6 μM with 0.1 mM Cbz-Gly-Gly-Leu-AMC, comparable to the IC_{50} determined in Section 2.3.2. **MD08** inhibits ClpYQ with an IC_{50} of 11.0 μM and a Hill slope of -4.5. Each data point is collected in triplicate (n = 3).

One possible explanation for this steep dose-response curve is cooperative binding[237,238], where initial binding of inhibitor influences subsequent binding of inhibitors to active sites of the ClpQ multimer. However, this mechanism seems unlikely given that it has not been observed for any other analog of **1**, all of which maintain the same core scaffold. Instead, the steep IC_{50} curve is more likely a function of stoichiometric inhibition caused by an enzyme concentration higher than the K_i of a competitive inhibitor[239,240]. Most enzyme systems, including Michaelis-Menten kinetics, operate under the assumption that enzyme concentration is very small and therefore the concentration of enzyme-inhibitor complex is negligible[239]. However, in cases where enzyme concentration is large, or K_i is very small as is the case with potent inhibitors, then the enzyme-inhibitor complex is no longer insignificant and inhibition is dependent on enzyme concentration[239,240]. A dose-response curve thus shows increasingly steeper slopes with increasing enzyme concentration[240]. Our standard assays were performed with 0.25 μM of purified ClpQ and ClpY and thus we should expect the true K_i value for **MD08** to be below this concentration. We can test this experimentally by decreasing the amount of enzyme in our assay. By dropping the ClpQ and ClpY concentration to 0.1 μM, we observe a prominent decrease in

the steepness of the slope with a Hill coefficient of -1.4 and an IC_{50} of 2.8 ± 1.1 μM (**Figure 4.7**). Decreasing the enzyme concentration even further to achieve a Hill coefficient of -1 will likely result in a lower IC_{50} and allow us to obtain a true K_i that is significantly lower than both **MD01** and **MD04**. Currently, this data is expected to be collected in the very near future.

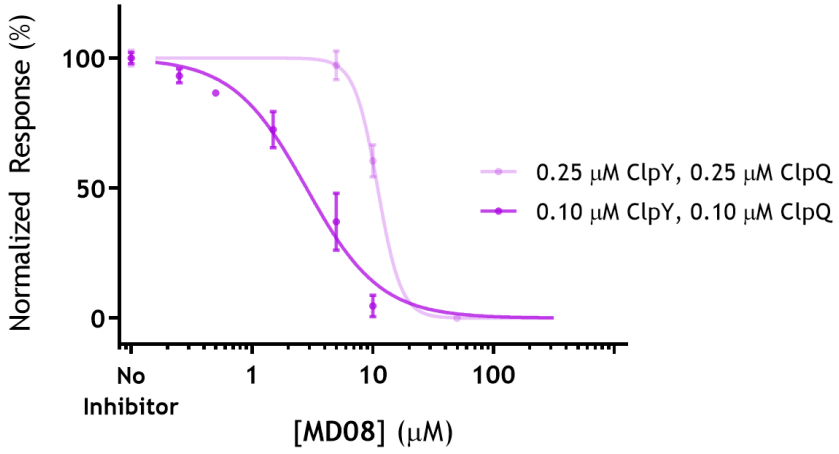

Figure 4.7. Stoichiometric inhibition: enzyme to K_i ratio. At 0.25 μM ClpYQ, **MD08** inhibits ClpYQ at an IC_{50} of 11.0 μM and a Hill slope of -4.5. At At 0.10 μM ClpYQ, **MD08** inhibits ClpYQ at an IC_{50} of 2.8 μM and a Hill slope of -1.4. Each data point was collected in triplicate (n = 3).

4.3 Conclusions

4.3.1 Armeniaspirol analogs display promising antibiotic activity

In summary, most first-generation analogs displayed comparable or improved antibiotic activity in comparison to **1**. Specifically, the first-generation analogs **MD01** and **MD04** both resulted in improved antibiotic activity and *in vitro* inhibition of the *B. subtilis* ClpYQ protease as compared to **1**. Meanwhile, the second-generation analog **MD08** showed only two-fold improved antibiotic activity in MRSA but appears to be the best inhibitor of the ClpYQ protease. Uniquely, **MD08** is also the only analog to have bactericidal activity. Examination of the first- and second-generation analogs revealed that armeniaspirol requires an extended alkyl chain to retain appreciable antibiotic activity either at the R_1 or R_2 position. However, this only holds true

to an extent as exemplified with **MD02**, which is fitted with a dodecyl chain at R_1 and a hexyl chain at R_2 but has poor antibiotic activity with MICs ≥ 8 μg/mL. Thus, we have identified three compounds for further *in vivo* characterization and drug development.

4.3.2 Limitations of Gram-positive ClpXP evaluation

The mechanism of action of armeniaspirol is predicated on the dual inhibition of ClpYQ and ClpXP proteases in Gram-positive bacteria. Thus, it is imperative that we characterize inhibition of both proteases with our analogs. We previously deferred to the Gram-negative *E. coli* ClpXP for the purposes of characterizing its mechanism of action. However, for lead optimization in the development of a Gram-positive antibiotic, tailoring armeniaspirol derivatives to this Gram-negative system is less sensible. Unfortunately, every attempt to recover activity from a Gram-positive ClpXP protease has thus far proven unsuccessful. Purified His-tagged *B. subtilis* ClpX and ClpP resulted in only single turnover of fluorogenic substrate as previously mentioned, and His-tagged *S. aureus* ClpX and ClpP was completely inactive in our proteolytic biochemical assays (data not shown).

However, another approach based on urease activity, provides a possible means for evaluating ClpXP inhibition in Gram-positive bacteria. Two genomic-based studies analyzing the transcriptional profiles of ClpX and ClpP deletions in *S. aureus* were previously reported[241,242]. A genomic-based comparison between wild-type *S. aureus* and *S. aureus* expressing an inactive ClpX mutant (I265E), revealed significant upregulation of genes in the urease operon *ureABCEFGHD*[241]. The induction of this operon was similarly identified in the transcriptional profile of a *S. aureus ΔclpP* deletion strain, and a high urease activity was observed using a commercial analytical profile index (API) test strip assay[242]. Together, this data strongly suggests ClpXP inhibition leads to increased urease activity, though the exact reason for

this consistent increase in urease activity in ClpXP-deficient *S. aureus* is uncertain. Notably, induction of the *ureABC* operon was not observed according to our *B. subtilis* quantitative proteomics. However, we proceeded to assay urease activity in *S. aureus* using Christensen media, which is supplemented with phenol red pH indicator[243]. Christensen media was originally formulated to evaluate urea decomposition for rapid diagnosis of enteric bacteria[243]. Hydrolysis of urea leads to production of ammonia and an increase in pH, which is responsible for a deep red colour change to the media. Alternatively, the absence of urease activity results in a culture that is yellow in colour at pH ≤ 6.8, within the optimal range for most bacterial growth. This colour difference provides a mechanism to evaluate urease activity in *S. aureus*, specifically as it relates to ClpXP inhibition. Specifically, in the presence of a ClpXP inhibitor, induced expression of the urease operon in *S. aureus* should lead to hydrolysis of urea and a red colour change in the media. Promisingly, this experimental rationale has been justified recently in *S. aureus* with a non-competitive small molecule inhibitor of ClpP[244]. Thus, we performed an identical liquid culture screen with MRSA USA300 in the presence or absence of a sub-inhibitory concentration of **1** (1 μg/ml – ¼ the MIC) (**Figure S10** in **Appendix III**). We observed a distinct colour change from yellow (in the absence of **1**) to pink (in the presence of **1**), proving urease activity and likely demonstrating ClpXP inhibition. This initial data provides groundwork for a promising alternative to evaluate ClpXP activity in response to our armeniaspirol analogs in *S. aureus.* Ideally, at a steady sub-inhibitory concentration for each analog, we hope to observe differences in colour intensity from yellow to orange to pink to red for our analogs ranging from poor antibiotic activity to potent antibiotic activity, respectively. Further optimization of this assay may also enable us to obtain a dose response for each analog,

whereby increasing inhibitor concentration leads to an increase in intensity of colour change. Currently, this data is expected to be collected in the very near future.

4.4 Contributions

The syntheses for chloro-armeniaspirol analogs **MD01-MD11** were performed by Michael Darnowski, Ph.D. candidate, University of Ottawa. MIC and MBC assays were performed in collaboration with Michael Darnowski, Ph.D. candidate, University of Ottawa and Claudia Natola, M.Sc. student, University of Ottawa.

CHAPTER FIVE:
Characterization of the ClpYQ Degradome

5.1 Introduction: unnatural amino acid incorporation

5.1.1 Expanding the genetic code in E. coli

The ability to encode an unnatural amino acid into a protein during translation enables incorporation of useful biochemical functional groups that can be used to modulate protein activity or characterize protein function[245]. For example, post-translationally modified amino acids, photocaged amino acids, and various label- or probe-derivatized amino acids have been successfully encoded into proteins to obtain new insights into biological processes and interactions[246]. This revolutionary development in synthetic biology is facilitated by two components that manipulate the genetic code and protein translation: (1) an evolved orthogonal tRNA/aminoacyl-tRNA synthetase (aaRS) pair, and (2) a cognate codon for specific incorporation during translation[247]. The aaRS charges its orthogonal tRNA with the unnatural amino acid, which is recognized by the ribosome in response to the site-directed placement of its cognate codon in mRNA (**Figure 5.1**). The amber stop codon, UAG, for unnatural amino acid incorporation in *E. coli* has been most widely used with great efficiency given its rare usage in the genome[247]. Two orthogonal $tRNA_{CUA}$/aaRS pairs have been evolved for amino acid incorporation in *E. coli* including the $tRNA_{CUA}$/tyrosyl-tRNA synthetase (TyrRS) from the archaebacterium *Methanococcus jannaschii*[248] and the $tRNA_{CUA}$/pyrrolysyl-tRNA synthetase (PylRS) from the archaebacterium *Methanosarcina barkeri*[249–251]. Considerable progress has since been made to expand the versatility of these orthogonal pairs in incorporating various unnatural amino acids in *E. coli*.

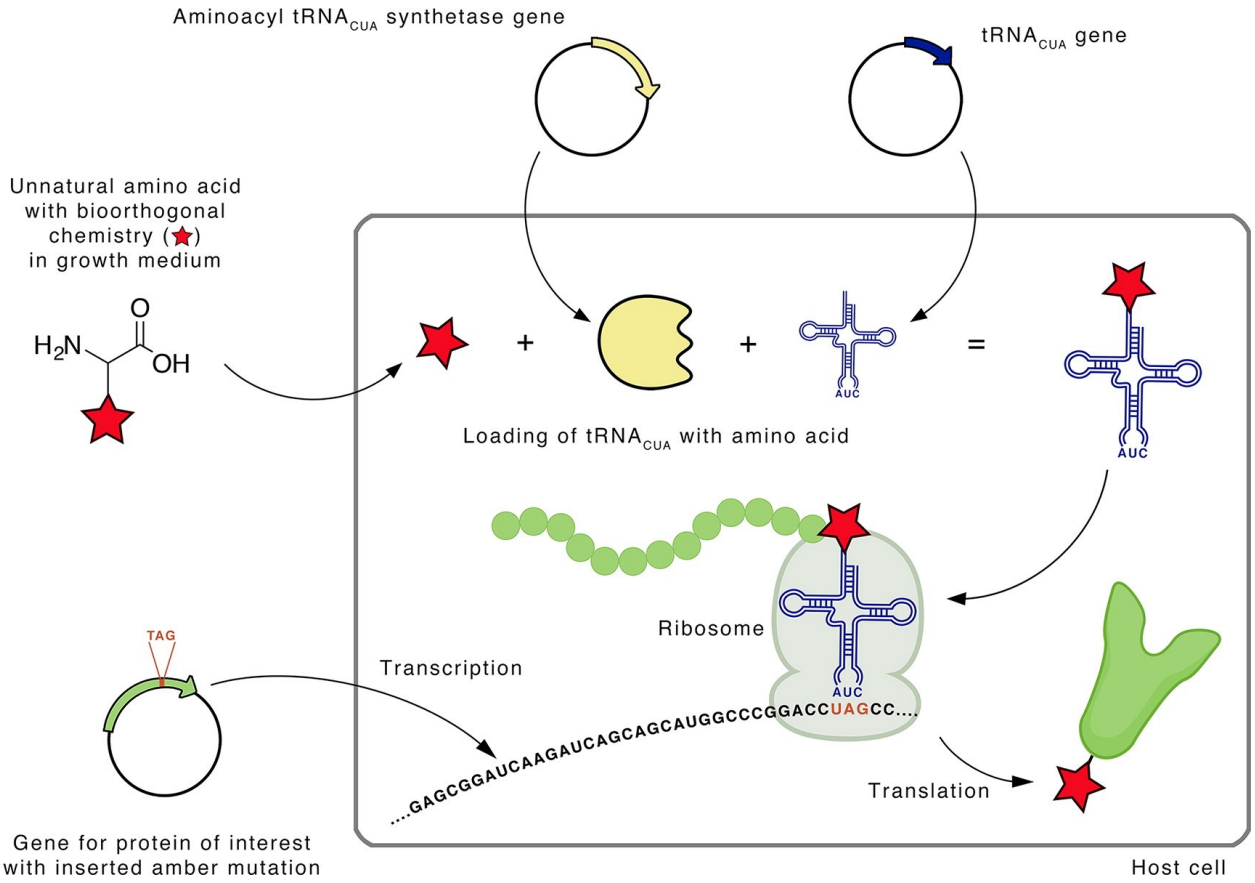

Figure 5.1. Principles of unnatural amino acid incorporation. An aminoacyl-tRNA synthetase charges an orthogonal tRNA$_{CUA}$ with an unnatural amino acid that is incorporated at an amber stop codon during translation. Reproduced (adapted) with permission from Redeker, E. S. et al. *Bioconjugate chem.* 2013, 24 (11), 1761-1777. Copyright 2013 American Chemical Society.

5.1.2 Development of a novel acyl-enzyme trapping strategy

Recently, a novel covalent trapping mechanism for acyl-enzyme intermediates was developed and implemented by encoding 2,3-diaminopropionic acid in place of active site cysteine and serine amino acid residues in the Tobacco Etch Virus (TEV) protease and valinomycin thioesterase, respectively[252]. The advantage of replacing the nucleophilic sulfhydryl or hydroxyl functional groups of cysteine or serine with an amine lies in the consequent formation of an acyl-enzyme intermediate that is linked via an amide bond. Amide intermediates are substantially more stable in aqueous solution and resistant to cleavage compared to thioester

or ester intermediates which are susceptible to nucleophilic attack. Using the TEV protease as an example, the acyl-enzyme intermediate formed through a labile thioester linkage in the Cys-His-Asp active site will normally undergo hydrolysis to release bound substrate and regenerate the enzyme active site[253] (**Figure 5.2A**). However, when the sulfhydryl functional group of the cysteine is instead replaced with an amine functional group, the resulting acyl-enzyme intermediate formed through a stable amide linkage is essentially trapped in place (**Figure 5.2B**). This prevents subsequent hydrolysis and regeneration of the active site from occurring.

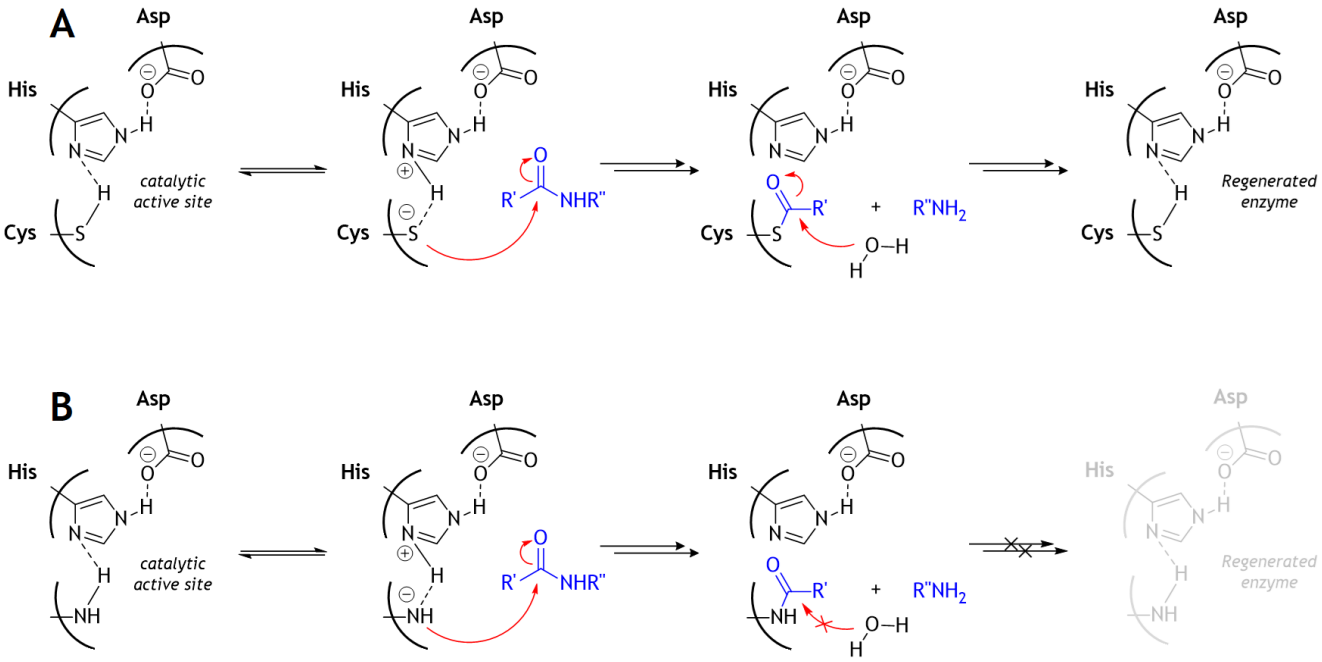

Figure 5.2. TEV protease Cys-His-Asp catalytic mechanism. (A) Catalytic mechanism that proceeds through a transient acyl-enzyme intermediate that is subsequently hydrolyzed. (B) Catalytic mechanism where the sulfhydryl functional group of cysteine is substituted with an amine, resulting in a stable acyl-enzyme intermediate that is unsusceptible to hydrolysis.

Evolving a $tRNA_{CUA}$/aaRS pair selective for 2,3-diaminopropionic acid provided a challenge due to its close structural similarity with serine and cysteine[252]. Instead, several protected versions of 2,3-diaminopropionic acid were synthesized and ultimately an orthogonal *Methanosarcina barkeri* $tRNA_{CUA}$/PylRS pair was evolved to enable the incorporation of a photocleavable

precursor of 2,3-diaminopropionic acid[252], here on referred to as **pcDAP**. Upon exposure to light (365 nm), **pcDAP** breaks down to reveal 2,3-diaminopropionic acid, DAP (**Figure 5.3**).

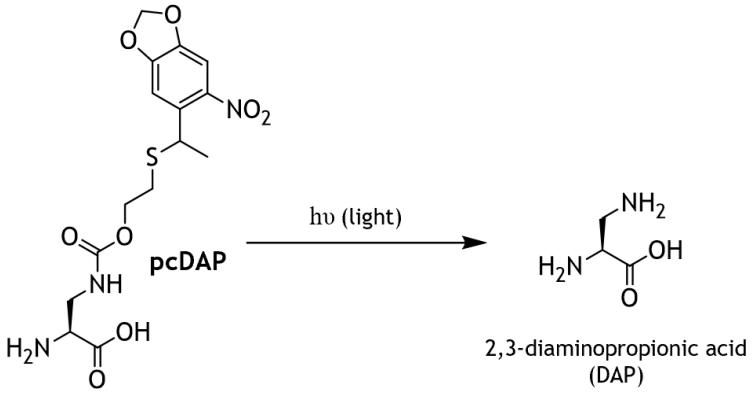

Figure 5.3. Photocleavable precursor of 2,3-diaminopropionic acid. A photocleavable amino acid precursor, **pcDAP**, is incorporated into a protein of interest, which is deprotected upon exposure to UV light (365 nm) to yield 2,3-diaminopropionic acid (DAP).

Promisingly, **pcDAP** was incorporated into a TEV protease construct as a proof-of-concept, replacing the active site cysteine ($TEV_{C151DAP}$). This mutant was able to covalently trap the model substrate ubiquitin flanked with a TEV protease recognition sequence *in vitro*[252].

5.2 Characterizing ClpYQ substrates in *B. subtilis*

5.2.1 Evaluating EzrA degradation by ClpYQ

The *ΔclpQ* deletion proteomics data in Chapter Three has provided initial insights into potential roles and client proteins of the ClpYQ protease. In *E. coli*, the ClpYQ protease (also called HslVU) is implicated in the degradation of SulA, a negative regulator of cell division[105]. The *B. subtilis* genome does not encode for SulA or any other protein of similar amino acid sequence. Instead, *B. subtilis* possesses a protein known as EzrA which functions in a similar fashion to SulA – that is, a negative regulator of cell division by facilitating the depolymerization of FtsZ and disassembling the Z-ring[254]. Biochemical assays have shown the *B. subtilis* ClpYQ protease is able to degrade purified EzrA *in vitro*[106], but we have been unsuccessful in corroborating these results. Notably, our *ΔclpQ* deletion proteomics does not show a significant

increase in EzrA abundance, as would be expected for the substrates of ClpYQ, though EzrA is also a proposed substrate for the FtsH protease[202] which may account for this observation. However, we were also unable to replicate *in vitro* degradation of cell-free translated EzrA by *B. subtilis* ClpYQ (**Figure S11** in **Appendix IV**). Thus, the direct biochemical substrates of the ClpYQ protease and even more importantly *in vivo* confirmation of these substrates remain elusive. Resolving the biological roles of the ClpYQ protease through characterization of the degradome will provide valuable information into its antibiotic implications observed with armeniaspirol.

The most prominent and successful strategy to characterize the substrates of ClpXP in *E. coli* and *S. aureus* has been through the expression of an inactive variant of ClpP, called Clp^{TRAP}, outlined in Chapter One. The active site serine is substituted for an alanine and substrate proteins are transferred into the $ClpP^{TRAP}$ proteolytic chamber following ClpX-mediated unfolding and translocation[97,98,170]. Rather than being degraded, the substrates are retained in the inactive $ClpP^{TRAP}$, enabling recovery and subsequent identification by mass spectrometry proteomics. However, this has yet to be accomplished for the ClpQ serine protease in any bacteria. Although this strategy has been instrumental in identifying key protease substrates, it is dependent on a noncovalent interaction between ClpP and its client proteins, which may reduce recovery efficiency during the experimental workup. Herein, we propose adapting the established acyl-enzyme trapping strategy to identify ClpQ substrates by substituting the active site serine amino acid residue with the unnatural amino acid DAP.

5.2.2 Construction of a B. subtilis $ClpQ_{DAP}$ protease system

As discussed above, the catalytic mechanism of serine proteases such as ClpP and ClpQ involve the formation of an acyl-enzyme intermediate with its protein substrate[255]. This transient

intermediate represents the protease covalently bound to its native substrate prior to cleavage. Thus, trapping the intermediate at this point using DAP would enable the stable recovery of the intermediate complex and identification of bound substrates. The active site serine of the ClpQ protease has been characterized at the N-terminal, at the second amino acid residue of the protein sequence[45]. Thus, we constructed an IPTG-inducible plasmid (pPL64) encoding *B. subtilis* ClpQ with serine-2 substituted for the amber suppressor codon, $ClpQ_{DAP}$ (**Figure 5.4**). Using pET21c as the parental vector, our construct includes a C-terminal His-tag. Thus, following expression of $ClpQ_{DAP}$ and covalent modification to protein substrate, the complex can be recovered by affinity purification. The DNA sequence of *clpQ*$_{DAP}$ was confirmed by Sanger Sequencing (Génome Québec) (**Table S7** in **Appendix IV**). Additionally, we synthesized **pcDAP** for expression following **Scheme S1** in **Appendix IV**.

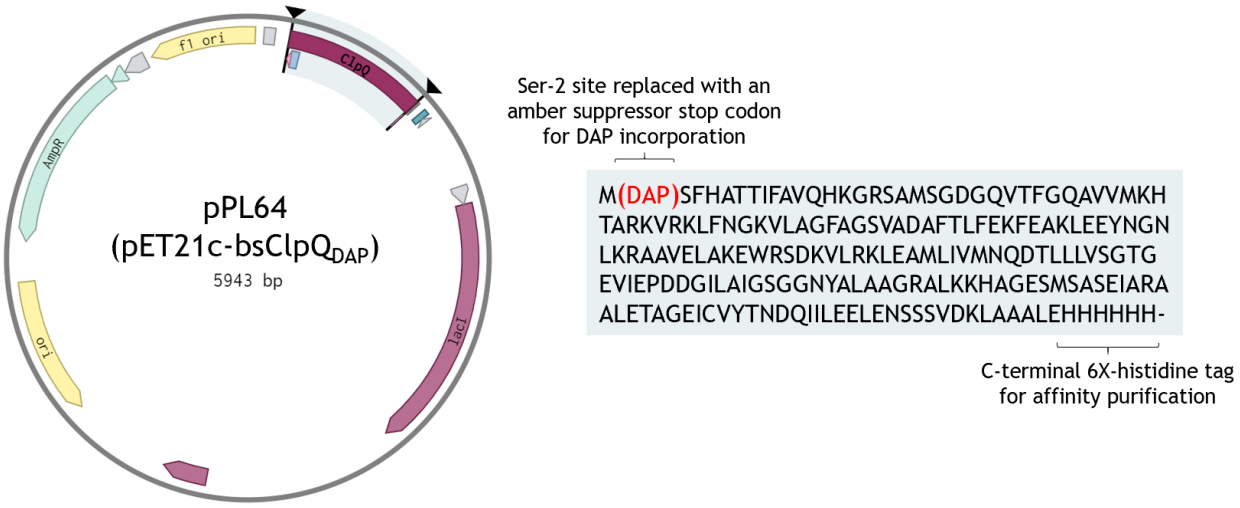

Figure 5.4. Plasmid construction for expression of ClpQ$_{DAP}$. $ClpQ_{DAP}$ encodes for *B. subtilis* ClpQ with the Ser-2 position substituted for an amber suppressor codon leading to DAP incorporation. A 6X His-tag is added to the C-terminal for affinity purification.

Given the challenges associated with plasmid transformation and expression in *B.* subtilis, our strategy to identify ClpQ substrates involves two steps. First is the heterologous

expression and purification of recombinant $ClpQ_{DAP}$ (and separately, ClpY) in chemically competent *E. coli* BL21(DE3) (**Figure 5.5**). *E. coli* BL21(DE3) is doubly transformed with our tailored plasmid encoding $ClpQ_{DAP}$ (pPL64) as well as a second plasmid (pDAPRS) that encodes for the $tRNA_{CUA}$/aminoacyl-tRNA synthetase required for **pcDAP** incorporation at the amber suppressor codon. In the presence of **pcDAP** in culture media, expression of His-tagged $ClpQ_{DAP}$ is induced using IPTG. Following affinity purification, the second step involves adding purified $ClpYQ_{DAP}$ to *B. subtilis* cell lysate to covalently trap native client proteins (**Figure 5.5**). Finally, after a second round of affinity purification of the $ClpYQ_{DAP}$-substrate complex from the lysate, proteins can be identified by tryptic digestion and LC-MS/MS. Based on our mechanism of action study of armeniaspirol, we expect to identify key regulators of the *B. subtilis* divisome and elongasome as substrates of ClpYQ.

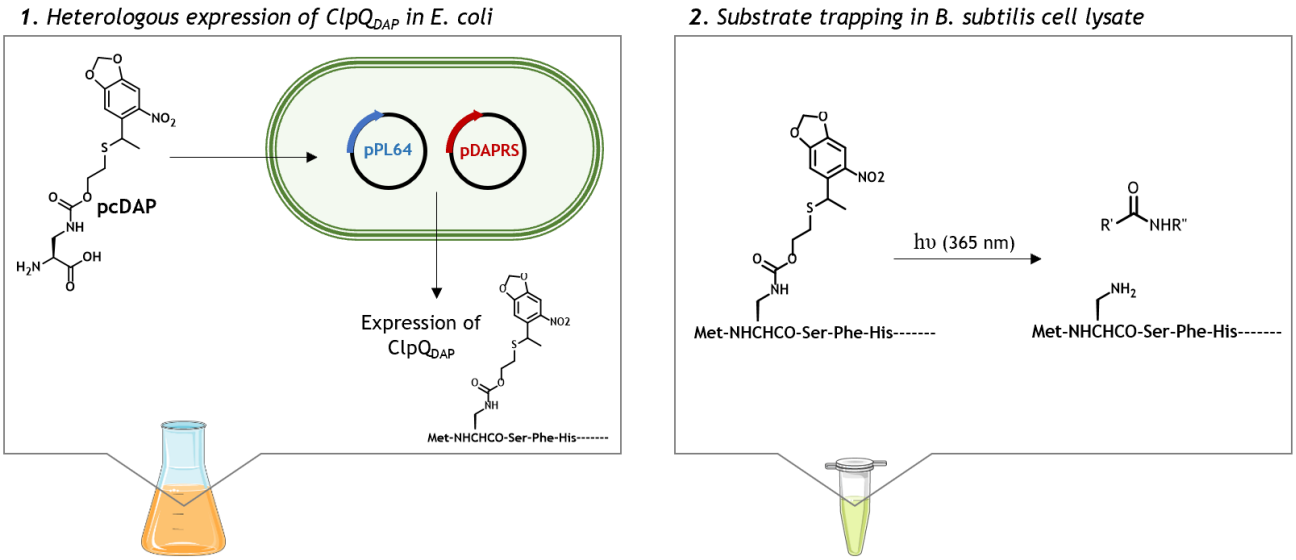

Figure 5.5. Heterologous expression of $ClpQ_{DAP}$. General schematic for heterologous expression of $ClpQ_{DAP}$ in *E. coli* BL21(DE3). **pcDAP** is added to culture media containing double transformants of *E. coli* with pPL64 and a pDAPRS encoding the $tRNA_{CUA}$/aaRS for **pcDAP** incorporation. The culture is induced with IPTG at an OD_{600} of 0.6 for overnight expression. Subsequently, $ClpYQ_{DAP}$ is incubated in *B. subtilis* cell lysate to facilitate protease-substrate trapping, which can be recovered by affinity purification for LC-MS/MS substrate identification.

Unfortunately, initial expression experiments performed as previously described[252] has yet to yield any observable production of $ClpQ_{DAP}$ (**Figure 5.6**). Thus, a critical re-evaluation of our strategy is required to overcome the lack of production of $ClpQ_{DAP}$.

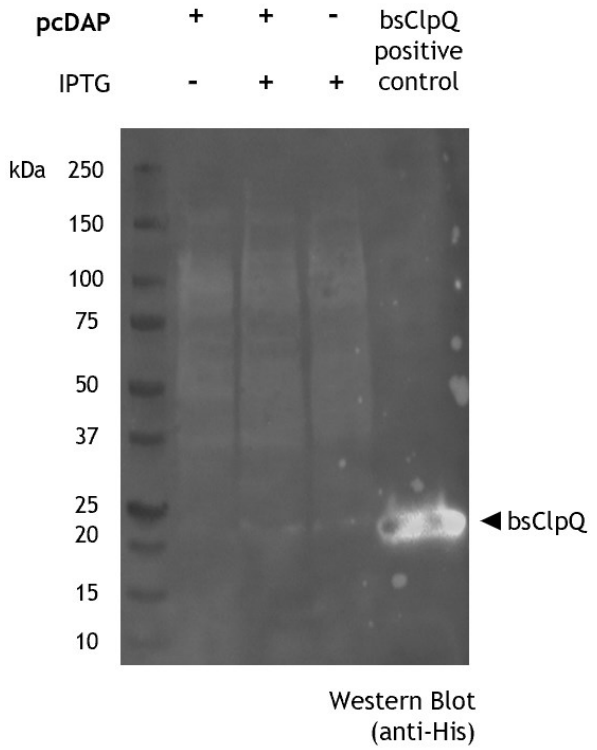

Figure 5.6. Western blot of $ClpQ_{DAP}$ following expression in *E. coli*. In the presence of **pcDAP** and IPTG, induced expression of $ClpQ_{DAP}$ is expected in the *E. coli* cell lysate. Anti-His antibody was used for chemiluminescence detection of the C-terminal His-tag of $ClpQ_{DAP}$. No production of $ClpQ_{DAP}$ was observed.

5.3 Conclusions (future work)

5.3.1 Reconsidering placement of the amber suppressor codon

The first consideration in our troubleshooting strategy is the placement of the amber suppressor codon in the sequence. One of the limitations of using the amber suppressor codon, despite its low prevalence in the *E. coli* genome[247], is that it can still be recognized by the translation termination machinery, specifically release factor proteins[256]. The result is translation termination and production of a truncated protein, which is a significant drawback responsible

for the typically low yields of unnatural amino acid incorporation[257]. Compounded to this is, at position two of the amino acid sequence, it is conceivable that translation efficiency is significantly reduced as opposed to incorporation into a growing polypeptide chain. Indeed, the examples reported by Huguenin-Dezot, N. et al. using the DAP system all involve successful incorporations well into translation, including at residue 150 of green fluorescence protein, residue 151 of TEV protease, and residue 2463 of the thioesterase domain from the valinomycin non-ribosomal peptide synthetase[252]. Thus, we may consider appending a cleavable N-terminal tag such as a maltose-binding protein tag to evaluate if it leads to improved expression of $ClpQ_{DAP}$.

5.3.2 E. coli ClpP as a proof-of-concept control

Building upon the hypothesis that placement of the amber suppressor codon is important as it relates to translation efficiency, we propose using *E. coli* ClpP as a control. The active site serine of ClpP in *E. coli* is at position 111 of the polypeptide sequence[43], placing the incorporation site well into translation. Thus, our current priority is to construct a plasmid encoding *E. coli clpP* with the active site serine substituted for the amber suppressor codon to obtain $ClpP_{DAP}$. There is significant additional value in having access to a $ClpP_{DAP}$ mutant; it would enable the optimization of the covalent trapping assay in cell lysate, or even *in vivo*. Given that several substrates for the ClpXP protease in *E. coli* have been identified[98], we are afforded a valuable foundation which would allow us to corroborate substrates obtained with $ClpP_{DAP}$.

5.4 Contributions

The plasmid (pDAPRS) for expression of the $tRNA_{CUA}$/aminoacyl-tRNA synthetase for **pcDAP** incorporation was provided by Prof. Martin Schmeing, McGill University.

CHAPTER SIX: **Conclusions and Perspectives**

6.1 General conclusions

Armeniaspirol mechanism of action study

Antimicrobial resistant pathogens present an urgent threat to modern medicine, creating a desperate need for antibiotics. The unique and diverse structures of bioactive natural products, shaped by evolution, represent ideal candidates for antibiotics with new mechanisms of action. The primary research objective of this thesis was to elucidate the mechanism of action of armeniaspirol, a novel polyketide Gram-positive antibiotic for which resistance does not readily emerge. Using a combination of chemical synthesis, chemical proteomics, and biochemical assays, we discovered armeniaspirol is a direct competitive inhibitor of the AAA+ proteases ClpXP and ClpYQ in the Gram-positive model organism *Bacillus subtilis*. Through quantitative proteomics and microscopy, we showed that inhibition of ClpXP and ClpYQ dysregulates key proteins of the divisome and elongasome – including FtsZ, DivIVA, and MreB – leading to cell division arrest (**Figure 6.1**).

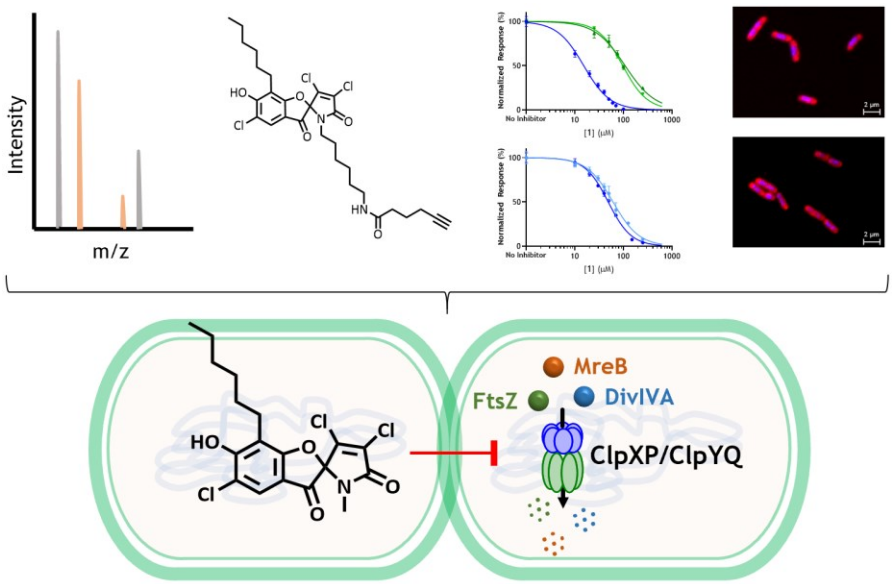

Figure 6.1. Armeniaspirol inhibits ClpXP and ClpYQ leading to cell division arrest.

Armeniaspirol medicinal chemistry study

The ClpXP protease is a highly coveted target in infectious disease due to its key role in virulence in Gram-positive pathogens. Armeniaspirol is the first known natural product inhibitor of the ClpXP protease, and the combined ClpXP ClpYQ inhibition to achieve antibiotic activity represents a unique pharmacology. Moreover, armeniaspirol is active against MRSA in an *in vivo* sepsis model, and resistant *S. aureus* strains could not be generated even after 30 serial passages under sub-lethal doses[110]. Thus, armeniaspirol represents an ideal candidate for lead optimization and clinical development. Our preliminary medicinal chemistry study identified three analogs – **MD01**, **MD04**, and **MD08** – with improved antibiotic activity towards a panel of clinically relevant Gram-positive pathogens including MRSA and VRE (**Figure 6.2**). Correspondingly, these three analogs displayed improved *in vitro* inhibition towards the ClpYQ protease.

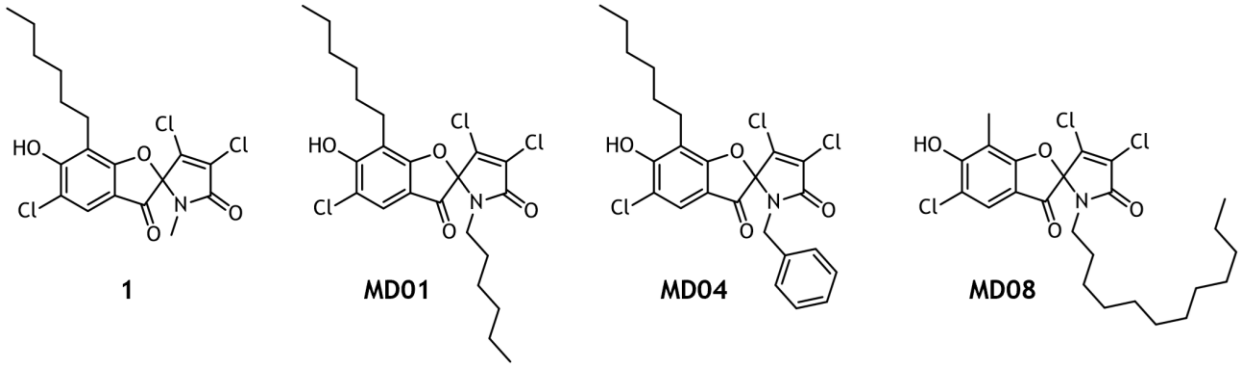

Figure 6.2. Structures of promising armeniaspirol analogs for drug development.

ClpQ degradome characterization study

Finally, our mechanism of action study identified ClpYQ as an important target responsible for the observed antibiotic activity of armeniaspirol. A proteomic profile of the *B. subtilis ΔclpQ* deletion strain provided insights into its degradome and allowed us to propose substrates of the uncharacterized ClpYQ protease. We identified several potential targets for this protease including DivIVA and Mbl proteins, integral components of the divisome and elongasome, respectively. To fully characterize the role of the ClpYQ protease and clarify its role in armeniaspirol mechanism of action, we have initiated a study for ClpQ substrate identification through an unnatural amino acid incorporation strategy (**Figure 6.3**). By replacing the N-terminal active site serine residue of ClpQ with 2,3-diaminopropionic acid, we hope to covalently trap acyl-enzyme intermediates through a highly stable amide bond that will ultimately be identified by LC-MS/MS.

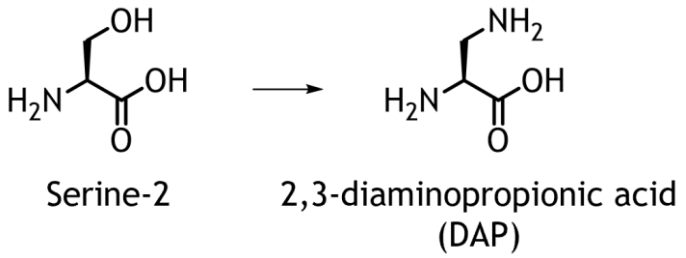

Figure 6.3. Acyl-enzyme trapping strategy to characterize the ClpYQ degradome.

6.2 Outlook

Deciphering the mechanism of action of armeniaspirol is just a first step in its development as an antibiotic. We believe armeniaspirol possesses significant upside for antibiotic development, with a promising new scaffold and a new strategy to target the divisome for antibiotic activity without detectable resistance. While we have identified a novel pharmacology and synthesized analogs with improved antibiotic activity, the future steps require collection of integral pre-clinical data including *in vivo* efficacy and safety. Current efforts are focused on the therapeutic evaluation of MRSA-infected wax moth *Galleria mellonella* larvae – an increasingly popular and rapid infection model for reporting on human pathogens[258,259]. *G. mellonella* possesses an immune system with professional phagocytes (hemocytes) that perform similar functions to human macrophages and neutrophils[260]. Thus, there is a good correlation between pathogenicity observed in *G. mellonella* versus mammalian models. However, evaluation of toxicity in mammalian cells, ability to clear intracellular MRSA in macrophage infection assays, and treatment of bacteremia animal models remain necessary to fully characterize and unveil the full potential of armeniaspirol.

Additionally, our proteomics demonstrated key new links between the regulation of the divisome and elongasome in rod shaped bacteria. This is particularly relevant for the ClpYQ protease, where few targets were known prior to our study and remains largely uncharacterized. Altering protein homeostasis has provided therapeutic strategies for anti-cancer and antimicrobial agents, as has been noted for the extensively characterized ClpP protease[37,93]. Similarly, characterizing ClpQ provides an opportunity to fully elucidate its biological roles and gain insights into its potential as an antimicrobial target. While our characterization of the ClpYQ degradome is currently in the initial stages, it provides an improved strategy to trap and

identify direct protease-substrate relationships that have not been determined previously. The success of this strategy will also enable transfer to other proteases of interest that are otherwise poorly understood.

CHAPTER SEVEN: **Experimental Procedures**

LC-MS/MS proteomics

The LC-MS/MS system consisted of an Ultimate 3000 nanoRLSC system (Dionex) coupled with an Orbitrap Fusion mass spectrometer (ThermoFisher Scientific) operated in positive ion mode. A 70 μm × 150 mm Luna C18(2) reverse phase column (3 μm; 100-Å pore size; Phenomenex) was packed in-house. The mobile phases consisted of 0.1% (v/v) formic acid in water as buffer A and 0.1% (v/v) formic acid in acetonitrile as buffer B. The sample was loaded onto the column using 2% buffer B at a flow rate of 0.30 μL/min for 105 minutes. The method was designed as follows: a gradient from 2% to 38% buffer B was performed for 70 minutes, a gradient from 38% to 98% buffer B for 9 minutes, 98% buffer B for 10 minutes, gradient from 98% to 2% buffer B for 3 minutes, concluded by a 2% buffer B wash for 10 minutes. The Orbitrap Fusion was run in top speed mode and the MS method consisted of a full MS scan from 350 - 2000 *m/z* with R = 60, 000. Precursor ions were filtered according to monoisotopic precursor selection, +2 to +7 charge state, and 30 seconds ± 10 ppm dynamic exclusion. Fragmentation was performed with collision-induced dissociation (CID) in the linear ion trap. Precursors were isolated using a 2 *m/z* isolation window, and fragmented with a normalized collision energy of 35%.

Mass spectrometry processing (inhibitor capture). Proteome Discoverer 2.1 (ThermoFisher Scientific) was used for protein identification. The precursor mass tolerance was set at 10 ppm, and 0.6 Da mass tolerance for fragment ions. Search engine SEQUEST-HT implemented in Proteome Discovery was applied for all MS raw files. Search parameters were set to allow for dynamic modification of methionine oxidation and static modification of cysteine carbamidomethylation. The search database consisted of nonredundant *B. subtilis* protein

sequences in FASTA file format from the UniProt/SwissProt database. The FDR was set to 0.05 for both peptide and protein identifications.

Mass spectrometry processing (dimethyl labeling). Proteome Discoverer 2.1 (ThermoFisher Scientific) was used for protein identification and quantification. The precursor mass tolerance was set at 10 ppm, and 0.6 Da mass tolerance for fragment ions. Search engine SEQUEST-HT implemented in Proteome Discovery was applied for all MS raw files. Search parameters were set to allow for dynamic modification of methionine oxidation, static modification of cysteine carbamidomethylation, and dimethyl modifications on lysine and N-terminus (light and medium labels). The raw files were searched separately with "light" or "medium" labels in the same workflow. The search database consisted of nonredundant *B. subtilis* protein sequences in FASTA file format from the UniProt/SwissProt database. The FDR was set to 0.01, 0.05, and 0.10 for high, medium, and low protein identifications, respectively. Quantification of peptides and proteins was performed using standard settings provided by Proteome Discoverer.

Proteomics data analysis. Proteins that were sparsely quantified were removed by a comprehensive data filtering. Only proteins with an FDR confidence of high and 2 or more peptides detected were used in the data analysis. Of these only protein hits that were detected in two of three or three of four replicates in either the treatment or control group were used for the analysis. The values were Log(2) transformed and each replicate dataset was normalized by subtracting the median of the Log(2) transformed distribution form all values. Missing values were imputed from a Gaussian distribution downshift 1.8 σ from the mean with a standard deviation of 0.3 σ.

Minimum inhibitory/bactericidal concentration (MIC/MBC) assays

MICs were performed in 96-well clear polystyrene microplates (Millipore Sigma). 100 µL of Mueller Hinton Broth (Fisher Scientific) was added to all wells. Two-fold serial dilutions of compound beginning at 32 µg/ml were pipetted across each row of the plate. 5 µL of bacterial culture (OD_{600} 0.07-0.1) was inoculated into each well and incubated at 37°C for 16-18 h. Growth was observed by OD_{600} readings using a Synergy H4 Microplate Reader (BioTek). The MIC was determined by observing the lowest concentration of compound resulting in growth inhibition. MIC assays were performed in triplicate per compound for each bacterium. MBCs were performed by streaking 100 µL of each MIC bacterial subculture on individual petri dishes of non-antibiotic containing Mueller-Hinton Agar (Fisher Scientific). The MBC was determined by a colony count resulting in a 3-log reduction (99.9%) of bacterial growth.

In vitro labeling and inhibitor capture

In vitro labeling and click reaction. Fresh *B. subtilis* 168 cell lysate (2 mg/mL) was incubated in 1 mL (2 x 0.5 mL) PBS containing 0.05% Triton X-100 with 1 mM of compound **1** for 2 h, followed by incubation with 20 µM of compound **2** for an additional 2 h. 500 µL of freshly prepared click chemistry mix (100 µM biotin-azide, 2 mM TCEP, 200 µM TBTA, and 2 mM $CuSO_4$) in PBS was added to each probe-labeled lysate and incubated for 2 h at room temperature with gentle shaking. Respective 0.5 mL reactions were combined and quenched by addition of 5 mL acetone and stored at -80 ºC overnight. The solution was centrifuged at maximum speed for 15 min at 4ºC. The resulting supernatant was discarded, and the pellet was resuspended with 750 µL cold methanol and sonicated for 5 one-second pulses (30% amplitude). The solution was centrifuged for 5 min at 6,500 g at 4°C. The supernatant was discarded, and this

process was repeated an additional 2X. 650 µL of 2.5% SDS in PBS was added to the pellet and sonicated for 15 one-second pulses (30% amplitude). Samples were heated for 5 min at 60°C and centrifuged for 4 min at 6,500 g. The supernatant was transferred to a 15 mL falcon tube and the volume was brought to 8 mL with PBS.

Streptavidin enrichment. 100 µL of 50% Pierce™ streptavidin-agarose beads (ThermoFisher Scientific) were washed 3X times with 700 µL PBS in a Bio-Spin chromatography column (Bio-Rad) at 1,000g. The beads were transferred to probe-labeled cell lysates using 500 µL PBS and incubated for 90 min at room temperature. Beads were pelleted for 2 min at 1,400 g at room temperature. 500 µL of supernatant was used to transfer beads to Bio-Spin columns. Beads were washed 3X with 1% SDS and 3X with fresh 6 M urea by short-spin centrifugation (1,000 g maximum speed).

On-bead digestion. Beads were washed 1X with PBS, 5X with 50 mM ammonium bicarbonate (ABC), and transferred to a 1.5 mL microcentrifuge tube with 700 µL ABC. Beads were pelleted for 2 min at 1,400 g and the supernatant was discarded. 500 µL of 50 mM ABC with 10 mM DTT was added to samples and heated for 15 min at 65ºC. 25 µL of 500 mM iodoacetamide was added and lysates were incubated at room temperature in the dark for 30 min. Samples were centrifuged for 2 min at 1,400 rpm and the supernatant was discarded. Beads were washed 3X with 500 µL TEAB (pH 8.5) and resuspended with 100 µL TEAB. 2 µL of 0.5 mg/mL trypsin was added to samples and were rotated at 37ºC overnight. The samples were pelleted, and the supernatant was centrifuged for 1 min at 1,000 g in new Bio-Spin columns. The flow-through was collected, desalted using Pierce C18 Tips (ThermoFisher Scientific), and dried by vacuum centrifugation prior to LC-MS/MS analysis.

Expression and purification of ClpYQ and ClpXP

B. subtilis clp genes were PCR amplified from *B. subtilis* 168 genomic DNA (Promega Wizard Genomic DNA Purification Kit) and was cloned into the pET21c vector (C-terminal His tag, Amp^R). The resulting plasmid (pPL29) was transformed into chemically competent *E. coli* BL21(DE3) for protein expression. 400 mL LB media was inoculated with 0.5% (*v/v*) of an overnight pre-culture. The culture was grown at 37°C (200 rpm) and expression was induced with 1 mM isopropyl-1-thio-β-D-galactopyranoside (IPTG) at an optical density (OD_{600}) of 0.5. The culture was grown at 37°C (200 rpm) for 4 h. The cells were pelleted at 4,000 rpm for 20 min and re-suspended in lysis buffer (50 mM Tris, 100 mM NaCl, 1 µg/mL leupeptin, 1 µg/mL pepstatin A, 1 mg/mL lysozyme, 10% glycerol, pH 8.0). Mechanical cell lysis was achieved by 30 s sonication. The cell debris was pelleted at 10,000 rpm for 60 min and the supernatant was incubated with 800 µL 50% Ni-NTA agarose resin (QIAGEN) for 30 min at 4°C with gentle shaking. The lysate was loaded onto a column and the flow-through was collected. The resin was washed sequentially with 5 mL elution buffer (100 mM Tris, 300 mM NaCl, pH 8.0) containing 0 mM, 20 mM, 100 mM and 250 mM imidazole. Fractions were analyzed by SDS-PAGE (4-20% Mini-PROTEAN TGX Precast Gels; Bio-Rad). Fractions containing purified protein were pooled and buffer exchanged (50 mM Tris, 250 mM NaCl, pH 8.0) using a 10 kDa Amicon Ultra-15 centrifugal filter unit (Millipore Sigma). The concentrated protein was stored at -80°C with 30% (w/w) glycerol. The *B. subtilis clpY* gene was cloned into pET28b (C-terminal His tag, Kan^R), and the resulting plasmid (pPL31) was purified as above. All protein concentrations were determined by Bradford assay.

The *E. coli clpX* plasmid (pProEx-Htb-ClpX) was expressed as above in 0.8 L LB media. The cells were pelleted at 4,000 rpm for 20 min and re-suspended in 20 mL lysis buffer (25 mM Tris, 500 mM NaCl, 10 mM imidazole, 1 µg/mL leupeptin, 1 µg/mL pepstatin A, 1 mg/mL lysozyme, 10% (w/w) glycerol, pH 8.0). Mechanical cell lysis was achieved by 30 s sonication. The cell debris was pelleted at 10,000 rpm for 60 min and the supernatant was incubated with 2.4 mL 50% Ni-NTA agarose resin (QIAGEN) for 30 min at 4°C with gentle shaking. The lysate was loaded onto a column and the flow-through was collected. The resin was washed 2X with 6 mL lysis buffer (25 mM Tris, 500 mM NaCl, 10 mM imidazole, 10% (w/w) glycerol, pH 8.0), 3X with 10 mL wash buffer (25 mM Tris, 500 mM NaCl, 50 mM imidazole, pH 8.0), and 2X with 5 mL elution buffer (25 mM Tris, 500 mM NaCl, 250 mM imidazole, pH 8.0). Fractions were analyzed by SDS-PAGE (4-20% Mini-PROTEAN TGX Precast Gels; Bio-Rad). Fractions containing purified protein were pooled and buffer exchanged (50 mM Tris, 200 mM KCl, 25 mM $MgCl_2$, 1 mM DTT, 0.1 mM EDTA, 10% (w/w) glycerol pH 8.0) overnight at 4°C. The concentrated protein was stored in small aliquots at -80°C.

The *E. coli clpP* plasmid (pET9a-ClpP) was expressed as above in 0.8 L LB media. The cells were pelleted at 4,000 rpm for 20 min and re-suspended in lysis buffer (50 mM Tris, 150 mM KCl, 1 µg/mL leupeptin, 1 µg/mL pepstatin A, 1 mg/mL lysozyme, 10% (w/w) glycerol, pH 8.0). Mechanical cell lysis was achieved by 60 s sonication. The cell debris was pelleted at 10,000 rpm for 60 min and saturated ammonium sulfate was added to the supernatant slowly with stirring until 40% saturation. Stirring was continued for 60 min at 4°C. The lysate was centrifuged at 10,000 rpm for 30 min and the pellet was discarded. Saturated ammonium sulfate was added further until 60% saturation. Stirring was continued for 60 min at 4°C. The lysate was

centrifuged at 10,000 rpm for 30 min and the pellet was discarded. The lysate was buffer exchanged into Buffer A (50 mM Tris, 150 mM KCl, 1 mM DTT, 10% (w/w) glycerol, pH 8.0) and filtered through a 0.2 μm syringe filter. The solution was injected onto a 1 mL Q sepharose column (GE Healthcare) and eluted with a step gradient of 0%, 10%, 15%, 20%, 25%, 30% and 50% Buffer B (50 mM Tris, 1 M KCl, 1 mM DTT, 10% (w/w) glycerol, pH 8.0) each over 1.5 column volumes. 0.5 mL fractions were collected and analyzed by SDS-PAGE. ClpP containing fractions were pooled and buffer exchanged into 50 mM MES pH 6.0 using a 10 kDa Amicon Ultra-15 centrifugal filter unit (Millipore Sigma). The solution was injected onto a 1 mL SP sepharose column (GE Healthcare) and eluted with a step gradient of 0%, 5%, 10%, 15%, 20%, 25% and 30% Buffer C (50 mM MES, 1 M KCl, 10% (w/w) glycerol, pH 6.0) each over 2 column volumes. 0.5 mL fractions were collected and analyzed by SDS-PAGE. Fractions containing ClpP were concentrated using a 10 kDa Amicon Ultra-15 centrifugal filter unit (Millipore Sigma). The concentrated protein was stored at -80^{o}C with 30% (w/w) glycerol.

Peptide hydrolysis assay

Peptide hydrolysis was assayed using the Cbz-Gly-Gly-Leu-AMC (Millipore Sigma) substrate. 0.1 mL reaction assays were done in Nunc 96-well microplates for fluorescence-based assays (ThermoFisher Scientific). Assays were composed of purified bsClpQ and bsClpY protein, 0.1 M Tris (pH 8.0), 0.1 mM Cbz-Gly-Gly-Leu-AMC, 10 mM $MgCl_2$, 1 mM ATP, 1 mM TCEP, and 1 mM EDTA. Peptide hydrolysis for ecClpX and ecClpP was monitored with the substrate Suc-Leu-Tyr-AMC (Millipore Sigma) under the same conditions. A continuous assay of AMC release was monitored at 37^{o}C using a Synergy H4 microplate reader (BioTek). Excitation and emission for Cbz-Gly-Gly-Leu-AMC were measured at 355 nm and 460 nm, respectively.

Excitation and emission for Suc-Leu-Try-AMC were measured at 360 nm and 440 nm, respectively. Inhibition was observed with varying concentrations of **1**.

ATP hydrolysis assay

ATP hydrolysis was monitored by a discontinuous assay with a malachite green colour reagent. 3 volumes 0.045% (w/v) malachite green in dH_2O and 1 volume 4.2% (w/v) ammonium molybdate in 4 M HCl were mixed to make the colour reagent. After 20 min of shaking at room temperature in the dark, 100 µL of 2% (w/v) Triton X-100 per 5 mL colour reagent was added, and the resulting solution was filtered through a 0.2 µm syringe filter. Reaction assays contained purified bsClpY and bsClpQ, 1 mM ATP, 10 mM $MgCl_2$, 1 mM TCEP, 1 mM EDTA, 0.1 M Tris (pH 8.0). At specified time intervals, 25 µL of the assay was added to 100 µL of the colour reagent in a 96-well plate. The mixture was incubated at room temperature for 5 min and the absorbance (A_{650}) was read using a Synergy H4 microplate reader (BioTek). Inhibition was observed with varying concentrations of **1**.

Non-denaturing polyacrylamide gel electrophoresis

Purified *B. subtilis* ClpY and ClpQ proteins (2 µM) were incubated at room temperature with various concentrations of **1** (100 µM, 10 µM, 1 µM, 0 µM) under proteolytic assay conditions (0.1 M Tris (pH 8.0), 0.1 mM Cbz-Gly-Gly-Leu-AMC, 10 mM $MgCl_2$, 1 mM ATP, 1 mM TCEP, and 1 mM EDTA). Following a 60 min incubation, 2X loading buffer (Tris-HCl pH 6.8/Glycerol/β-mercaptoethanol/Bromophenol blue) was added 1:1 to each sample. Samples were analyzed by polyacrylamide gel electrophoresis (4-20% Mini-PROTEAN TGX Precast Gels; Bio-Rad) under non-denaturing conditions (Tris/Glycine) at 150 V for 120 min.

Polyacrylamide gels were stained with Coomassie Blue (50% (v/v) ethanol and 0.25% (w/v) Coomassie R250).

Whole proteome extraction and dimethyl labeling

B. subtilis 168 was grown in 5 mL Mueller-Hinton broth overnight at 37°C. The culture was diluted 1/50 in fresh 50 mL Mueller-Hinton broth with (1 μg/mL) or without compound **1** and incubated for 6 hours at 37°C (200 rpm). The cells were pelleted at 4,000 rpm for 30 min and re-suspended in 1.25 mL lysis buffer (50 mM Tris, 100 mM NaCl, 1 μg/mL leupeptin, 1 μg/mL pepstatin A, 1 mg/mL lysozyme, pH 8.0). Mechanical cell lysis was achieved by 30 s sonication. The cell debris was pelleted at 10,000 rpm for 10 min. Cell lysate was quantified by Bradford assay. 50 μg were transferred to a 1.5 mL microcentrifuge tube and the volume was adjusted to 100 μL with 100 mM TEAB buffer. 5 μL of 200 mM TCEP was added to the mixture and incubated at 55°C for 1 h. 5 μL of 375 mM iodoacetamide was added and further incubated at room temperature for 30 min in the dark. A methanol/chloroform precipitation was performed to obtain protein pellet. The pellet was re-suspended in 100 μL of 50 mM TEAB buffer containing 0.015% Triton X-100. Protein was digested with trypsin overnight at 37°C. A pellet was obtained by vacuum centrifugation and re-suspended with 100 μL of 100 mM TEAB buffer. 4 μL of 4% (*v/v*) formaldehyde was added to the control reaction, while deuterated formaldehyde was added to **1**-containing reactions. 4 μL of 0.6 M $NaBH_3CN$ was added to all samples and incubated in a fumehood for 1 h with rotation. 16 μL of 1% (v/v) ammonia solution was added to quench the reaction. 8 μL of 5% formic acid (FA) was added and differentially labeled samples were mixed 1:1. All samples were desalted with Pierce C18 Tips (ThermoFisher Scientific) prior to LC-MS/MS analysis.

Microscopy and image analysis

10 mL Mueller-Hinton broth with (1 µg/ml) and without **1** was inoculated with 1% (*v/v*) of overnight *B. subtilis* 168 pre-culture. Cultures were incubated for 5 hours at 37°C. Cultures with **1** reached an OD_{600} of 0.2-0.25, while cultures without **1** were diluted to an OD_{600} of 0.2-0.25. 1 mL bacterial culture was prepared on #1.5 coverslips (ThermoFisher Scientific) washed with poly-lysine(K) in phosphate-buffered saline (PBS). The bacterial dilution was fixed with 4% paraformaldehyde-PBS for 10 min at room temperature, and subsequently washed with filter-sterilized 100 mM glycine-PBS for 5 min. The membrane was stained with 5 µg/ml FM 4-64FX (Invitrogen) fluorescent dye while the nucleoid was stained with 2 µg/mL DAPI (Millipore Sigma) fluorescent dye. Coverslips were mounted on Superfrost Plus microscope slides (ThermoFisher Scientific) with Mowiol mounting medium. The slides were left to dry overnight in the dark. Images were obtained with an LSM 880 confocal microscope (Zeiss) using a 100X/1.4 oil immersion objective. Image analysis and cell length measurements were conducted using ZEN Blue (Zeiss) software.

***Staphylococcus aureus* urease activity assay**

Christensen urease broth (pH 6.8) was prepared as follows: 1 g/L peptone, 1 g/L glucose, 5 g/L NaCl, 1.2 g/L Na_2HPO_4, 0.8 g/L KH_2PO_4, 0.004 g/L phenol red. 5 mL of 40% (w/v) urea was added to 95 mL of Christensen urease broth. 5 mL of Christensen urease broth with (1 µg/ml) and without **1** was inoculated with 1% (*v/v*) of an overnight MRSA USA300 pre-culture. Cultures were grown overnight at 37°C and resulting colour change was observed.

Cell-free EzrA expression and degradation assay

The *B. subtilis ezrA* gene was PCR amplified from *B. subtilis* 168 genomic DNA (Promega Wizard Genomic DNA Purification Kit) and cloned into the pET21c vector (C-terminal His tag, Amp^R). Cell-free expression was carried out using the PURExpress® In Vitro Protein Synthesis Kit (New England BioLabs) supplemented with BODIPY-Lysine for imaging. Expression was validated by SDS-PAGE (4-20% Mini-PROTEAN TGX Precast Gels; Bio-Rad). Purified *B. subtilis* ClpY and ClpQ proteins (5 μM) were incubated at room temperature with cell-free expressed EzrA under proteolytic assay conditions (0.1 M Tris (pH 8.0), 10 mM $MgCl_2$, 1 mM ATP, 1 mM TCEP, and 1 mM EDTA). Following overnight incubation, 2X Lammli sample buffer (Bio-Rad) was added 1:1 to each sample and analyzed by SDS-PAGE (4-20% Mini-PROTEAN TGX Precast Gels; Bio-Rad).

Expression of $ClpQ_{DAP}$

B. subtilis $clpQ_{DAP}$ was PCR amplified from *B. subtilis* 168 genomic DNA (Promega Wizard Genomic DNA Purification Kit) and was cloned into the pET21c vector (C-terminal His tag, Amp^R). The resulting plasmid (pPL64) and pDAPRS were transformed into chemically competent *E. coli* BL21(DE3) for protein expression. 50 mL LB media was inoculated with 0.5% (*v/v*) of an overnight pre-culture. The culture was grown at 37°C (200 rpm) and expression was induced with 0.1 mM isopropyl-1-thio-β-D-galactopyranoside (IPTG) at an optical density (OD_{600}) of 0.6. The culture was grown at 16°C (200 rpm) overnight. The cells were pelleted at 4,000 rpm for 20 min and re-suspended in B-PER Bacterial Protein Extraction Reagent (Thermo Scientific). The re-suspension was centrifuged at 10,000 rpm for 10 min. 2X Lammli sample

buffer (Bio-Rad) was added 1:1 to the supernatant and analyzed on SDS-PAGE (4-20% Mini-PROTEAN TGX Precast Gels; Bio-Rad).

Western Blot immunoassay

Transfer from SDS-PAGE on to an Immun-Blot PVDF membrane (Bio-Rad) was performed in transfer buffer (3.03 g/L Tris-base, 14.41 g glycine, 20% methanol) and run at 40 V for 90 min. The membrane was incubated in 15 mL blocking buffer (5 g powdered milk, 100 mL Tris-buffered saline, 100 µL Tween-20) at 4°C overnight with gentle shaking. Note: Tris-buffered saline composition is 7.88 g/L Tris-HCl, 8.77 g/L NaCl, pH adjusted to 7.5. The blocking buffer was decanted, and 5 mL blocking buffer was added to the membrane with HRP His-tag antibody. The membrane was incubated at 37°C for 1 h (50 rpm). The blocking buffer was decanted, and 10 mL wash buffer (100 mL tris-buffered saline, 100 µL Tween-20) was added to the membrane. The membrane was incubated at room temperature for 5 min (50 rpm) and wash buffer was decanted. This washing step was repeated three additional times. Imaging was performed with Immobilon Western Chemiluminescent HRP substrate (Millipore Sigma). 2 mL of the luminol reagent was mixed with 2 mL peroxide solution and added to the membrane. The membrane was equilibrated for 30 seconds and imaged for chemiluminescence using a ChemiDoc imaging system (Bio-Rad).

Synthesis of photocleavable DAP precursor (pcDAP)

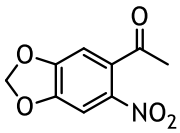

5.2

1-(6-nitrobenzo[d][1,3]dioxol-5-yl)ethan-1-one

10 g (0.07 mol) of **5.1** (Sigma-Aldrich) was dissolved in 40 mL glacial acetic acid and added dropwise to a three-necked round-bottom flask containing 70% HNO_3 at 0°C over 1 h with stirring under nitrogen. Following addition of starting material, the solution was stirred further for an additional 45 min at room temperature. The solution was poured slowly over crushed ice in a beaker, resulting in a yellow precipitate collected by filtration and triturated in methanol. The final compound was collected by vacuum filtration (6.43 g, 51%). ^{1}H NMR (400 MHz, Acetone-d_6) δ 7.57 (s, 1H), 7.07 (s, 1H), 6.31 (s, 2H), 2.48 (s, 3H).

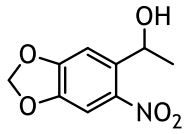

5.3

1-(6-nitrobenzo[d][1,3]dioxol-5-yl)ethan-1-ol

6.43 g (0.030 mol, 1.0 eq.) of **5.2** was dissolved in THF (70 mL) and methanol (130 mL) and cooled to 0°C. $NaBH_4$ (1.59 g, 0.042 mol, 1.4 eq.) was added portion-wise. The solution was stirred for 30 min at 0°C and monitored by TLC. The solvent was evaporated, diluted with water and extracted with ethyl acetate. The organic phase was collected, dried with $MgSO_4$ and evaporated producing a yellow oil. The final product was crystallized with ether/hexanes resulting in light yellow solid (5.69 g, 87%). ^{1}H NMR (400 MHz, Chloroform-*d*) δ 7.46 (s, 1H), 7.27 (s, 1H), 6.17 – 6.08 (m, 2H), 5.46 (q, J = 6.3 Hz, 1H), 2.17 (s, 1H), 1.54 (d, J = 6.3 Hz, 3H).

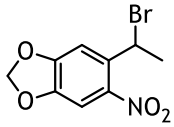

5.4

5-(1-bromoethyl)-6-nitrobenzo[d][1,3]dioxole

5.69 g (0.027 mol, 1.0 eq.) of **5.3** was dissolved in dry CH_2Cl_2 (135 mL) and kept under nitrogen. The solution was cooled to 0°C for 20 min. PBr_3 (0.011 mol, 0.4 eq.) was added dropwise over 10 min, followed by 0.18 mL pyridine. The reaction was stirred for 15 min at 0°C, then brought to room temperature and stirred further for 1.5 h. The reaction was monitored by TLC. The reaction was cooled to 0°C and quenched by addition of 10 mL dry methanol. The reaction was warmed to room temperature and stirred for 30 min. The solvent was evaporated producing a dark brown, thick liquid. The product was dissolved in CH_2Cl_2 and extracted with saturated $NaHCO_3$ followed by saturated NaCl. The organic phase was collected, dried with $MgSO_4$ and evaporated. The crude product was purified by flash chromatography on SiO_2 [eluent: ethyl acetate/n-hexane (1:10)] to obtain **5.4** (4.35 g, 59%). ^{1}H NMR (400 MHz, Chloroform-*d*) δ 7.34 (s, 1H), 7.26 (s, 1H), 6.15 – 6.08 (m, 2H), 5.89 (q, *J* = 6.8 Hz, 1H), 2.03 (d, *J* = 6.8 Hz, 3H).

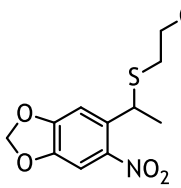

5.5

2-((1-(6-nitrobenzo[d][1,3]dioxol-5-yl)ethyl)thio)ethan-1-ol

0.63 g NaOH dissolved in 31.5 mL water (0.5 M, 1.0 eq) was added to a three-necked round-bottom flask. The solution was degassed through a stream of nitrogen. 1.2 mL mercaptoethanol (0.017 mol, 1.05 eq.) was added to the solution and further degassed. Separately, 4.35 g of **5.4**

was dissolved in 16 mL 1,4-dioxane and degassed through a stream of nitrogen. The NaOH/mercaptoethanol mixture was added to **5.4** using a cannula. The solution was stirred for 1 h resulting in a precipitate. 50 mL of 1,4-dioxane was added to the reaction and stirred for 12 h at room temperature. The reaction was monitored by TLC [ethyl acetate:n-hexane (3:7)]. The solvent was evaporated and extracted with ethyl acetate. The organic phase was washed with saturated NH_4Cl and extracted with saturated NaCl. The organic phase was evaporated. The crude product was purified by flash chromatography on SiO_2 [eluent: ethyl acetate/n-hexane (3:7)] to obtain **5.5** (2.40 g, 55%). ^{1}H NMR (400 MHz, Chloroform-*d*) δ 7.27 (s, 1H), 7.25 (s, 1H), 6.11 – 6.06 (m, 2H), 4.77 (q, *J* = 6.9 Hz, 1H), 3.71 – 3.55 (m, 2H), 2.62 – 2.45 (m, 2H), 1.86 (s, 1H), 1.54 (d, *J* = 7.0 Hz, 3H).

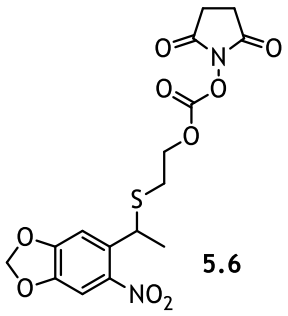

5.6

2,5-dioxopyrrolidin-1-yl (2-((1-(6-nitrobenzo[d][1,3]dioxol-5-yl)ethyl)thio)ethyl) carbonate

2.4 g (0.009 mol, 1.0 eq) of **5.6** was dissolved in dry CH_3CN (45 mL) under nitrogen. Dry DIPEA (4.62 mL, 0.027 mol, 3.0 eq.) was added to the reaction, followed by DSC (3.17 g, 0.012 mol, 1.4 eq.). The reaction was stirred o/n at room temperature. The reaction was monitored by TLC [ethyl acetate:n-hexane (3:7)] and immediately carried forward to the next step.

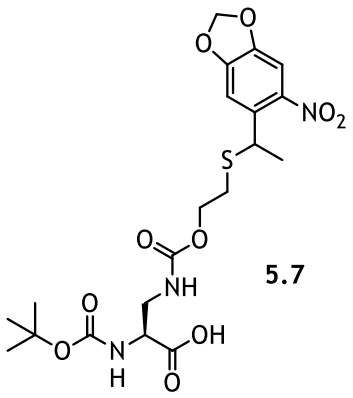

5.7

(2S)-2-((tert-butoxycarbonyl)amino)-3-(((2-((1-(6-nitrobenzo[d][1,3]dioxol-5-yl)ethyl)thio)ethoxy)carbonyl)amino)propanoic acid

2 g of Boc-L-DAP-OH (0.010 mol, 1.1 eq.) was added to the reaction above under nitrogen. The reaction was stirred o/n at room temperature. The reaction was monitored by TLC (4% methanol in CH_2Cl_2). The solvent was evaporated. The crude product was purified by flash chromatography on SiO_2 (eluent: 3% methanol in CH_2Cl_2) to obtain **5.7** (4.96 g). ^{1}H NMR (400 MHz, Chloroform-*d*) δ 7.27 – 7.26 (m, 1H), 7.25 (d, *J* = 0.8 Hz, 1H), 6.11 – 6.07 (m, 2H), 5.74 (d, *J* = 6.5 Hz, 1H), 5.49 (d, *J* = 9.2 Hz, 1H), 4.81 (p, *J* = 7.1 Hz, 1H), 4.31 (t, *J* = 7.1 Hz, 1H), 4.11 (tt, *J* = 11.2, 6.1 Hz, 2H), 3.59 (s, 2H), 2.60 – 2.42 (m, 2H), 1.52 (dd, *J* = 6.9, 0.8 Hz, 3H), 1.42 (s, 9H).

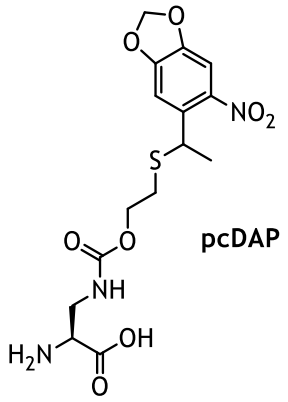

(2S)-2-amino-3-(((2-((1-(6-nitrobenzo[d][1,3]dioxol-5-yl)ethyl)thio)ethoxy)carbonyl)amino)propanoic acid

4.96 g of **5.7** (0.010 mol, 1.0 eq.) is dissolved in dry CH_2Cl_2 (55 mL). 16 mL of triethylsilane (0.100 mol, 10 eq.) was added to the solution and stirred for 5 min. Next, 15 mL of TFA was added to the solution and the reaction was stirred for 5 h at room temperature. The reaction was monitored by TLC (10% methanol in CH_2Cl_2). The solvent was evaporated. The product was washed with 15 mL methanol and evaporated again. The product was dried in high vacuum (<0.1 mbar) o/n. The compound was dissolved in 15 mL methanol and cooled to 0°C. Cold dry ether (75 mL) was added to the reaction under nitrogen. The solution was stirred first for 15 min at 0°C and then for 2 h at room temperature. The resulting precipitate was filtered, washed with ether (three times) and n-hexane. The product was dried in high vacuum (<0.1 mbar) o/n. ^{1}H NMR (400 MHz, Methanol-d_4) δ 7.33 (s, 1H), 7.30 (s, 1H), 6.13 (dd, J = 6.5, 1.0 Hz, 2H), 4.81 (qd, J = 7.0, 1.4 Hz, 1H), 4.24 – 3.99 (m, 3H), 3.79 (ddd, J = 15.1, 4.0, 2.2 Hz, 1H), 3.71 – 3.59 (m, 1H), 2.61 (ddt, J = 36.7, 13.9, 6.6 Hz, 2H), 1.57 (d, J = 6.9 Hz, 3H).

References

(1) Ruiz, B.; Chávez, A.; Forero, A.; García-huante, Y.; Romero, A.; Sánchez, M.; Rocha, D.; Sánchez, B.; Rodríguez-Sanoja, R.; Sánchez, S.; et al. Production of microbial secondary metabolites : Regulation by the carbon source. *Crit. Rev. Microbiol.* **2010**, *36* (2), 146–167.

(2) Genilloud, O. Actinomycetes: Still a source of novel antibiotics. *Nat. Prod. Rep.* **2017**, *34* (10), 1203–1232.

(3) Katz, E.; Demain, A. L. The peptide antibiotics of Bacillus: chemistry, biogenesis, and possible functions. *Bacteriol. Rev.* **1977**, *41* (2), 449–474.

(4) Martin, J. F.; Demain, A. L. Control of Antibiotic Biosynthesis. *Microbiol. Rev.* **1980**, *44* (2), 230–251.

(5) Romero, D.; Traxler, M. F.; López, D.; Kolter, R. Antibiotics as Signal Molecules. *Chem. Rev.* **2011**, *111* (9), 5492–5505.

(6) Davies, J. Are antibiotics naturally antibiotics ? *J Ind Microbiol Biotechnol* **2006**, *33* (7), 496–499.

(7) Discovery and Development of Penicillin https://www.acs.org/content/acs/en/education/whatischemistry/landmarks/flemingpenicillin.html (accessed Jul 11, 2017).

(8) Fleming, A. On the antibacterial action of cultures of a penicillium, with special reference to their use in the isolation of B. influenzae. *Br J Exp Pathol* **1929**, *10* (3), 226–236.

(9) Brown, E. D.; Wright, G. D. Antibacterial drug discovery in the resistance era. *Nature* **2016**, *529* (7586), 336–343.

(10) Gould, K. Antibiotics : from prehistory to the present day. *J Antimicrob Chemother* **2018**, *71* (3), 572–575.

(11) Davies, J. Where have All the Antibiotics Gone? *Can. J. Infect. Dis. Med. Microbiol.* **2006**, *17* (5), 287–290.

(12) Ventola, C. L. The antibiotic resistance crisis: part 1: causes and threats. *P&T* **2015**, *40* (4), 277–283.

(13) Von Nussbaum, F.; Brands, M.; Hinzen, B.; Weigand, S.; Häbich, D. Antibacterial natural products in medicinal chemistry - Exodus or revival? *Angew. Chemie - Int. Ed.* **2006**, *45* (31), 5072–5129.

(14) Lipinski, C. A.; Lombardo, F.; Dominy, B. W.; Feeney, P. J. Experimental and computational approaches to estimate solubility and permeability in drug discovery and

development settings. *Adv. Drug Deliv. Rev.* **1997**, *23* (1–3), 3–25.

(15) Waksman, S. A.; Woodruff, H. B. The soil as a source of microorganisms antagonistic to disease-producing bacteria. *J. Bacteriol.* **1940**, *40*, 581–600.

(16) Frost, W. D. The antagonism exhibited by certain saprophytic bacteria against the Bacillus typhosis Gaffky. *J. Infect. Dis.* **1904**, *1* (4), 599–640.

(17) Pasteur, L.; Joubert, J. Charbon et septicémie. *Compt. Rend. Acad. Sci.* **1877**, *85*, 101–105.

(18) Waksman, S. A. What Is an Antibiotic or an Antibiotic Substance? *Mycologia* **1947**, *39* (5), 565–569.

(19) Waksman, S. A.; Woodruff, H. B. Actinomyces antibioticus, a new soil organism antagonistic to pathogenic and non-pathogenic bacteria. *J. Bacteriol.* **1941**, *42*, 231–249.

(20) Silver, L. L. Challenges of Antibacterial Discovery. *Clin. Microbiol. Rev.* **2011**, *24* (1), 71–109.

(21) Reen, F. J.; Romano, S.; Dobson, A. D. W.; Gara, F. O. The Sound of Silence: Activating Silent Biosynthetic Gene Clusters in Marine Microorganisms. *Mar. Drugs* **2015**, *13* (8), 4754–4783.

(22) Amann, R. I.; Ludwig, W.; Schleifer, K.-H. Phylogenetic identification and in situ detection of individual microbial cells without cultivation. *Microbiol. Rev.* **1995**, *59*, 143–169.

(23) Onaka, H. Novel antibiotic screening methods to awaken silent or cryptic secondary metabolic pathways in actinomycetes. *J. Antibiot. (Tokyo).* **2017**, *70* (8), 865–870.

(24) Atanasov, A. G.; Zotchev, S. B.; Dirsch, V. M.; Orhan, I. E.; Banach, M.; Rollinger, J. M.; Barreca, D.; Weckwerth, W.; Bauer, R.; Bayer, E. A.; et al. Natural products in drug discovery: advances and opportunities. *Nat. Rev. Drug Discov.* **2021**, *20* (3), 200–216.

(25) Aminov, R. I. A brief history of the antibiotic era: Lessons learned and challenges for the future. *Front. Microbiol.* **2010**, *1* (134), 1–7.

(26) Pankey, G. A.; Sabath, L. D. Clinical relevance of bacteriostatic versus bactericidal mechanisms of action in the treatment of gram-positive bacterial infections. *Clin. Infect. Dis.* **2004**, *38* (6), 864–870.

(27) Reygaert, W. C. An overview of the antimicrobial resistance mechanisms of bacteria. *AIMS Microbiol.* **2018**, *4* (3), 482–501.

(28) Monserrat-Martinez, A.; Gambin, Y.; Sierecki, E. Thinking outside the bug: molecular targets and strategies to overcome antibiotic resistance. *Int. J. Mol. Sci.* **2019**, *20* (6),

1255.

(29) Antimicrobial resistance http://www.who.int/mediacentre/factsheets/fs194/en/ (accessed Nov 28, 2016).

(30) Methicillin-resistant Staphylococcus aureus in Canadian acute-care hospitals https://www.canada.ca/en/public-health/services/infectious-diseases/nosocomial-occupational-infections/healthcare-acquired-infections-currently-under-surveillance/methicillin-resistant-staphylococcus-aureus-canadian-acute-care-hospitals-surveillance-repor (accessed Oct 31, 2020).

(31) Canadian Antimicrobial Resistance Surveillance System Report 2016 http://healthycanadians.gc.ca/publications/drugs-products-medicaments-produits/antibiotic-resistance-antibiotique/antimicrobial-surveillance-antimicrobioresistance-eng.php#a4-2-3 (accessed Nov 28, 2016).

(32) About antibiotic resistance https://www.canada.ca/en/public-health/services/antibiotic-antimicrobial-resistance/about-antibiotic-resistance.html#a3 (accessed Sep 17, 2018).

(33) Payne, D. J.; Gwynn, M. N.; Holmes, D. J.; Pompliano, D. L. Drugs for bad bugs: confronting the challenges of antibacterial discovery. *Nat. Rev. Drug Discov.* **2007**, *6* (1), 29–40.

(34) Wanted: a reward for antibiotic development. *Nat. Biotechnol.* **2018**, *36* (7), 555.

(35) Bittner, L. M.; Arends, J.; Narberhaus, F. Mini review: ATP-dependent proteases in bacteria. *Biopolymers* **2016**, *105* (8), 505–517.

(36) Wong, K. S.; Houry, W. A. Recent advances in targeting human mitochondrial AAA+ proteases to develop novel cancer therapeutics. *Adv. Exp. Med. Biol.* **2019**, *1158*, 119–142.

(37) Wong, K. S.; Houry, W. A. Chemical modulation of human mitochondrial ClpP: potential application in cancer therapeutics. *ACS Chem. Biol.* **2019**, *14*, 2349–2360.

(38) Kirstein, J.; Molière, N.; Dougan, D. A.; Turgay, K. Adapting the machine: adaptor proteins for Hsp100/Clp and AAA+ proteases. *Nat. Rev. Microbiol.* **2009**, *7* (8), 589–599.

(39) Grimaud, R.; Kessel, M.; Beuron, F.; Steven, A. C.; Maurizi, M. R. Enzymatic and structural similarities between the Escherichia coli ATP- dependent proteases, ClpXP and ClpAP. *J. Biol. Chem.* **1998**, *273* (20), 12476–12481.

(40) Flanagan, J. M.; Wall, J. S.; Capel, M. S.; Schneider, D. K.; Shanklin, J. Scanning transmission electron microscopy and small-angle scattering provide evidence that native Escherichia coli ClpP is a tetradecamer with an axial pore. *Biochemistry* **1995**, *34* (34), 10910–10917.

(41) Rho, S.-H.; Park, H. H.; Kang, G. B.; Im, Y. J.; Kang, M. S.; Lim, B. K.; Seong, I. S.; Seol, J.; Chung, C. H.; Wang, J.; et al. Crystal structure of Bacillus subtilis CodW, a noncanonical HslV-like peptidase with an impaired catalytic apparatus. *Proteins* **2008**, *71* (2), 1020–1026.

(42) Baker, T. A.; Sauer, R. T. ATP-dependent proteases of bacteria: recognition logic and operating principles. *Trends Biochem. Sci.* **2006**, *31* (12), 647–653.

(43) Maurizi, M. R.; Clark, W. P.; Kim, S. H.; Gottesman, S. Clp P represents a unique family of serine proteases. *J. Biol. Chem.* **1990**, *265* (21), 12546–12552.

(44) Choi, K. H.; Licht, S. Control of peptide product sizes by the energy-dependent protease ClpAP. *Biochemistry* **2005**, *44* (42), 13921–13931.

(45) Kang, M. S.; Lim, B. K.; Seong, I. S.; Seol, J. H.; Tanahashi, N.; Tanaka, K.; Chung, C. H. The ATP-dependent CodWX (HslVU) protease in Bacillus subtilis is an N- terminal serine protease. *EMBO J.* **2001**, *20* (4), 734-42.

(46) Rohrwild, M.; Coux, O.; Huang, H.; Moerschell, R. P.; Ji, S. HslV-HslU: A novel ATP-dependent protease complex in Escherichia coli related to the eukaryotic proteasome. *Proc. Natl. Acad. Sci.* **1996**, *93* (12), 5808–5813.

(47) Seol, J. H.; Yoo, S. J.; Shin, D. H.; Shim, Y. K.; Kang, M.-S.; Goldberg, A. L.; Chung, C. H. The heat-shock protein HslVU from Escherichia Coli is a protein-activated ATPase as well as an ATP-dependent proteinase. *Eur. J. Biochem.* **1997**, *247* (3), 1143–1150.

(48) Seong, I. S.; Kang, M. S.; Choi, M. K.; Lee, J. W.; Koh, O. J.; Wang, J.; Eom, S. H.; Chung, C. H. The C-terminal tails of HslU ATPase act as a molecular switch for activation of HslV peptidase. *J. Biol. Chem.* **2002**, *277* (29), 25976–25982.

(49) Rotanova, T. V.; Melnikov, E. E.; Khalatova, A. G.; Makhovskaya, O. V.; Botos, I.; Wlodawer, A.; Gustchina, A. Classification of ATP-dependent proteases Lon and comparison of the active sites of their proteolytic domains. *Eur. J. Biochem.* **2004**, *271* (23–24), 4865–4871.

(50) Bieniossek, C.; Schalch, T.; Bumann, M.; Meister, M.; Meier, R.; Baumann, U. The molecular architecture of the metalloprotease FtsH. *Proc. Natl. Acad. Sci. U. S. A.* **2006**, *103* (9), 3066–3071.

(51) Sauer, R. T.; Baker, T. A. AAA+ proteases: ATP-fueled machines of protein destruction. *Annu. Rev. Biochem.* **2011**, *80*, 587–612.

(52) Keiler, K. C.; Waller, P. R.; Sauer, R. T. Role of a peptide tagging system in degradation of proteins synthesized from damaged messenger RNA. *Science (80-.).* **1996**, *271* (5251), 990–993.

(53) Wiegert, T.; Schumann, W. SsrA-mediated tagging in Bacillus subtilis. *J. Bacteriol.* **2001**,

183 (13), 3885–3889.

(54) Gottesman, S.; Roche, E.; Zhou, Y.; Sauer, R. T. The ClpXP and ClpAP proteases degrade proteins with carboxy-terminal peptide tails added by the SsrA-tagging system. *Genes Dev.* **1998**, *12* (9), 1338–1347.

(55) Gerth, U.; Krüger, E.; Derré, I.; Msadek, T.; Hecker, M. Stress induction of the Bacillus subtilis clpP gene encoding a homologue of the proteolytic component of the Clp protease and the involvement of ClpP and ClpX in stress tolerance. *Mol. Microbiol.* **2002**, *28* (4), 787–802.

(56) Gur, E.; Sauer, R. T. Recognition of misfolded proteins by Lon, a AAA+ protease. *Genes Dev.* **2008**, *22* (16), 2267–2277.

(57) Chung, C. H.; Goldberg, A. L. The product of the lon (capR) gene in Escherichia coli is the ATP-dependent protease, protease La. *Proc. Natl. Acad. Sci. U. S. A.* **1981**, *78* (8 I), 4931–4935.

(58) Krüger, E.; Witt, E.; Ohlmeier, S.; Hanschke, R.; Hecker, M. The Clp proteases of Bacillus subtilis are directly involved in degradation of misfolded proteins. *J. Bacteriol.* **2000**, *182* (11), 3259–3265.

(59) Lies, M.; Maurizi, M. R. Turnover of endogenous SsrA-tagged proteins mediated by ATP-dependent proteases in Escherichia coli. *J. Biol. Chem.* **2008**, *283* (34), 22918–22929.

(60) Herman, C.; Thévenet, D.; Bouloc, P.; Walker, G. C.; D'Ari, R. Degradation of carboxy-terminal-tagged cytoplasmic proteins by the Escherichia coli protease HflB (FtsH). *Genes Dev.* **1998**, *12* (9), 1348–1355.

(61) Dougan, D. A. Regulated proteolysis in microorganisms. *Subcell. Biochem.* **2013**, *66*, 1–327.

(62) Chiba, S.; Akiyama, Y.; Mori, H.; Matsuo, E. I.; Ito, K. Length recognition at the N-terminal tail for the initiation of FtsH-mediated proteolysis. *EMBO Rep.* **2000**, *1* (1), 47–52.

(63) Chiba, S.; Akiyama, Y.; Ito, K. Membrane protein degradation by FtsH can be initiated from either end. *J. Bacteriol.* **2002**, *184* (17), 4775–4782.

(64) Mei, J.; Nourbakhsh, F.; Ford, C. W.; Holden, D. W. Identification of Staphylococcus aureus virulence genes in a murine model of bacteraemia using signature-tagged mutagenesis . *Mol. Microbiol.* **1997**, *26* (2), 399–407.

(65) Hensel, M.; Shea, J. E.; Gleeson, C.; Jones, M. D.; Dalton, E.; Holden, D. W. Simultaneous identification of bacterial virulence genes by negative selection. *Science (80-.).* **1995**, *269* (5222), 400–403.

(66) Mazurkiewicz, P.; Tang, C. M.; Boone, C.; Holden, D. W. Signature-tagged mutagenesis: barcoding mutants for genome-wide screens. *Nat. Rev. Genet.* **2006**, *7* (12), 929–939.

(67) Frees, D.; Qazi, S. N. A.; Hill, P. J.; Ingmer, H. Alternative roles of ClpX and ClpP in Staphylococcus aureus stress tolerance and virulence. *Mol. Microbiol.* **2003**, *48* (6), 1565–1578.

(68) Robertson, G. T.; Ng, W.-L.; Foley, J.; Gilmour, R.; Winkler, M. E. Global transcriptional analysis of clpP mutations of type 2 Streptococcus pneumoniae and their effects on physiology and virulence. *J. Bacteriol.* **2002**, *184* (13), 3508–3520.

(69) Yamamoto, T.; Sashinami, H.; Takaya, A.; Tomoyasu, T.; Matsui, H.; Kikuchi, Y.; Hanawa, T.; Kamiya, S.; Nakane, A. Disruption of the genes for clpXP protease in Salmonella enterica serovar Typhimurium results in persistent infection in mice, and development of persistence requires endogenous gamma interferon and tumor necrosis factor alpha. *Infect. Immun.* **2001**, *69* (5), 3164–3174.

(70) Dickey, S. W.; Cheung, G. Y. C.; Otto, M. Different drugs for bad bugs: antivirulence strategies in the age of antibiotic resistance. *Nat. Rev. Drug Discov.* **2017**, *16* (7), 457–471.

(71) Clatworthy, A. E.; Pierson, E.; Hung, D. T. Targeting virulence: a new paradigm for antimicrobial therapy. *Nat. Chem. Biol.* **2007**, *3* (9), 541–548.

(72) Cegelski, L.; Marshall, G. R.; Eldridge, G. R.; Hultgren, S. J. The biology and future prospects of antivirulence therapies. *Nat. Rev. Microbiol.* **2008**, *6* (1), 17–27.

(73) Andersson, D. I.; Hughes, D. Antibiotic resistance and its cost: is it possible to reverse resistance? *Nat. Rev. Microbiol.* **2010**, *8* (4), 260–271.

(74) Rasko, D. A.; Sperandio, V. Anti-virulence strategies to combat bacteria-mediated disease. *Nat. Rev. Drug Discov.* **2010**, *9* (2), 117–128.

(75) Böttcher, T.; Sieber, S. A. β-lactones as specific inhibitors of ClpP attenuate the production of extracellular virulence factors of Staphylococcus aureus. *J. Am. Chem. Soc.* **2008**, *130* (44), 14400–14401.

(76) Hackl, M. W.; Lakemeyer, M.; Dahmen, M.; Glaser, M.; Pahl, A.; Lorenz-Baath, K.; Menzel, T.; Sievers, S.; Böttcher, T.; Antes, I.; et al. Phenyl esters are potent inhibitors of caseinolytic protease P and reveal a stereogenic switch for deoligomerization. *J. Am. Chem. Soc.* **2015**, *137* (26), 8475–8483.

(77) Global Tuberculosis Report 2020 (World Health Organization) https://apps.who.int/iris/bitstream/handle/10665/336069/9789240013131-eng.pdf (accessed Mar 7, 2021).

(78) Raju, R. M.; Unnikrishnan, M.; Rubin, D. H. F.; Krishnamoorthy, V.; Kandror, O.;

Akopian, T. N.; Goldberg, A. L.; Rubin, E. J. Mycobacterium tuberculosis ClpP1 and ClpP2 function together in protein degradation and are required for viability in vitro and during infection. *PLoS Pathog.* **2012**, *8* (2), e1002511.

(79) Schmitt, E. K.; Riwanto, M.; Sambandamurthy, V.; Roggo, S.; Miault, C.; Zwingelstein, C.; Krastel, P.; Noble, C.; Beer, D.; Rao, S. P. S.; et al. The natural product cyclomarin kills mycobacterium tuberculosis by targeting the ClpC1 subunit of the caseinolytic protease. *Angew. Chemie - Int. Ed.* **2011**, *50* (26), 5889–5891.

(80) Vasudevan, D.; Rao, S. P. S.; Noble, C. G. Structural basis of mycobacterial inhibition by Cyclomarin A. *J. Biol. Chem.* **2013**, *288* (43), 30883–30891.

(81) Gavrish, E.; Sit, C. S.; Cao, S.; Kandror, O.; Spoering, A.; Peoples, A.; Ling, L.; Fetterman, A.; Hughes, D.; Bissell, A.; et al. Lassomycin, a ribosomally synthesized cyclic peptide, kills Mycobacterium tuberculosis by targeting the ATP-dependent protease ClpC1P1P. *Chem. Biol.* **2014**, *21* (4), 509–518.

(82) Gao, W.; Kim, J.-Y.; Anderson, J. R.; Akopian, T.; Hong, S.; Jin, Y.-Y.; Kandror, O.; Kim, J.-W.; Lee, I.-A.; Lee, S.-Y.; et al. The cyclic peptide ecumicin targeting ClpC1 is active against Mycobacterium tuberculosis in vivo. *Antimicrob. Agents Chemother.* **2015**, *59* (2), 880–889.

(83) Ollinger, J.; O'Malley, T.; Kesicki, E. A.; Odingo, J.; Parish, T. Validation of the essential ClpP protease in Mycobacterium tuberculosis as a novel drug target. *J. Bacteriol.* **2012**, *194* (3), 663–668.

(84) Brötz-Oesterhelt, H.; Beyer, D.; Kroll, H. P.; Endermann, R.; Ladel, C.; Schroeder, W.; Hinzen, B.; Raddatz, S.; Paulsen, H.; Henninger, K.; et al. Dysregulation of bacterial proteolytic machinery by a new class of antibiotics. *Nat. Med.* **2005**, *11* (10), 1082–1087.

(85) Michel, K. H.; Kastner, R. E. A54556 Antibiotics and process for production thereof. US patent 4492650, 1985.

(86) Kirstein, J.; Hoffmann, A.; Lilie, H.; Schmidt, R.; Helga, R. W.; Heike, B. O.; Mogk, A.; Turgay, K. The antibiotic ADEP reprogrammes ClpP, switching it from a regulated to an uncontrolled protease. *EMBO Mol. Med.* **2009**, *1* (1), 37–49.

(87) Lee, B. G.; Park, E. Y.; Lee, K. E.; Jeon, H.; Sung, K. H.; Paulsen, H.; Rübsamen-Schaeff, H.; Brötz-Oesterhelt, H.; Song, H. K. Structures of ClpP in complex with acyldepsipeptide antibiotics reveal its activation mechanism. *Nat. Struct. Mol. Biol.* **2010**, *17* (4), 471–478.

(88) Li, D. H. S.; Chung, Y. S.; Gloyd, M.; Joseph, E.; Ghirlando, R.; Wright, G. D.; Cheng, Y. Q.; Maurizi, M. R.; Guarné, A.; Ortega, J. Acyldepsipeptide antibiotics induce the formation of a structured axial channel in ClpP: A model for the ClpX/ClpA-bound state of ClpP. *Chem. Biol.* **2010**, *17* (9), 959–969.

(89) Lavey, N. P.; Coker, J. A.; Ruben, E. A.; Duerfeldt, A. S. Sclerotiamide: the first non-peptide-based natural product activator of bacterial caseinolytic protease P. *J. Nat. Prod.* **2016**, *79* (4), 1193–1197.

(90) López-Otín, C.; Overall, C. M. Protease degradomics: a new challenge for proteomics. *Nat. Rev. Mol. Cell Biol.* **2002**, *3* (7), 509–519.

(91) Patick, A. K.; Potts, K. E. Protease inhibitors as antiviral agents. *Clin. Microbiol. Rev.* **1998**, *11* (4), 614–627.

(92) Miladi, B.; Marjou, A. El; Boeuf, G.; Bouallagui, H.; Dufour, F.; Di Martino, P.; Elm'selmi, A. Oriented immobilization of the tobacco etch virus protease for the cleavage of fusion proteins. *J. Biotechnol.* **2012**, *158* (3), 97–103.

(93) Bhandari, V.; Wong, K. S.; Zhou, J. L.; Mabanglo, M. F.; Batey, R. A.; Houry, W. A. The role of ClpP protease in bacterial pathogenesis and human diseases. *ACS Chem. Biol.* **2018**, *13*, 1413–1425.

(94) Weibezahn, J.; Schlieker, C.; Bukau, B.; Mogk, A. Characterization of a trap mutant of the AAA+ chaperone ClpB. *J. Biol. Chem.* **2003**, *278* (35), 32608–32617.

(95) Goloubinoff, P.; Mogk, A.; Ben Zvi, A. P.; Tomoyasu, T.; Bukau, B. Sequential mechanism of solubilization and refolding of stable protein aggregates by a bichaperone network. *Proc. Natl. Acad. Sci. U. S. A.* **1999**, *96* (24), 13732–13737.

(96) Graham, J. W.; Lei, M. G.; Lee, C. Y. Trapping and identification of cellular substrates of the Staphylococcus aureus ClpC chaperone. *J. Bacteriol.* **2013**, *195* (19), 4506–4516.

(97) Feng, J.; Michalik, S.; Varming, A. N.; Andersen, J. H.; Albrecht, D.; Jelsbak, L.; Krieger, S.; Ohlsen, K.; Hecker, M.; Gerth, U.; et al. Trapping and proteomic identification of cellular substrates of the ClpP protease in staphylococcus aureus. *J. Proteome Res.* **2013**, *12* (2), 547–558.

(98) Flynn, J. M.; Neher, S. B.; Kim, Y. I.; Sauer, R. T.; Baker, T. A. Proteomic discovery of cellular substrates of the ClpXP protease reveals five classes of ClpX-recognition signals. *Mol. Cell* **2003**, *11* (3), 671–683.

(99) Bhat, N. H.; Vass, R. H.; Stoddard, P. R.; Shin, D. K.; Chien, P. Identification of ClpP substrates in Caulobacter crescentus reveals a role for regulated proteolysis in bacterial development. *Mol. Microbiol.* **2013**, *88* (6), 1083–1092.

(100) Van Melderen, L.; Gottesman, S. Substrate sequestration by a proteolytically inactive Lon mutant. *Proc. Natl. Acad. Sci. U. S. A.* **1999**, *96*, 6064–6071.

(101) Westphal, K.; Langklotz, S.; Thomanek, N.; Narberhaus, F. A trapping approach reveals novel substrates and physiological functions of the essential protease FtsH in Escherichia coli. *J. Biol. Chem.* **2012**, *287* (51), 42962–42971.

(102) Tsilibaris, V.; Maenhaut-Michel, G.; Van Melderen, L. Biological roles of the Lon ATP-dependent protease. *Res. Microbiol.* **2006**, *157* (8), 701–713.

(103) Tomoyasu, T.; Gamer, J.; Bukau, B.; Kanemori, M.; Mori, H.; Rutman, A. J.; Oppenheim, A. B.; Yura, T.; Yamanaka, K.; Niki, H.; et al. Escherichia coli FtsH is a membrane-bound, ATP-dependent protease which degrades the heat-shock transcription factor σ32. *EMBO J.* **1995**, *14* (11), 2551–2560.

(104) Herman, C.; Thevenet, D.; D'Ari, R.; Bouloc, P. Degradation of σ32, the heat shock regulator in Escherichia coli, is governed by HflB. *Proc. Natl. Acad. Sci. U. S. A.* **1995**, *92* (8), 3516–3520.

(105) Seong, I. S.; Oh, J. Y.; Yoo, S. J.; Seol, J. H.; Chung, C. H. ATP-dependent degradation of SulA, a cell division inhibitor, by the HslVU protease in Escherichia coli. *FEBS Lett.* **1999**, *456* (1), 211–214.

(106) Kang, M. S.; Kim, S. R.; Kwack, P.; Lim, B. K.; Ahn, S. W.; Rho, Y. M.; Seong, I. S.; Park, S. C.; Eom, S. H.; Cheong, G. W.; et al. Molecular architecture of the ATP-dependent CodWX protease having an N-terminal serine active site. *EMBO J.* **2003**, *22* (12), 2893–2902.

(107) Couturier, C.; Bauer, A.; Rey, A.; Schroif-Dufour, C.; Broenstrup, M. Armeniaspiroles, a new class of antibacterials: antibacterial activities and total synthesis of 5-chloro-Armeniaspirole A. *Bioorg. Med. Chem. Lett.* **2012**, *22* (19), 6292–6296.

(108) Fu, C.; Xie, F.; Hoffmann, J.; Wang, Q.; Bauer, A.; Brönstrup, M.; Mahmud, T.; Müller, R. Armeniaspirol antibiotic biosynthesis: chlorination and oxidative dechlorination steps affording spiro[4.4]non-8-ene. *ChemBioChem* **2019**, *20* (6), 764–769.

(109) Qiao, Y.; Yan, J.; Jia, J.; Xue, J.; Qu, X.; Hu, Y.; Deng, Z.; Bi, H.; Zhu, D. Characterization of the biosynthetic gene cluster for the antibiotic armeniaspirols in streptomyces armeniacus. *J. Nat. Prod.* **2019**, *82* (2), 318–323.

(110) Dufour, C.; Wink, J.; Kurz, M.; Kogler, H.; Olivan, H.; Sablé, S.; Heyse, W.; Gerlitz, M.; Toti, L.; Nußer, A.; et al. Isolation and structural elucidation of armeniaspirols A-C: Potent antibiotics against gram-positive pathogens. *Chem. - A Eur. J.* **2012**, *18* (50), 16123–16128.

(111) Valderrama, K.; Pradel, E.; Firsov, A. M.; Drobecq, H.; Roy, H. B. le; Villemagne, B.; Antonenko, Y. N.; Hartkoorn, R. C. Pyrrolomycins are potent natural protonophores. *Antimicrob. Agents Chemother.* **2019**, *63* (10), e01450-19.

(112) Hughes, C. C.; Prieto-Davo, A.; Jensen, P. R.; Fenical, W. The marinopyrroles, antibiotics of an unprecedented structure class from a marine Streptomyces sp. *Org. Lett.* **2008**, *10* (4), 629–631.

(113) Alvarez-Mico, X.; Jensen, P. R.; Fenical, W.; Hughes, C. C. Chlorizidine, a cytotoxic 5H-pyrrolo[2,1-a]isoindol-5-one-containing alkaloid from a marine Streptomyces sp. *Org. Lett.* **2013**, *15* (5), 988–991.

(114) Andrews, J. M. Determination of minimum inhibitory concentrations. *J. Antimicrob. Chemother.* **2001**, *48* (Suppl 1), 5–16.

(115) French, G. L. Bactericidal agents in the treatment of MRSA infections-the potential role of daptomycin. *J. Antimicrob. Chemother.* **2006**, *58*, 1107–1117.

(116) Michna, R. H.; Commichau, F. M.; Tödter, D.; Zschiedrich, C. P.; Stülke, J. SubtiWiki-A database for the model organism Bacillus subtilis that links pathway, interaction and expression information. *Nucleic Acids Res.* **2014**, *42* (D1), 692–698.

(117) Zhu, B.; Stülke, J. SubtiWiki in 2018: From genes and proteins to functional network annotation of the model organism Bacillus subtilis. *Nucleic Acids Res.* **2018**, *46* (D1), D743–D748.

(118) Peters, J. M.; Colavin, A.; Shi, H.; Czarny, T. L.; Larson, M. H.; Wong, S.; Hawkins, J. S.; Lu, C. H. S.; Koo, B.-M.; Marta, E.; et al. A comprehensive, CRISPR-based functional analysis of essential genes in bacteria. *Cell* **2016**, *165* (6), 1493–1506.

(119) Koo, B. M.; Kritikos, G.; Farelli, J. D.; Todor, H.; Tong, K.; Kimsey, H.; Wapinski, I.; Galardini, M.; Cabal, A.; Peters, J. M.; et al. Construction and analysis of two genome-scale deletion libraries for Bacillus subtilis. *Cell Syst.* **2017**, *4* (3), 291–305.

(120) Cravatt, B. F.; Wright, A. T.; Kozarich, J. W. Activity-based protein profiling: from enzyme chemistry to proteomic chemistry. *Annu. Rev. Biochem.* **2008**, *77*, 383–414.

(121) Deng, H.; Lei, Q.; Wu, Y.; He, Y.; Li, W. Activity-based protein profiling: recent advances in medicinal chemistry. *Eur. J. Med. Chem.* **2020**, *191*, 112151.

(122) Wright, M. H.; Sieber, S. A. Chemical proteomics approaches for identifying the cellular targets of natural products. *Nat. Prod. Rep.* **2016**, *33* (5), 681–708.

(123) Shannon, D. A.; Weerapana, E. Covalent protein modification: the current landscape of residue-specific electrophiles. *Curr. Opin. Chem. Biol.* **2015**, *24*, 18–26.

(124) Jeffery, D. A.; Bogyo, M. Chemical proteomics and its application to drug discovery. *Curr. Opin. Biotechnol.* **2003**, *14* (1), 87–95.

(125) Kolb, H. C.; Finn, M. G.; Sharpless, K. B. Click chemistry: diverse chemical function from a few good reactions. *Angew. Chemie Int. Ed.* **2001**, *40* (11), 2004–2021.

(126) Speers, A. E.; Cravatt, B. F. Profiling enzyme activities in vivo using click chemistry methods. *Chem. Biol.* **2004**, *11* (4), 535–546.

(127) Martell, J.; Weerapana, E. Applications of copper-catalyzed click chemistry in activity-based protein profiling. *Molecules* **2014**, *19* (2), 1378–1393.

(128) Speers, A. E.; Adam, G. C.; Cravatt, B. F. Activity-based protein profiling in vivo using a copper(I)-catalyzed azide-alkyne [3 + 2] cycloaddition. *J. Am. Chem. Soc.* **2003**, *125* (16), 4686–4687.

(129) Speers, A. E.; Cravatt F., B. Activity-Based Protein Profiling (ABPP) and Click Chemistry (CC)-ABPP by MudPIT Mass Spectrometry. *Curr. Protoc. Chem. Biol.* **2009**, *1*, 29–41.

(130) Wang, S.; Tian, Y.; Wang, M.; Wang, M.; Sun, G.; Sun, X. Advanced activity-based protein profiling application strategies for drug development. *Front. Pharmacol.* **2018**, *9*, 353.

(131) Muntel, J.; Fromion, V.; Goelzer, A.; Maa, S.; Mäder, U.; Büttner, K.; Hecker, M.; Becher, D. Comprehensive absolute quantification of the cytosolic proteome of bacillus subtilis by data independent, parallel fragmentation in liquid chromatography/mass spectrometry (LC/MSE). *Mol. Cell. Proteomics* **2014**, *13* (4), 1008–1019.

(132) Gribun, A.; Kimber, M. S.; Ching, R.; Sprangers, R.; Fiebig, K. M.; Houry, W. A. The ClpP double ring tetradecameric protease exhibits plastic ring-ring interactions, and the N termini of its subunits form flexible loops that are essential for ClpXP and ClpAP complex formation. *J. Biol. Chem.* **2005**, *280* (16), 16185–16196.

(133) Woo, K. M.; Chung, W. J.; Ha, D. B.; Goldberg, A. L.; Chung, C. H. Protease Ti from Escherichia coli requires ATP hydrolysis for protein breakdown but not for hydrolysis of small peptides. *J. Biol. Chem.* **1989**, *264* (4), 2088–2091.

(134) Yoo, S. J.; Seol, J. H.; Shin, D. H.; Rohrwild, M.; Kang, M. S.; Tanaka, K.; Goldberg, A. L.; Chung, C. H. Purification and characterization of the heat shock proteins HsIV and HsIU that form a new ATP-dependent protease in Escherichia coli. *J. Biol. Chem.* **1996**, *271* (24), 14035–14040.

(135) Strelow, J.; Dewe, W.; Iversen, P. W.; Brooks, H. B.; Radding, J. A.; McGee, J.; Weidner, J. *Mechanism of Action Assays for Enzymes*; Eli Lilly & Company and the National Center for Advancing Translational Sciences, 2004.

(136) Yung-Chi, C.; Prusoff, W. H. Relationship between the inhibition constant (KI) and the concentration of inhibitor which causes 50 per cent inhibition (I50) of an enzymatic reaction. *Biochem. Pharmacol.* **1973**, *22* (23), 3099–3108.

(137) Lanzetta, P. A.; Alvarez, L. J.; Reinach, P. S.; Candia, O. A. An improved assay for nanomole amounts of inorganic phosphate. *Anal. Biochem.* **1979**, *100* (1), 95–97.

(138) Doyle, S. M.; Wickner, S. Hsp104 and ClpB: protein disaggregating machines. *Trends*

Biochem. Sci. **2009**, *34* (1), 40–48.

(139) Elsholz, A. K. W.; Birk, M. S.; Charpentier, E.; Turgay, K. Functional diversity of AAA+ protease complexes in Bacillus subtilis. *Front. Mol. Biosci.* **2017**, *4* (44), 1–15.

(140) Frees, D.; Thomsen, L. E.; Ingmer, H. Staphylococcus aureus ClpYQ plays a minor role in stress survival. *Arch. Microbiol.* **2005**, *183* (4), 286–291.

(141) Gray, D. A.; Wenzel, M. Multitarget approaches against multiresistant superbugs. *ACS Infect. Dis.* **2020**, *6* (6), 1346–1365.

(142) Böttcher, T.; Sieber, S. A. Structurally refined β-lactones as potent inhibitors of devastating bacterial virulence factors. *ChemBioChem* **2009**, *10* (4), 663–666.

(143) Culp, E.; Wright, G. D. Bacterial proteases, untapped antimicrobial drug targets. *J. Antibiot. (Tokyo).* **2017**, *70* (4), 366–377.

(144) Moreno-Cinos, C.; Goossens, K.; Salado, I. G.; Van Der Veken, P.; De Winter, H.; Augustyns, K. ClpP protease, a promising antimicrobial target. *Int. J. Mol. Sci.* **2019**, *20* (9), 2232.

(145) Wright, G. D. Something old, something new: Revisiting natural products in Antibiotic drug discovery. *Can. J. Microbiol.* **2014**, *60* (3), 147–154.

(146) Böttcher, T.; Sieber, S. A. β-lactones decrease the intracellular virulence of Listeria monocytogenes in macrophages. *ChemMedChem* **2009**, *4* (8), 1260–1263.

(147) Malik, I. T.; Brötz-Oesterhelt, H. Conformational control of the bacterial Clp protease by natural product antibiotics. *Nat. Prod. Rep.* **2017**, *34* (7), 815–831.

(148) Gominet, M.; Seghezzi, N.; Mazodier, P. Acyl depsipeptide (ADEP) resistance in streptomyces. *Microbiology* **2011**, *157* (8), 2226–2234.

(149) Schubert, O. T.; Röst, H. L.; Collins, B. C.; Rosenberger, G.; Aebersold, R. Quantitative proteomics: challenges and opportunities in basic and applied research. *Nat. Protoc.* **2017**, *12* (7), 1289–1294.

(150) Wasinger, V. C.; Zeng, M.; Yau, Y. Current Status and Advances in Quantitative Proteomic Mass Spectrometry. *Int. J. Proteomics* **2013**, *2013*, 1–12.

(151) Boersema, P. J.; Raijmakers, R.; Lemeer, S.; Mohammed, S.; Heck, A. J. R. Multiplex peptide stable isotope dimethyl labeling for quantitative proteomics. *Nat. Protoc.* **2009**, *4* (4), 484–494.

(152) Boersema, P. J.; Aye, T. T.; Van Veen, T. A. B.; Heck, A. J. R.; Mohammed, S. Triplex protein quantification based on stable isotope labeling by peptide dimethylation applied to cell and tissue lysates. *Proteomics* **2008**, *8* (22), 4624–4632.

(153) Eymann, C.; Dreisbach, A.; Albrecht, D.; Bernhardt, J.; Becher, D.; Gentner, S.; Tam, L. T.; Büttner, K.; Buurman, G.; Scharf, C.; et al. A comprehensive proteome map of growing Bacillus subtilis cells. *Proteomics* **2004**, *4*, 2849–2876.

(154) Bandow, J. E.; Brötz, H.; Leichert, L. I. O.; Labischinski, H.; Hecker, M. Proteomic approach to understanding antibiotic action. *Antimicrob. Agents Chemother.* **2003**, *47* (3), 948–955.

(155) Stepanek, J. J.; Lukežič, T.; Teichert, I.; Petković, H.; Bandow, J. E. Dual mechanism of action of the atypical tetracycline chelocardin. *Biochim. Biophys. Acta - Proteins Proteomics* **2016**, *1864* (6), 645–654.

(156) Wenzel, M.; Patra, M.; Albrecht, D.; Chen, D. Y. K.; Nicolaou, K. C.; Metzler-Nolte, N.; Bandow, J. E. Proteomic signature of fatty acid biosynthesis inhibition available for in vivo mechanism-of-action studies. *Antimicrob. Agents Chemother.* **2011**, *55* (6), 2590–2596.

(157) Wenzel, M.; Kohl, B.; Münch, D.; Raatschen, N.; Albada, H. B.; Hamoen, L.; Metzler-Nolte, N.; Sahl, H.-G.; Bandow, J. E. Proteomic response of Bacillus subtilis to lantibiotics reflects differences in interaction with the cytoplasmic membrane. *Antimicrob. Agents Chemother.* **2012**, *56* (11), 5749–5757.

(158) Freiberg, C.; Brunner, N.; Macko, L.; Fischer, H. P. Discovering Antibiotic Efficacy Biomarkers. *Mol. Cell. Proteomics* **2006**, *5* (12), 2326–2335.

(159) Sender, U.; Bandow, J.; Engelmann, S.; Lindequist, U.; Hecker, M. Proteomic signatures for daunomycin and adriamycin in Bacillus subtilis. *Pharmazie* **2004**, *59* (1), 65–70.

(160) Jawetz, E. The use of combinations of antimicrobial drugs. *Annu. Rev. Pharmacol.* **1968**, *8*, 151–170.

(161) Yeh, P. J.; Hegreness, M. J.; Aiden, A. P.; Kishony, R. Drug interactions and the evolution of antibiotic resistance. *Nat. Rev. Microbiol.* **2009**, *7* (6), 460–466.

(162) Hall, M. J.; Middleton, R. F.; Westmacott, D. The fractional inhibitory concentration (FIC) index as a measure of synergy. *J. Antimicrob. Chemother.* **1983**, *11* (5), 427–433.

(163) Odds, F. C. Synergy, antagonism, and what the chequerboard puts between them. *J. Antimicrob. Chemother.* **2003**, *52* (1), 1.

(164) Johnson, M. D.; MacDougall, C.; Ostrosky-Zeichner, L.; Perfect, J. R.; Rex, J. H. Combination antifungal therapy. *Antimicrob. Agents Chemother.* **2004**, *48* (3), 693–715.

(165) Errington, J.; Wu, L. J. Cell cycle machinery in Bacillus subtilis. *Subcell. Biochem.* **2017**, *84*, 67–101.

(166) Bottomley, A. L.; Liew, A. T. F.; Kusuma, K. D.; Peterson, E.; Seidel, L.; Foster, S. J.;

Harry, E. J. Coordination of chromosome segregation and cell division in Staphylococcus aureus. *Front. Microbiol.* **2017**, *8*, 1575.

(167) Sugimoto, S.; Saruwatari, K.; Higashi, C.; Sonomoto, K. The proper ratio of GrpE to DnaK is important for protein quality control by the DnaK–DnaJ–GrpE chaperone system and for cell division. *Microbiology* **2008**, *154* (7), 1876–1885.

(168) Sinai, L.; Rosenberg, A.; Segev, E.; Correspondence, B.-Y.; Smith, Y.; Ben-Yehuda, S. The Molecular Timeline of a Reviving Bacterial Spore. *Mol. Cell* **2015**, *57*, 695–707.

(169) Vega-Cabrera, L. A.; Guerrero, A.; Rodríguez-Mejía, J. L.; Tabche, M. L.; Wood, C. D.; Gutiérrez-Rios, R. M.; Merino, E.; Pardo-López, L. Analysis of Spo0M function in Bacillus subtilis. *PLoS One* **2017**, *12* (2), e0172737.

(170) Neher, S. B.; Villén, J.; Oakes, E. C.; Bakalarski, C. E.; Sauer, R. T.; Gygi, S. P.; Baker, T. A. Proteomic profiling of ClpXP substrates after DNA damage reveals extensive instability within SOS regulon. *Mol. Cell* **2006**, *22* (2), 193–204.

(171) Gerth, U.; Kock, H.; Kusters, I.; Michalik, S.; Switzer, R. L.; Hecker, M. Clp-dependent proteolysis down-regulates central metabolic pathways in glucose-starved Bacillus subtilis. *J. Bacteriol.* **2008**, *190* (1), 321–331.

(172) Dajkovic, A.; Lan, G.; Sun, S. X.; Wirtz, D.; Lutkenhaus, J. MinC Spatially Controls Bacterial Cytokinesis by Antagonizing the Scaffolding Function of FtsZ. *Curr. Biol.* **2008**, *18* (4), 235–244.

(173) Scheffers, D. J. The effect of MinC on FtsZ polymerization is pH dependent and can be counteracted by ZapA. *FEBS Lett.* **2008**, *582* (17), 2601–2608.

(174) Blasios, V.; Bisson-Filho, A. W.; Castellen, P.; Nogueira, M. L. C.; Bettini, J.; Portugal, R. V.; Zeri, A. C. M.; Gueiros-Filho, F. J. Genetic and Biochemical Characterization of the MinC-FtsZ Interaction in Bacillus subtilis. *PLoS One* **2013**, *8* (4), e60690.

(175) Marston, A. L.; Errington, J. Selection of the midcell division site in Bacillus subtilis through MinD-dependent polar localization and activation of MinC. *Mol. Microbiol.* **1999**, *33* (1), 84–96.

(176) Eswaramoorthy, P.; Erb, M. L.; Gregory, J. A.; Silverman, J.; Pogliano, K.; Pogliano, J.; Ramamurthi, K. S. Cellular architecture mediates DivIVA ultrastructure and regulates min activity in Bacillus subtilis. *MBio* **2011**, *2* (6), e00257-11.

(177) Jana, B.; Tao, L.; Biswas, I. Strain-Dependent Recognition of a Unique Degradation Motif by ClpXP in Streptococcus mutans. *mSphere* **2016**, *1* (6), e00287-16.

(178) Yu, Y.; Yan, F.; He, Y.; Qin, Y.; Chen, Y.; Chai, Y.; Guo, J. H. The ClpY-ClpQ protease regulates multicellular development in Bacillus subtilis. *Microbiology* **2018**, *164* (5), 848–862.

(179) Trip, E. N.; Veening, J.; Stewart, E. J.; Errington, J.; Scheffers, D. Balanced transcription of cell division genes in Bacillus subtilis as revealed by single cell analysis. *Environ. Microbiol.* **2013**, *15* (12), 3196–3209.

(180) Begg, K.; Nikolaichik, Y.; Crossland, N.; Donachie, W. D. Roles of FtsA and FtsZ in activation of division sites. *J. Bacteriol.* **1998**, *180* (4), 881–884.

(181) Dai, K.; Lutkenhaus, J. The proper ratio of FtsZ to FtsA is required for cell division to occur in Escherichia coli. *J. Bacteriol.* **1992**, *174* (19), 6145–6151.

(182) Dewar, S. J.; Begg, K. J.; Donachie, W. D. Inhibition of cell division initiation by an imbalance in the ratio of FtsA to FtsZ. *J. Bacteriol.* **1992**, *174* (19), 6314–6316.

(183) Ma, X.; Ehrhardt, D. W.; Margolin, W. Colocalization of cell division proteins FtsZ and FtsA to cytoskeletal structures in living Escherichia coli cells by using green fluorescent protein. *Proc. Natl. Acad. Sci. U. S. A.* **1996**, *93* (23), 12998–13003.

(184) Cha, J. H.; Stewart, G. C. The DivIVA minicell locus of Bacillus subtilis. *J. Bacteriol.* **1997**, *179* (5), 1671–1683.

(185) Levin, P. A.; Schwartz, R. L.; Grossman, A. D. Polymer stability plays an important role in the positional regulation of FtsZ. *J. Bacteriol.* **2001**, *183* (18), 5449–5452.

(186) Szwedziak, P.; Löwe, J. Do the divisome and elongasome share a common evolutionary past? *Curr. Opin. Microbiol.* **2013**, *16* (6), 745–751.

(187) Abhayawardhane, Y.; Stewart, G. C. Bacillus subtilis possesses a second determinant with extensive sequence similarity to the escherichia coli mreB morphogene. *J. Bacteriol.* **1995**, *177* (3), 765–773.

(188) Carballido-López, R.; Formstone, A.; Li, Y.; Ehrlich, S. D.; Noirot, P.; Errington, J. Actin Homolog MreBH Governs Cell Morphogenesis by Localization of the Cell Wall Hydrolase LytE. *Dev. Cell* **2006**, *11* (3), 399–409.

(189) Salje, J.; van den Ent, F.; de Boer, P.; Löwe, J. Direct Membrane Binding by Bacterial Actin MreB. *Mol. Cell* **2011**, *43* (3), 478–487.

(190) Garti-Levi, S.; Hazan, R.; Kain, J.; Fujita, M.; Ben-Yehuda, S. The FtsEX ABC transporter directs cellular differentiation in Bacillus subtilis. *Mol. Microbiol.* **2008**, *69* (4), 1018–1028.

(191) De Leeuw, E.; Graham, B.; Phillips, G. J.; Ten Hagen-Jongman, C. M.; Oudega, B.; Luirink, J. Molecular characterization of Escherichia coli FtsE and FtsX. *Mol. Microbiol.* **1999**, *31* (3), 983–993.

(192) Yamaguchi, H.; Furuhata, K.; Fukushima, T.; Yamamoto, H.; Sekiguchi, J. Characterization of a new Bacillus subtilis peptidoglycan hydrolase gene, yvcE (named

cwlO), and the enzymatic properties of its encoded protein. *J. Biosci. Bioeng.* **2004**, *98* (3), 174–181.

(193) Kawai, Y.; Daniel, R. A.; Errington, J. Regulation of cell wall morphogenesis in Bacillus subtilis by recruitment of PBP1 to the MreB helix. *Mol. Microbiol.* **2009**, *71* (5), 1131–1144.

(194) Kawai, Y.; Asai, K.; Errington, J. Partial functional redundancy of MreB isoforms, MreB, Mbl and MreBHp in cell morphogenesis of Bacillus subtilis. *Mol. Microbiol.* **2009**, *73* (4), 719–731.

(195) Wachi, M.; Matsuhashi, M. Negative control of cell division by mreB, a gene that functions in determining the rod shape of Escherichia coli cells. *J. Bacteriol.* **1989**, *171* (6), 3123–3127.

(196) Ranjit, D. K.; Liechti, G. W.; Maurelli, A. T. Chlamydial MreB directs cell division and peptidoglycan synthesis in Escherichia coli in the absence of FtsZ activity. *MBio* **2020**, *11* (1).

(197) Schirner, K.; Errington, J. Influence of heterologous MreB proteins on cell morphology of Bacillus subtilis. *Microbiology* **2009**, *155* (11), 3611–3621.

(198) Brunet, Y. R.; Wang, X.; Rudner, D. Z. SweC and SweD are essential co-factors of the FtsEX-CwlO cell wall hydrolase complex in Bacillus subtilis. *PLoS Genet.* **2019**, *15* (8), e1008296.

(199) Do, T.; Page, J. E.; Walker, S. Uncovering the activities, biological roles, and regulation of bacterial cell wall hydrolases and tailoring enzymes. *J. Biol. Chem.* **2020**, *295* (10), 3347–3361.

(200) Hughes, A. C.; Subramanian, S.; Dann, C. E.; Kearns, D. B. The C-terminal region of Bacillus subtilis SwrA is required for activity and adaptor-dependent LonA proteolysis. *J. Bacteriol.* **2018**, *200* (6), e00659-17.

(201) Mukherjee, S.; Bree, A. C.; Liu, J.; Patrick, J. E.; Chien, P.; Kearns, D. B. Adaptor-mediated Lon proteolysis restricts Bacillus subtilis hyperflagellation. *Proc. Natl. Acad. Sci. U. S. A.* **2015**, *112* (1), 250–255.

(202) Mielich-Süss, B.; Schneider, J.; Lopez, D. Overproduction of flotillin influences cell differentiation and shape in Bacillus subtilis. *MBio* **2013**, *4* (6), e00719-13.

(203) Miethke, M.; Hecker, M.; Gerth, U. Involvement of Bacillus subtilis ClpE in CtsR degradation and protein quality control. *J. Bacteriol.* **2006**, *188* (13), 4610–4619.

(204) Shajani, Z.; Sykes, M. T.; Williamson, J. R. Assembly of bacterial ribosomes. *Annu. Rev. Biochem.* **2011**, *80* (1), 501–526.

(205) Corrigan, R. M.; Bellows, L. E.; Wood, A.; Gründling, A. PpGpp negatively impacts ribosome assembly affecting growth and antimicrobial tolerance in Gram-positive bacteria. *Proc. Natl. Acad. Sci.* **2016**, *113* (12), E1710–E1719.

(206) Irving, S. E.; Corrigan, R. M. Triggering the stringent response: signals responsible for activating (p)ppGpp synthesis in bacteria. *Microbiology* **2018**, *164* (3), 268–276.

(207) Starosta, A. L.; Lassak, J.; Jung, K.; Wilson, D. N. The bacterial translation stress response. *FEMS Microbiol. Rev.* **2014**, *38* (6), 1172–1201.

(208) Ollinger, J.; Song, K. B.; Antelmann, H.; Hecker, M.; Helmann, J. D. Role of the Fur regulon in iron transport in Bacillus subtilis. *J. Bacteriol.* **2006**, *188* (10), 3664–3673.

(209) Miethke, M.; Westers, H.; Blom, E.-J.; Kuipers, O. P.; Marahiel, M. A. Iron starvation triggers the stringent response and induces amino acid biosynthesis for bacillibactin production in Bacillus subtilis. *J. Bacteriol.* **2006**, *188* (24), 8655–8657.

(210) Kobayashi, K.; Ehrlich, S. D.; Albertini, A.; Amati, G.; Andersen, K. K.; Arnaud, M.; Asai, K.; Ashikaga, S.; Aymerich, S.; Bessieres, P.; et al. Essential Bacillus subtilis genes. *Proc. Natl. Acad. Sci.* **2003**, *100* (8), 4678–4683.

(211) Sprinzl, M. Elongation factor Tu: a regulatory GTPase with an integrated effector. *Trends Biochem. Sci.* **1994**, *19* (6), 245–250.

(212) Giegé, R.; Springer, M. Aminoacyl-tRNA synthetases in the bacterial world. *EcoSal Plus* **2016**, *7* (1), 1–83.

(213) Klaeger, S.; Gohlke, B.; Perrin, J.; Gupta, V.; Heinzlmeir, S.; Helm, D.; Qiao, H.; Bergamini, G.; Handa, H.; Savitski, M. M.; et al. Chemical proteomics reveals ferrochelatase as a common off-target of kinase inhibitors. *ACS Chem. Biol.* **2016**, *11* (5), 1245–1254.

(214) Potter, K. D.; Merlino, N. M.; Jacobs, T.; Gollnick, P. TRAP binding to the Bacillus subtilis trp leader region RNA causes efficient transcription termination at a weak intrinsic terminator. *Nucleic Acids Res.* **2011**, *39* (6), 2092–2102.

(215) Yang, W.-J.; Yanofsky, C. Effects of Tryptophan Starvation on Levels of the trp RNA-Binding Attenuation Protein (TRAP) and Anti-TRAP Regulatory Protein and Their Influence on trp Operon Expression in Bacillus subtilis. *J. Bacteriol.* **2005**, *187* (6), 1884–1891.

(216) Hobley, L.; Ostrowski, A.; Rao, F. V.; Bromley, K. M.; Porter, M.; Prescott, A. R.; MacPhee, C. E.; Van Aalten, D. M. F.; Stanley-Wall, N. R. BslA is a self-assembling bacterial hydrophobin that coats the Bacillus subtilis biofilm. *Proc. Natl. Acad. Sci. U. S. A.* **2013**, *110* (33), 13600–13605.

(217) Girish, T. S.; Gopal, B. Crystal structure of Staphylococcus aureus metallopeptidase

(Sapep) reveals large domain motions between the manganese-bound and apo-states. *J. Biol. Chem.* **2010**, *285* (38), 29406–29415.

(218) Lesniak, J.; Barton, W. A.; Nikolov, D. B. Structural and functional features of the *Escherichia coli* hydroperoxide resistance protein OsmC. *Protein Sci.* **2003**, *12* (12), 2838–2843.

(219) Auger, S.; Gomez, M. P.; Danchin, A.; Martin-Verstraete, I. The PatB protein of Bacillus subtilis is a C-S-lyase. *Biochimie* **2005**, *87* (2), 231–238.

(220) Gentry-Weeks, C. R.; Spokes, J.; Thompson, J. β-Cystathionase from *Bordetella avium*. *J. Biol. Chem.* **1995**, *270* (13), 7695–7702.

(221) Ejim, L. J.; Blanchard, J. E.; Koteva, K. P.; Sumerfield, R.; Elowe, N. H.; Chechetto, J. D.; Brown, E. D.; Junop, M. S.; Wright, G. D. Inhibitors of bacterial cystathionine β-lyase: leads for new antimicrobial agents and probes of enzyme structure and function. *J. Med. Chem.* **2007**, *50* (4), 755–764.

(222) Haranahalli, K.; Tong, S.; Ojima, I. Recent advances in the discovery and development of antibacterial agents targeting the cell-division protein FtsZ. *Bioorg. Med. Chem* **2016**, *24* (24), 6354–6369.

(223) Sass, P.; Brötz-Oesterhelt, H. Bacterial cell division as a target for new antibiotics. *Curr. Opin. Microbiol.* **2013**, *16* (5), 522–530.

(224) Tommasi, R.; Brown, D. G.; Walkup, G. K.; Manchester, J. I.; Miller, A. A. ESKAPEing the labyrinth of antibacterial discovery. *Nat. Rev. Drug Discov.* **2015**, *14* (8), 529–542.

(225) Pawlowski, A. C.; Johnson, J. W.; Wright, G. D. Evolving medicinal chemistry strategies in antibiotic discovery. *Curr. Opin. Biotechnol.* **2016**, *42*, 108–117.

(226) Lima, L. M.; Silva, B. N. M. da; Barbosa, G.; Barreiro, E. J. β-lactam antibiotics: an overview from a medicinal chemistry perspective. *Eur. J. Med. Chem.* **2020**, *208*, 112829.

(227) Ying, L.; Tang, D. Recent advances in the medicinal chemistry of novel erythromycin-derivatized antibiotics. *Curr. Top. Med. Chem.* **2010**, *10* (14), 1441–1469.

(228) Kharel, M. K.; Nybo, S. E.; Shepherd, M. D.; Rohr, J. Cloning and characterization of the ravidomycin and chrysomycin biosynthetic gene clusters. *ChemBioChem* **2010**, *11* (4), 523–532.

(229) Chang, Z.; Sitachitta, N.; Rossi, J. V.; Roberts, M. A.; Flatt, P. M.; Jia, J.; Sherman, D. H.; Gerwick, W. H. Biosynthetic pathway and gene cluster analysis of curacin A, an antitubulin natural product from the tropical marine cyanobacterium Lyngbya majuscula. *J. Nat. Prod.* **2004**, *67* (8), 1356–1367.

(230) Fudou, R.; Iizuka, T.; Yamanaka, S. Haliangicin, a novel antifungal metabolite produced

by a marine myxobacterium. 1. Fermentation and biological characteristics. *J. Antibiot.* **2001**, *54* (2), 149–152.

(231) Edwards, D. J.; Marquez, B. L.; Nogle, L. M.; McPhail, K.; Goeger, D. E.; Roberts, M. A.; Gerwick, W. H. Structure and biosynthesis of the Jamaicamides, new mixed polyketide-peptide neurotoxins from the marine cyanobacterium Lyngbya majuscula. *Chem. Biol.* **2004**, *11* (6), 817–833.

(232) Cheng, X. C.; Kihara, T.; Ying, X.; Uramoto, M.; Osada, H.; Kusakabe, H.; Wang, B. N.; Kobayashi, Y.; Ko, K.; Yamaguchi, I.; et al. A new antibiotic, tautomycetin. *J. Antibiot.* **1989**, *42* (1), 141–144.

(233) Cheng, X.-C.; Ubukata, M.; Isono, K. The structure of tautomycetin, a dialkylmaleic anhydride antibiotic. *J. Antibiot.* **1990**, *43* (7), 890–896.

(234) Klar, U.; Buchmann, B.; Schwede, W.; Skuballa, W.; Hoffmann, J.; Lichtner, R. B. Total synthesis and antitumor activity of ZK-EPO: the Ffirst fully synthetic epothilone in clinical development. *Angew. Chemie Int. Ed.* **2006**, *45* (47), 7942–7948.

(235) Klar, U.; Hoffmann, J.; Giurescu, M. Sagopilone (ZK-EPO): From a natural product to a fully synthetic clinical development candidate. *Expert Opin. Investig. Drugs* **2008**, *17* (11), 1735–1748.

(236) King, J. M.; Kulhankova, K.; Stach, C. S.; Vu, B. G.; Salgado-Pabón, W. Phenotypes and virulence among Staphylococcus aureus USA100, USA200, USA300, USA400, and USA600 clonal lineages. *mSphere* **2016**, *1* (3), e00071-16.

(237) Copeland, R. A. *Evaluation of Enzyme Inhibitors in Drug Discovery: A Guide for Medicinal Chemists and Pharmacologists*; Hoboken, NJ, USA, 2005.

(238) Shoichet, B. K. Interpreting steep dose-response curves in early inhibitor discovery. *J. Med. Chem.* **2006**, *49* (25), 7274–7277.

(239) Straus, O. H.; Goldstein, A.; Plachte, F. L. Zone behavior of enzymes: Illustrated by the effect of dissociation constant and dilution on the system cholinesterase-physostigmine. *J. Gen. Physiol.* **1943**, *26* (6), 559–585.

(240) Goldstein, A. The mechanism of enzyme-inhibitor-substrate reactions. *J. Gen. Physiol.* **1944**, *27* (6), 529–580.

(241) Stahlhut, S. G.; Alqarzaee, A. A.; Jensen, C.; Fisker, N. S.; Pereira, A. R.; Pinho, M. G.; Thomas, V. C.; Frees, D. The ClpXP protease is dispensable for degradation of unfolded proteins in Staphylococcus aureus. *Sci. Rep.* **2017**, *7*, 11739.

(242) Michel, A.; Agerer, F.; Hauck, C. R.; Herrmann, M.; Ullrich, J.; Hacker, J.; Ohlsen, K. Global regulatory impact of ClpP protease of Staphylococcus aureus on regulons involved in virulence, oxidative stress response, autolysis, and DNA repair. *J. Bacteriol.* **2006**, *188*

(16), 5783–5796.

(243) Christensen, W. B. Urea decomposition as a means of differentiating Proteus and Paracolon cultures from each other and from Salmonella and Shigella types. *J. Bacteriol.* **1946**, *52* (4), 461–466.

(244) Gao, P.; Ho, P. L.; Yan, B.; Sze, K. H.; Davies, J.; Kao, R. Y. T. Suppression of Staphylococcus aureus virulence by a small-molecule compound. *Proc. Natl. Acad. Sci. U. S. A.* **2018**, *115* (31), 8003–8008.

(245) Davis, L.; Chin, J. W. Designer proteins: applications of genetic code expansion in cell biology. *Nat. Rev. Mol. Cell Biol.* **2012**, *13* (3), 168–182.

(246) Neumann-Staubitz, P.; Neumann, H. The use of unnatural amino acids to study and engineer protein function. *Curr. Opin. Struct. Biol.* **2016**, *38*, 119–128.

(247) Xie, J.; Schultz, P. G. Adding amino acids to the genetic repertoire. *Curr. Opin. Chem. Biol.* **2005**, *9* (6), 548–554.

(248) Wang, L.; Brock, A.; Herberich, B.; Schultz, P. G. Expanding the genetic code of Escherichia coli. *Science (80-.).* **2001**, *292* (5516), 498–500.

(249) Hao, B.; Gong, W.; Ferguson, T. K.; James, C. M.; Krzycki, J. A.; Chan, M. K. A New UAG-Encoded Residue in the Structure of a Methanogen Methyltransferase. *Science (80-.).* **2002**, *296* (5572), 1462–1466.

(250) Srinivasan, G.; James, C. M.; Krzycki, J. A. Pyrrolysine encoded by UAG in archaea: Charging of a UAG-decoding specialized tRNA. *Science (80-.).* **2002**, *296* (5572), 1459–1462.

(251) Blight, S. K.; Larue, R. C.; Mahapatra, A.; Longstaff, D. G.; Chang, E.; Zhao, G.; Kang, P. T.; Green-Church, K. B.; Chan, M. K.; Krzycki, J. A. Direct charging of tRNACUA with pyrrolysine in vitro and in vivo. *Nature* **2004**, *431* (7006), 333–335.

(252) Huguenin-Dezot, N.; Alonzo, D. A.; Heberlig, G. W.; Mahesh, M.; Nguyen, D. P.; Dornan, M. H.; Boddy, C. N.; Schmeing, T. M.; Chin, J. W. Trapping biosynthetic acyl-enzyme intermediates with encoded 2,3-diaminopropionic acid. *Nature* **2019**, *565*, 112–117.

(253) Dougherty, W. G.; Parks, T. D.; Cary, S. M.; Bazan, J. F.; Fletterick, R. J. Characterization of the catalytic residues of the tobacco etch virus 49-kDa proteinase. *Virology* **1989**, *172* (1), 302–310.

(254) Levin, P. A.; Kurtser, I. G.; Grossman, A. D. Identification and characterization of a negative regulator of FtsZ ring formation in Bacillus subtilis. *Proc. Natl. Acad. Sci.* **1999**, *96* (17), 9642–9647.

(255) Hedstrom, L. Serine protease mechanism and specificity. *Chem. Rev.* **2002**, *102* (12), 4501–4523.

(256) Wals, K.; Ovaa, H. Unnatural amino acid incorporation in E. coli: current and future applications in the design of therapeutic proteins. *Front. Chem.* **2014**, *2* (15), 1–12.

(257) Smolskaya, S.; Andreev, Y. A. Site-specific incorporation of unnatural amino acids into escherichia coli recombinant protein: Methodology development and recent achievement. *Biomolecules* **2019**, *9* (7), 255.

(258) Harding, C. R.; Schroeder, G. N.; Collins, J. W.; Frankel, G. Use of Galleria mellonella as a model organism to study Legionella pneumophila infection. *J. Vis. Exp.* **2013**, No. 81, 50964.

(259) El-Halfawy, O. M.; Czarny, T. L.; Flannagan, R. S.; Day, J.; Bozelli, J. C.; Kuiack, R. C.; Salim, A.; Eckert, P.; Epand, R. M.; McGavin, M. J.; et al. Discovery of an antivirulence compound that reverses β-lactam resistance in MRSA. *Nat. Chem. Biol.* **2020**, *16* (2), 143–149.

(260) Bergin, D.; Reeves, E. P.; Renwick, J.; Wientjes, F. B.; Kavanagh, K. Superoxide production in Galleria mellonella hemocytes: Identification of proteins homologous to the NADPH oxidase complex of human neutrophils. *Infect. Immun.* **2005**, *73* (7), 4161–4170.

Appendices

Appendix I: Supplementary Figures and Tables for Chapter Two

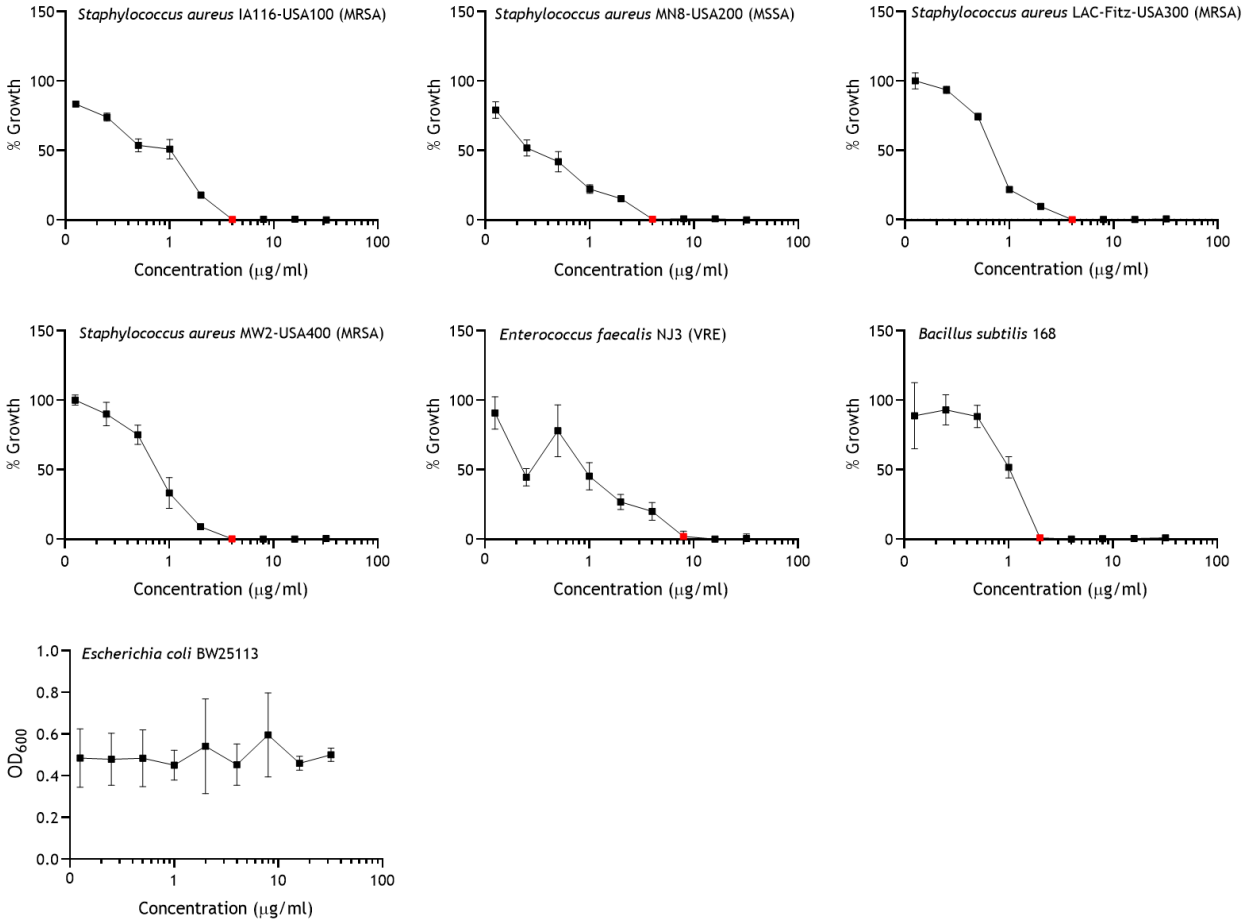

Figure S1. Minimum inhibitory concentration (MIC) assays. Assays of various Gram-positive bacteria and the Gram-negative *E. coli*. **1** is active against Gram-positive bacteria, including clinically relevant MRSA and VRE strains. Data points in red indicate the MIC value. Each MIC was performed in triplicate (n = 3).

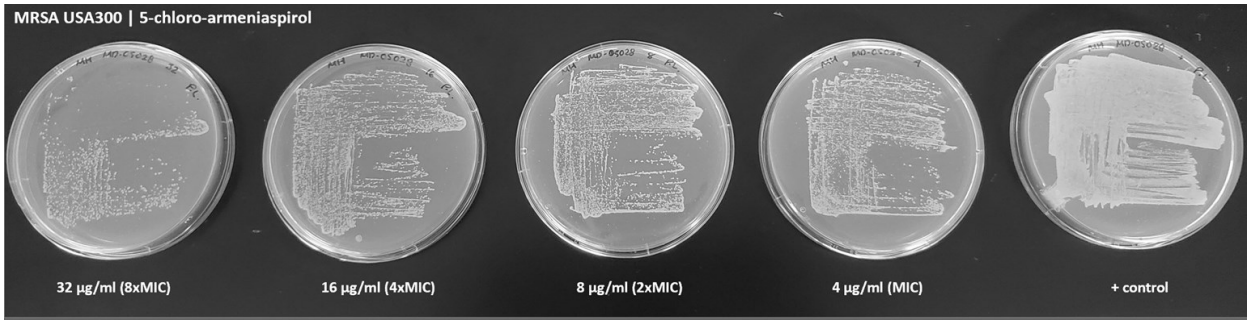

Figure S2. MRSA USA300 minimum bactericidal concentration assay. Reconstitution of MIC subcultures of **1** on non-antibiotic containing plates resulted in growth >32 μg/ml (>8X MIC), indicating a bacteriostatic mechanism of action.

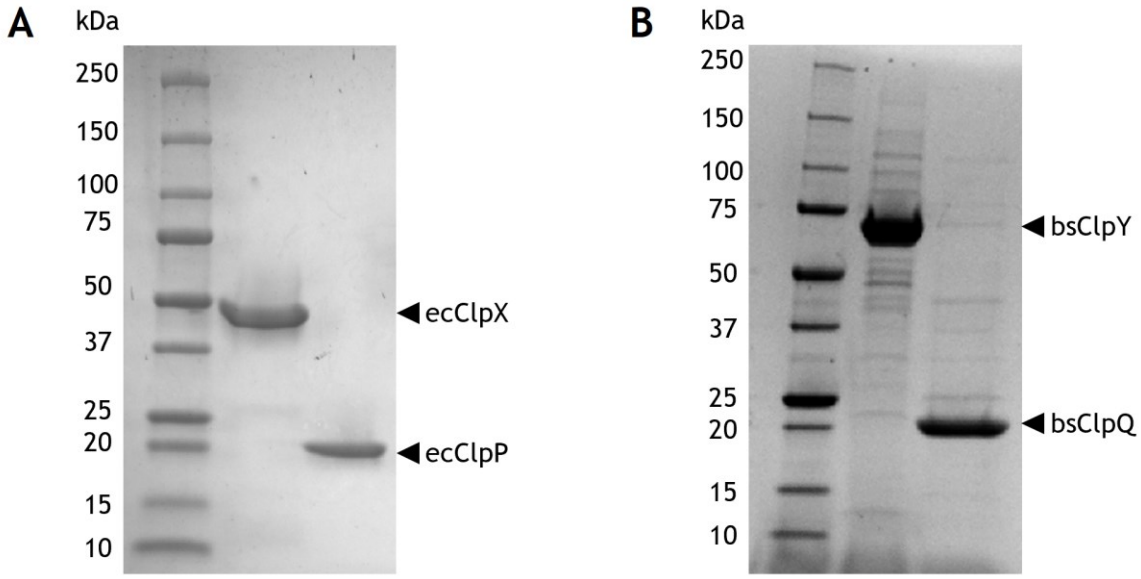

Figure S3. Purification of ecClpX/P and bsClpY/Q. SDS-PAGE following purification of (A) ecClpX and ecClpP and (B) bsClpY and bsClpQ proteins. Proteins were heterologously expressed in *E. coli* BL21(DE3) cells. Bio-Rad 4-20% Mini-PROTEAN TGX™ precast gels were used for SDS-PAGE and subsequently imaged with Coomassie dye. Molecular weight reference standards were obtained using Bio-Rad Precision Plus Protein™ All Blue Prestained Protein Standards.

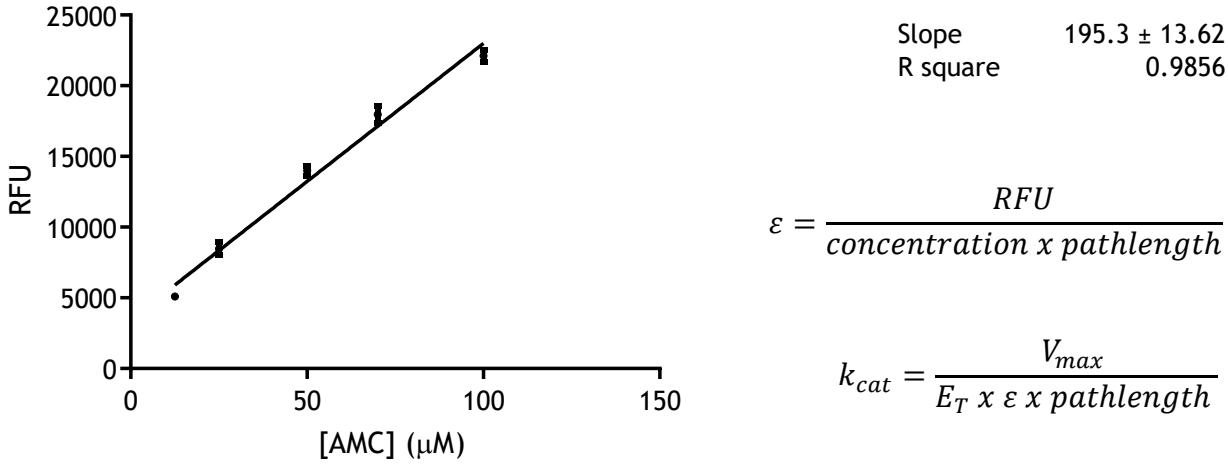

Figure S4. Standard curve used to determine AMC concentration from relative fluorescent units (RFU). This standard curve was used to obtain the extinction coefficient, ε, to calculate k_{cat} of Clp(X)P and ClpYQ proteolysis of an AMC peptidic substrate. Both variables were calculated as indicated by the equations above. A pathlength of 0.246 cm was obtained from the Synergy H4 microplate reader (BioTek). All data points were collected in triplicate (n = 3).

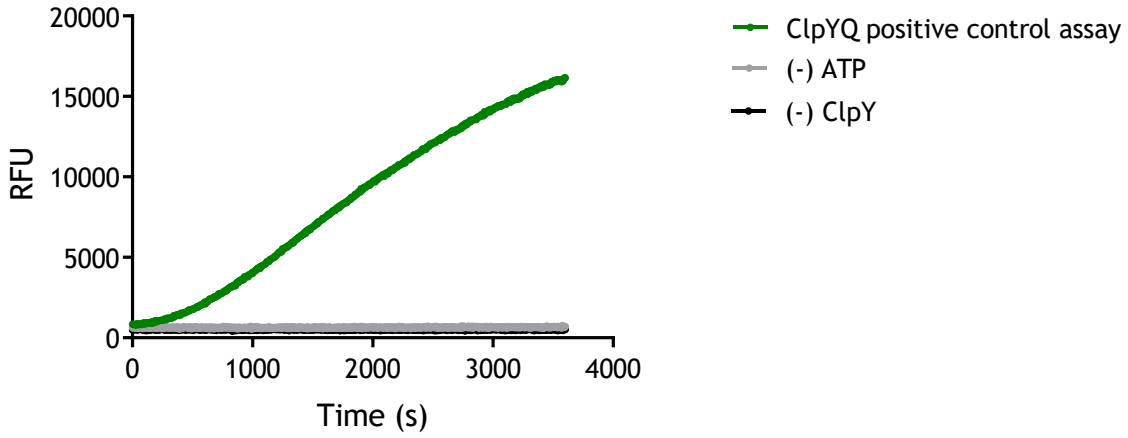

Figure S5. ATP- and ClpY-dependence of bsClpYQ proteolysis activity. Assay conditions for the positive control were set up with 0.25 µM ClpY, 0.25 µM ClpYQ, 1 mM ATP, and 0.1 mM Cbz-Gly-Gly-Leu-AMC (green). The bsClpYQ complex requires ATP to degrade the fluorogenic peptide substrate *in vitro* (grey). Additionally, bsClpQ does not possess peptidase activity in the absence of ClpY (black).

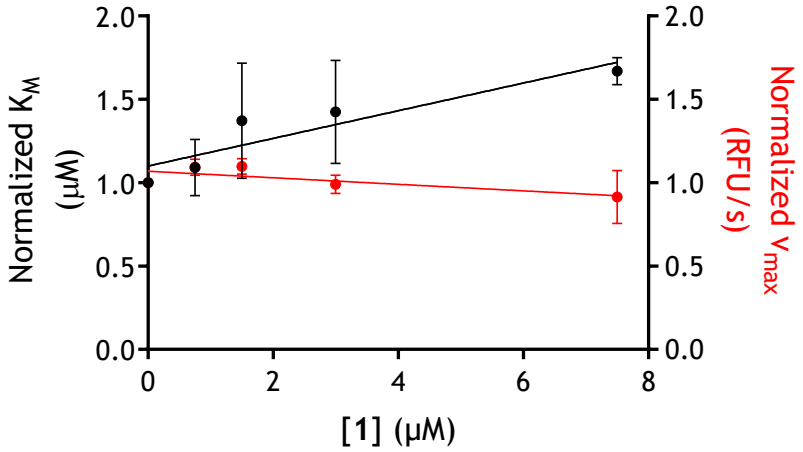

Figure S6. Competitive inhibition of bsClpYQ proteolysis of Cbz-Gly-Gly-Leu-AMC. Normalized plot of Michaelis-Menten parameters showing an increase of K_M and stable v_{max} with increasing inhibitor concentrations, the hallmark of competitive inhibition.

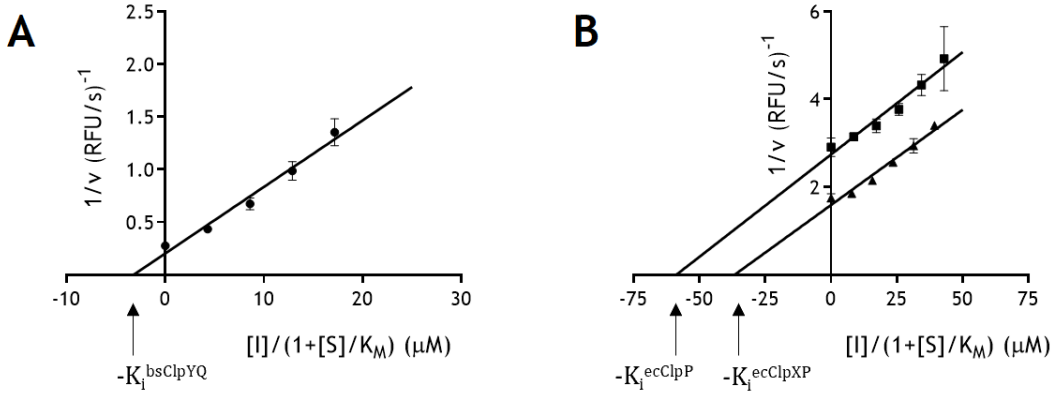

	Theoretical K_i (μM)	$-K_i$ (μM) (95% Confidence Interval)
bsClpYQ	6.524	-3.213 (-8.189 to -0.2279)
ecClpP	52.35	-58.82 (-90.07 to -41.00)
ecClpXP	38.16	-36.68 (-55.54 to -25.14)

Figure S7. Cheng-Prusoff alteration of a Dixon plot. The x-intercepts correspond to inhibitor constants, K_i. (A) The K_i of bsClpYQ is 3.21 μM. (B) The K_i of ecClpP and ecClpXP are 58.82 μM and 36.68 μM, respectively. Each data point was collected in triplicate (n = 3).

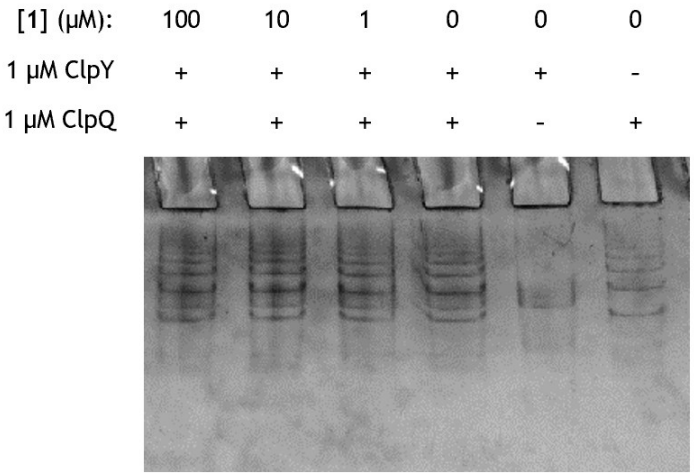

Figure S8. Non-denaturing polyacrylamide gel electrophoresis. *B. subtilis* ClpYQ was incubated with various concentrations of inhibitor **1** under proteolytic assay conditions. Samples were run under non-denaturing conditions (tris/glycine buffer) to visualize multimeric complexes. Bio-Rad 4-20% Mini-PROTEAN TGX™ precast gels were used for PAGE and subsequently imaged with Coomassie dye. No differences in band profiles were observed in absence or presence inhibitor.

Table S1. IC80 values of armeniaspirol A against Gram-positive and Gram-negative bacteria. Armeniaspirol A is active against Gram-positive bacteria at low micromolar concentrations. Armeniaspirol A is not active against Gram-negative bacteria. Data obtained from Couturier, C. et al. *Bioorg. Med. Chem. Lett.* 2012, *22* (19), 6292–6296.

Growth inhibition IC_{80} (μM)	Methicillin-resistant *S. aureus* (MRSA)	Penicillin-resistant *S. pneumoniae* (PRSP)	Vancomycin-resistant *E. faecium* (VRE)	*E. coli*	*P. aeruginosa*
Armeniaspirol A	0.125	2.3	8.2	>30	>30

Table S2. LC-MS/MS results of inhibitor capture in *B. subtilis* cell lysate. Experiments were performed in the absence or presence of 10 μM **2**. A competition assay involving pre-incubation of **1** followed by **2** was performed to establish the most optimal candidates. LC-MS/MS proteomics data was analyzed as described in Chapter Seven.

Accession	**Protein**	**Function**	**Essential**	**Fold-change**	**p-value**
P46906	ArgS	Arginine--tRNA ligase	Yes	2.19937	0.02012
P71014	BslA	Biofilm-surface layer protein A	No	9.99254	0.01058
P80244	ClpP	ATP-dependent Clp protease proteolytic subunit	No	3.32824	0.04084
P32396	HemH	Ferrochelatase	No	10.8583	0.02093
P19466	MtrB	Transcription attenuation protein	No	10.7687	0.00814
Q08432	PatB	Cystathionine beta-lyase	No	3.37298	0.00443
P08838	PtsI	Phosphoenolpyruvate-protein phosphotransferase	No	4.78435	0.00498
P08065	SdhA	Succinate dehydrogenase flavoprotein	No	2.02044	0.01502
P54375	SodA	Superoxide dismutase	No	3.38786	0.02560
P33166	TufA	Elongation factor Tu	Yes	2.19048	0.00001
O31790	YmaD	Uncharacterized protein	No	5.66526	0.01748
O34944	YtjP	Putative dipeptidase	No	6.42074	0.00185

Appendix II: Supplementary Figures and Tables for Chapter Three

Table S3. Comparison of 1-treatment in relation to protein biomarkers of known antibiotic mechanisms. Protein fold-change and p-values are identified for specific proteins associated with certain antibiotic treatments and are shown in tabular format. Each protein marker has been shown to have significant upregulation with its corresponding antibiotic treatment. LC-MS/MS proteomics data was analyzed as described in Chapter Seven.

Accession	Description	Fold-change	p-value
Protein Biosynthesis Biomarkers [ref antibiotics: tetracycline, chelocardin]			
P21464	30S ribosomal protein S2, RpsB	4.101	0.007
P21468	30S ribosomal protein S6, RpsF	7.062	0.002
P42923	50S ribosomal protein L10, RplJ	0.646	0.555
P80868	Elongation factor G, FusA	1.426	0.098
P33166	Elongation factor Tu, TufA	0.906	0.767
Fatty Acid Biosynthesis Biomarkers [ref antibiotics: platencin, platensimycin, cerulenin, triclosan]			
O34746	3-oxoacyl-[acyl-carrier-protein] synthase 3 protein 1, FabHA	0.614	0.412
O34340	3-oxoacyl-[acyl-carrier-protein] synthase 2, FabF	0.742	0.587
P54616	Enoyl-[acyl-carrier-protein] reductase [NADH], FabI	0.254	0.025
Cell Envelope Stress Biomarkers [ref antibiotics: merscadin, bacitracin, vancomycin]			
P81100	Stress response protein SCP2, YceC	1.320	0.163
O34833	Uncharacterized protein YceH	0.572	0.436
DNA Damage Response Biomarkers [ref antibiotics: mitomycin, daunomycin, Adriamycin]			
P16971	Protein RecA	0.832	0.526

Table S4. Enrichment of divisome- and elongasome-related proteins in 1-treated, *ΔclpP*, and *ΔclpQ B. subtilis*. Protein fold-change and p-values are provided (*n.d.*; not detected). LC-MS/MS proteomics data was analyzed as described in Chapter Seven.

Divisome Proteins		**1-treatment**		***ΔclpP* deletion**		***ΔclpQ* deletion**	
Accession	Description	Fold-change	p-value	Fold-change	p-value	Fold-change	p-value
P17865	Cell division protein, FtsZ	9.351	0.0312	8.324	0.0002	1.796	0.0150
P28598	60 kDa chaperonin, GroEL	2.860	0.0303	2.906	0.0005	1.085	0.5113
P17820	Chaperone protein, DnaK	4.795	0.0014	2.744	0.0994	1.067	0.8579
P80698	Trigger factor, Tig	11.539	0.0020	3.802	0.0002	0.797	0.3494
P71021	Septum site-determining protein, DivIVA	7.360	0.0029	4.584	0.1126	4.792	0.0397
P0CI74	Cell cycle protein, GpsB	3.903	0.1247	*n.d.*		*n.d.*	
Q01464	Septum site-determining protein, MinD	3.686	0.1711	8.070	4.9E-05	*n.d.*	
Elongasome Proteins		**1-treatment**		***ΔclpP* deletion**		***ΔclpQ* deletion**	
Accession	Description	Fold-change	p-value	Fold-change	p-value	Fold-change	p-value
Q01465	Rod shape-determining protein, MreB	5.123	0.0098	6.052	0.0002	1.282	0.1680
P39751	MreB-like protein, Mbl	*n.d.*		16.574	0.0052	14.242	2.1E-05
O32023	Uncharacterized protein, YqzC	11.245	0.0016	8.023	0.0014	*n.d.*	

Table S5. Enrichment of several known ClpXP substrates in 1-treated and *ΔclpP B. subtilis*, supporting a mechanism involving inhibition of ClpXP. Protein fold-change and p-values are identified for proteins known to be ClpP substrates (*n.d.*; not detected). Significance is defined as fold-change > 2 and p-value < 0.05. LC-MS/MS proteomics data was analyzed as described in Chapter Seven.

ClpP Substrates		**1-treatment**		***ΔclpP* deletion**	
Accession	Description	Fold-change	p-value	Fold-change	p-value
P80698	Trigger factor, Tig	11.539	0.002	3.802	0.0001
P17865	Cell division protein, FtsZ	9.351	0.031	8.324	0.0002
P02394	50S ribosomal protein L7/L12, RplL	4.732	0.002	3.601	0.0005
P28598	60 kDa chaperonin, GroEL	2.860	0.030	2.906	0.0005
P37945	Lon protease, LonA	2.408	0.011	13.409	0.0014
P17820	Chaperone protein, DnaK	4.795	0.001	*n.d.*	
P21883	Dihydrolipoyllysine-residue acetyltransferase component of pyruvate dehydrogenase complex, PdhC	3.468	0.035	*n.d.*	
P09124	Glyceraldehyde-3-phosphate dehydrogenase, GapA	3.441	0.007	*n.d.*	
P13243	Probable fructose-bisphosphate aldolase, FbaA	2.212	0.003	*n.d.*	
P05653	DNA gyrase subunit A, GyrA	*n.d.*		54.839	0.0085
P42923	50S ribosomal protein L10, RplJ	*n.d.*		12.007	0.0008
O31602	Regulatory protein Spx, SpxA	*n.d.*		10.222	0.0001
P12875	50S ribosomal protein L14, RplN	*n.d.*		6.521	1.07E-05
P39610	Pyridoxine kinase. ThiD	*n.d.*		4.691	0.0380
P12877	50S ribosomal protein L5, RplE	*n.d.*		4.219	0.0001
P37570	Protein-arginine kinase, McsB	*n.d.*		4.068	0.0005
P37958	Adapter protein, MecA	*n.d.*		3.224	0.0024
P21469	30S ribosomal protein S7, RpsG	*n.d.*		2.705	0.0026
P42921	50S ribosomal protein L4, RplD	*n.d.*		2.590	0.0479
P37571	Negative regulator of genetic competence, ClpC	*n.d.*		2.254	0.0017
P0CI73	Glutamine--fructose-6-phosphate aminotransferase [isomerizing], GlmS	*n.d.*		2.181	0.0011
P39912	Protein, AroA	*n.d.*		2.116	0.0046
P14193	Ribose-phosphate pyrophosphokinase, Prs	*n.d.*		2.019	0.0018

Appendix III: Supplementary Figures and Tables for Chapter Four

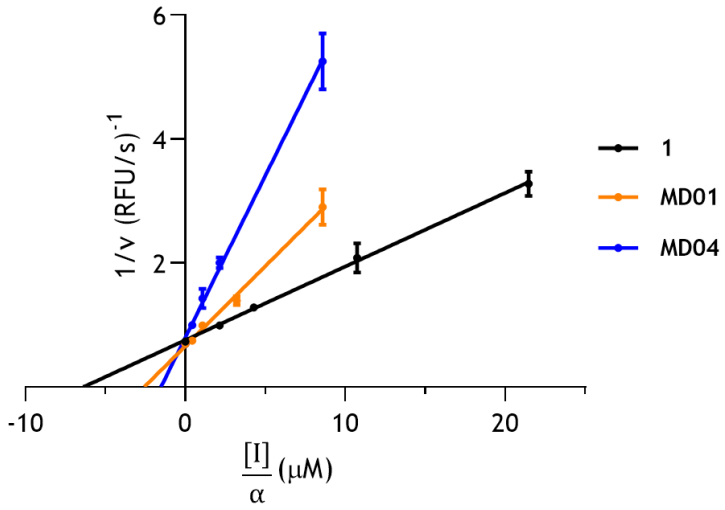

Compound	-K_i (μM) (95% Confidence Interval)
1	-6.361 (-7.690 to -5.201)
MD01	-2.560 (-3.155 to -2.050)
MD04	-1.522 (-1.893 to -1.190)

Figure S9. Cheng-Prusoff alteration of a Dixon plot. The x-intercepts correspond to inhibitor constants, K_i. The inhibitor constants for **MD01** and **MD04** were obtained for inhibition of ClpYQ proteolysis activity. Each data point was collected in triplicate (n = 3).

Figure S10. ClpXP inhibition assay in Christensen media. MRSA USA300 was grown in Christensen media in the presence or absence of **1**. Urease activity was detected with phenol red pH indicator. From left to right: MRSA USA300 + 1 μg/mL **1**, MRSA USA300 + 0 μg/mL **1**, Christensen media blank control.

Table S6. MBC (μg/mL) evaluation of first and second armeniaspirol analogs. Analogs were screened for antibiotic activity against clinically relevant Gram-positive and Gram-negative pathogens.

Compound	*S. aureus* IA116-USA100 (MRSA)	*S. aureus* MN8-USA200 (MSSA)	*S. aureus* LAC-Fitz-USA300 (MRSA)	*S. aureus* MW2-USA400 (MRSA)	*E. faecalis* NJ3 (VRE)	*P. aeruginosa* PA01
1	32	32	>32	>32	>32	>32
MD01	8	16	8	8	32	>32
MD02	16	16	32	16	>32	>32
MD03	32	32	>32	>32	>32	>32
MD04	8	>32	>32	>32	>32	>32
MD05	>32	32	16	16	>32	>32
MD06	>32	>32	>32	>32	>32	>32
MD07	32	>32	>32	>32	>32	>32
MD08	4	8	2	8	8	>32
MD09	>32	>32	>32	>32	>32	>32
MD10	>32	>32	>32	>32	>32	>32
MD11	>32	>32	>32	>32	>32	>32

Appendix IV: Supplementary Figures and Tables for Chapter Five

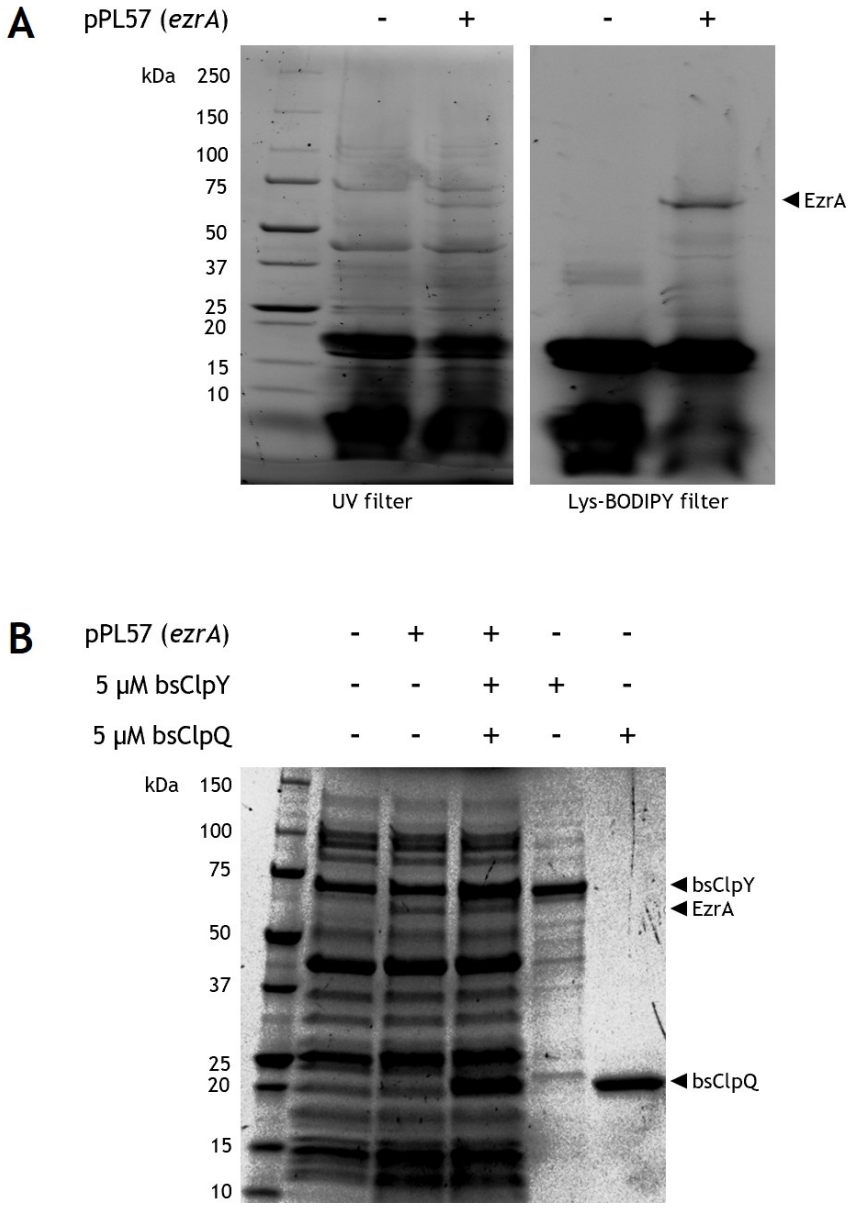

Figure S11. In vitro degradation assay of EzrA by ClpYQ. (A) EzrA was expressed by cell-free translation using the PURExpress® In Vitro Protein Synthesis Kit (New England BioLabs) and supplemented with BODIPY-Lys for easier visualization of expression. The molecular weight of EzrA is ~65 kDa. (B) 5 μM of bsClpYQ under proteolytic assay conditions was added to the mixture. No degradation of EzrA was observed following overnight incubation.

Table S7. Sequencing data for selected plasmids. Sanger sequencing data was obtained from Génome Québec using T7 primers.

Plasmid	Sequencing data (5' → 3')
pPL64	GAAGGAGATATACATATGTAGTCTTTTCATGNNNCCACAATATTTGCCGTA CAGCATAAAGGACGAAGCGCTATGTCCGGAGACGGCCAAGTAACATTTG GTCAGGCTGTTGTCATGAAACACACGGCACGGAAAGTGAGAAAACTGTT TAACGGCAAAGTTCTTGCTGGTTTTGCGGGATCTGTTGCAGACGCTTTCA CTTTATTCGAAAAGTTTGAAGCTAAGCTTGAAGAATATAACGGCAACTTA AAACGGGCGGCTGTTGAGCTTGCAAAGGAATGGCGCAGTGATAAAGTGC TAAGAAAGCTCGAAGCCATGCTGATTGTTATGAATCAGGATACTTTGCTT CTCGTATCGGGAACAGGCGAGGTGATCGAACCAGATGACGGCATTCTCG CGATTGGATCAGGAGGCAATTACGCTTTGGCAGCGGGAAGAGCACTGAA AAAGCATGCCGGGGAAAGCATGTCTGCAAGTGAGATTGCCAGAGCCGCG TTAGAAACAGCAGGCGAAATTTGTGTTTACACGAACGATCAAATCATACT GGAAGAGCTTGAGAATTCGAGCTCCGTCGACAAGCTTGCGGCCGCACTC GAGCACCACCACCACCACCACTGAGATCCGGCTGCTAACAAAGCCCGAA AGGAAGCTGAGTTGGCTGCTGCCACCGCTGAGCAATAACTAGCATAACC CCTTGGGGCCTCTAAACGGGTCTTGAGGGGTTTTTTGCTGAAAGGAGGA ACTATATCCGGATTGGCGAATGGGACGCGCCCTGTAGCGGCGCATNANGC GCGGCGGGTGTGGTGGT

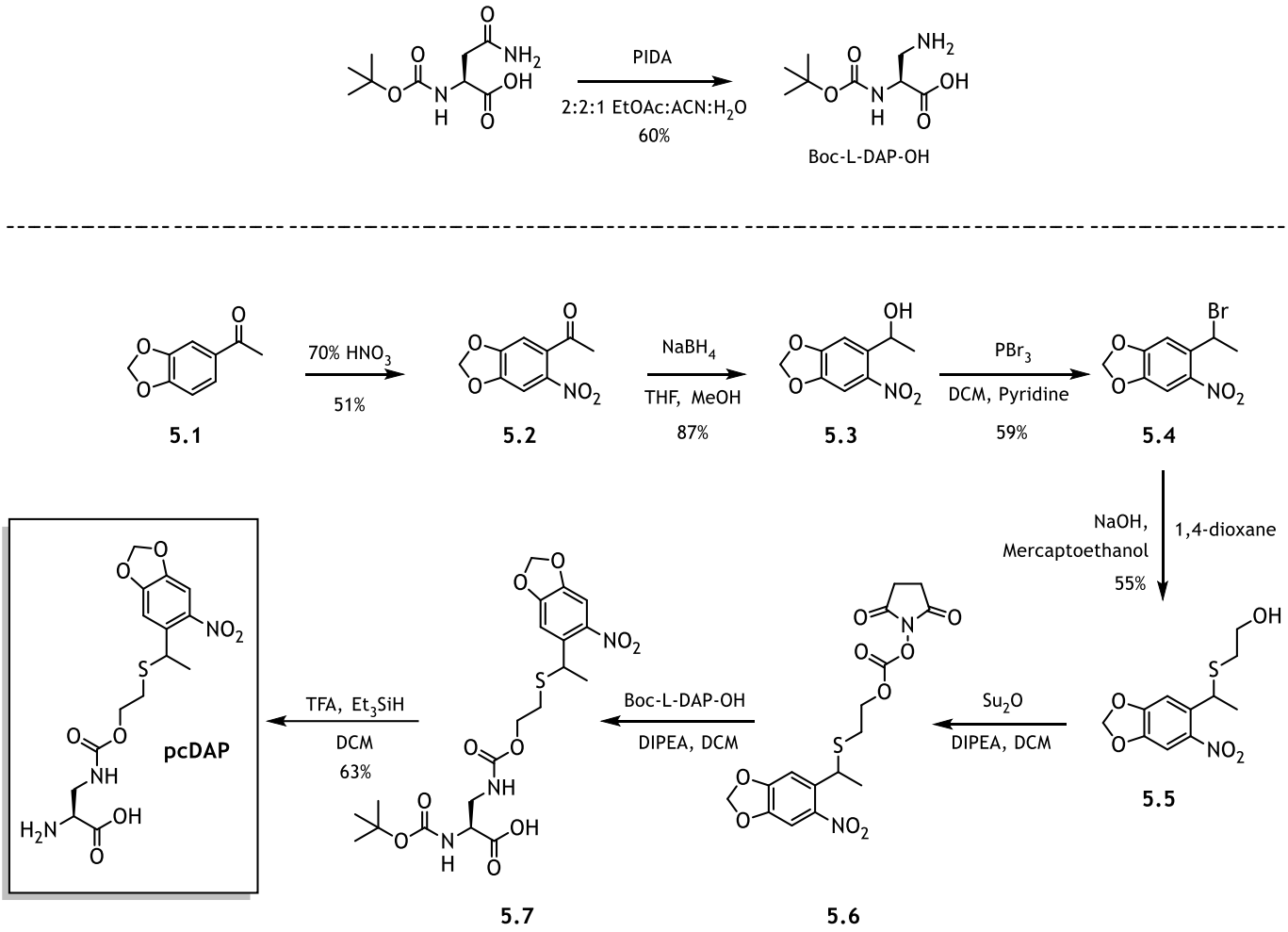

Scheme S1. Synthesis of photocleavable precursor (DAP) for amino acid incorporation. Synthesis was largely adapted from Huguenin-Dezot, N. et al. *Nature* **2019**, *565*, 112–117. Synthesis procedures are outlined in Capter Seven.

Appendix V: Key Resources

Table S8. List of *Bacillus subtilis* 168 gene deletion strains used in study.

[a]BGSC N^{o}	Original Strain	Genotype	PMID Ref.	MIC of 1 (µg/mL)
BKE16150	*Bacillus subtilis 168*	ΔclpQ::erm trpC2	28189581	2
BKK34540	*Bacillus subtilis 168*	ΔclpP::kan trpC2	28189581	2

[a]BGSC, Bacillus Genetic Stock Center, Columbus, OH

Table S9. List of plasmids used in study. All plasmids were heterologously expressed in *Escherichia coli* BL21 (DE3).

Plasmid	Gene	Marker	Vector	Primers (5' – 3')
pPL29	*clpQ* (*B. subtilis*)	Amp^R	pET21c	PCR amplified from *B. subtilis* gDNA F: CGTACATATGTCATCTTTTCATGCGACCAC R: CGTAGAATTCTCAAGCTCTTCCAGTATGATTTG
pPL31	*clpY* (*B. subtilis*)	Kan^R	pET28b	PCR amplified from *B. subtilis* gDNA F: AATTGCTAGCAACTTGAGGCGCATGGA R: CGTAGAATTCAATATAAATTGACTTAAATC
pProEx-Htb-ClpX	*clpX* (*E. coli*)	Amp^R	pProEx Htb	Generously provided by Prof. Walid Houry (University of Toronto)
pET9a-ClpP	*clpP* (*E. coli*)	Kan^R	pET9a	Generously provided by Prof. Walid Houry (University of Toronto)
pPL57	*ezrA* (*B. subtilis*)	Amp^R	pET21c	PCR amplified from *B. subtilis* gDNA F: CGTACATATGGAGTTTGTCATTGGATTATTAATTGTACTGCTTGCGCTGTTTGC R: CGTAGAATTCCTTATCGTCGTCATCCTTGTAATCCTAAGCGGATATGTCAGCTTTGAT
pPL64	$clpQ_{DAP}$ (*B. subtilis*)	Amp^R	pET21c	PCR amplified from *B. subtilis* gDNA F: CGTACATATGTAGTCTTTTCATGCGACCAC R: CGTAGAATTCTCAAGCTCTTCCAGTATGATTTG
pDAPRS	$tRNA_{CUA}$/*aaRS*	Kan^R		Generously provided by Prof. Martin Schmeing (McGill University)

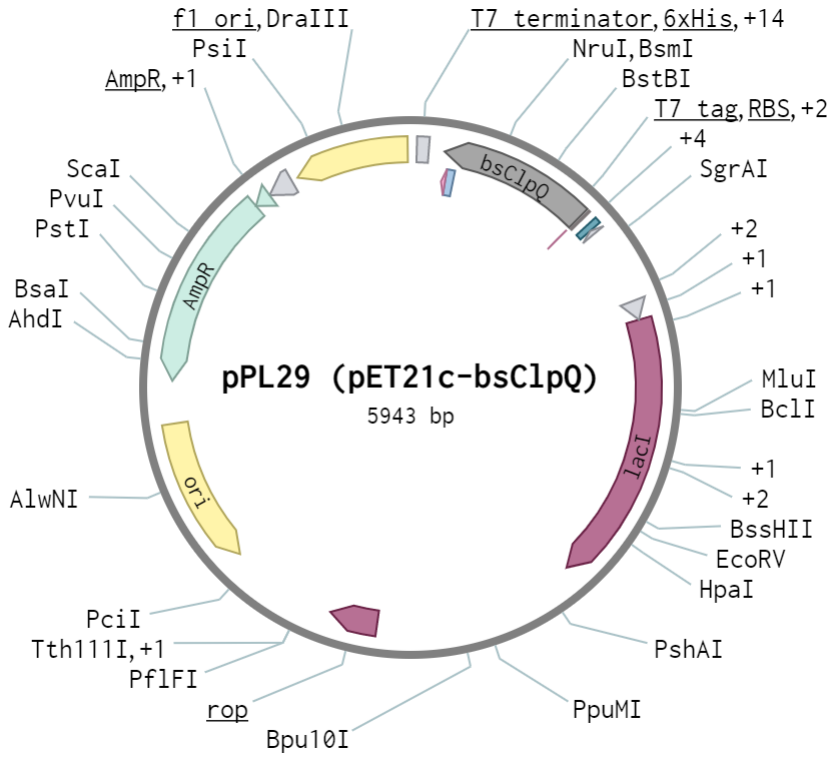
f1 ori, DraIII
PsiI
AmpR, +1
ScaI
PvuI
PstI
BsaI
AhdI
AlwNI
PciI
Tth111I, +1
PflFI
rop
Bpu10I
PpuMI
PshAI
HpaI
EcoRV
BssHII
+1
+2
MluI
BclI
+2
+1
+1
SgrAI
+4
T7 tag, RBS, +2
BstBI
NruI, BsmI
T7 terminator, 6xHis, +14
bsClpQ
AmpR
ori
lacI
pPL29 (pET21c-bsClpQ)
5943 bp

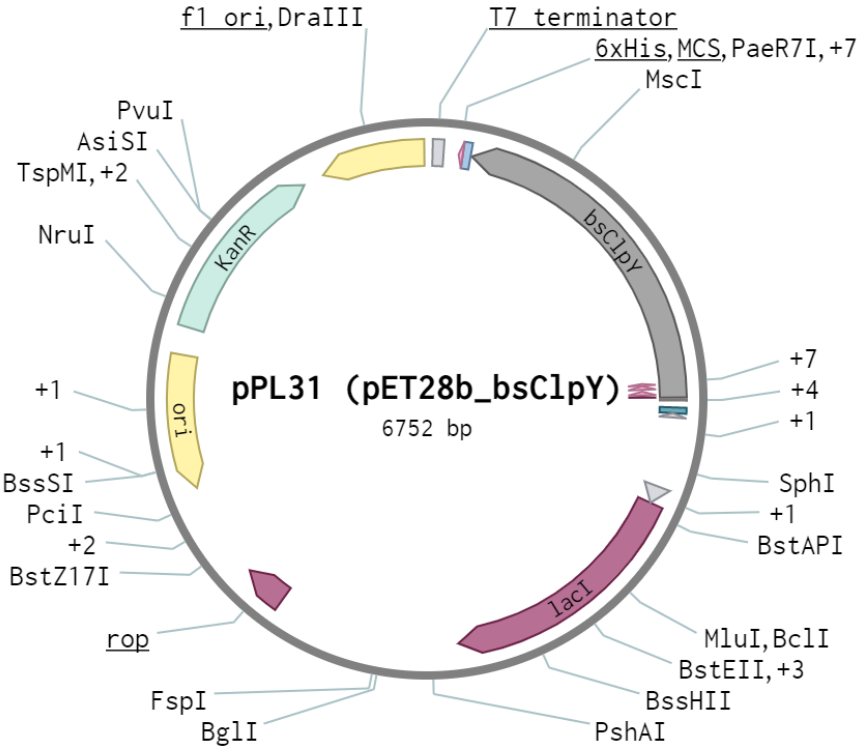
f1 ori, DraIII
T7 terminator
6xHis, MCS, PaeR7I, +7
MscI
PvuI
AsiSI
TspMI, +2
NruI
+1
+1
BssSI
PciI
+2
BstZ17I
rop
FspI
BglI
PshAI
BssHII
BstEII, +3
MluI, BclI
BstAPI
+1
SphI
+1
+4
+7
KanR
ori
lacI
bsClpY
pPL31 (pET28b_bsClpY)
6752 bp

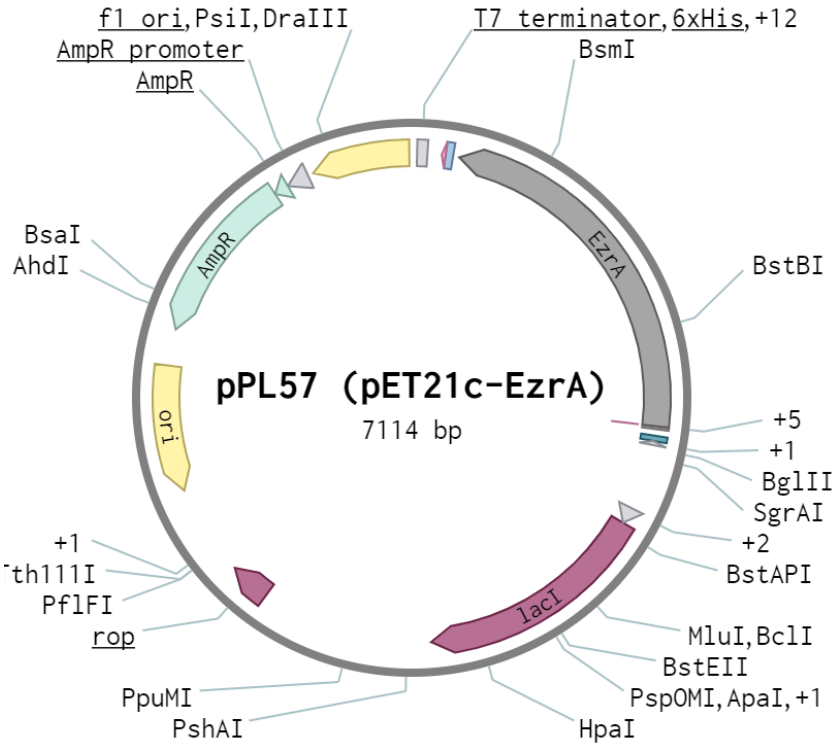
f1 ori, PsiI, DraIII
AmpR promoter
AmpR
T7 terminator, 6xHis, +12
BsmI
BsaI
AhdI
AmpR
EzrA
BstBI
pPL57 (pET21c-EzrA)
7114 bp
ori
+5
+1
BglII
SgrAI
+2
BstAPI
+1
Tth111I
PflFI
rop
lacI
MluI, BclI
BstEII
PspOMI, ApaI, +1
PpuMI
PshAI
HpaI

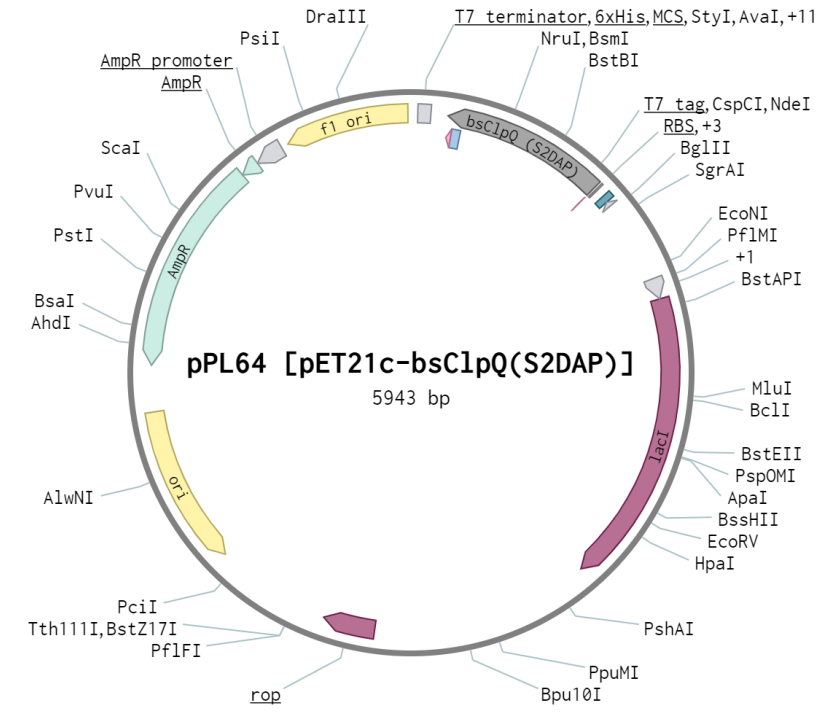
DraIII
PsiI
T7 terminator, 6xHis, MCS, StyI, AvaI, +11
NruI, BsmI
BstBI
AmpR promoter
AmpR
f1 ori
bsClpQ (S2DAP)
T7 tag, CspCI, NdeI
RBS, +3
BglII
SgrAI
ScaI
PvuI
PstI
AmpR
EcoNI
PflMI
+1
BstAPI
BsaI
AhdI
pPL64 [pET21c-bsClpQ(S2DAP)]
5943 bp
MluI
BclI
lacI
BstEII
PspOMI
ApaI
BssHII
EcoRV
HpaI
AlwNI
ori
PciI
Tth111I, BstZ17I
PflFI
PshAI
PpuMI
Bpu10I
rop

Appendix VI: Rights and Permissions

Permission rights to **Figure 1.4**:

License Number	5022061020573
License date	Mar 04, 2021
Licensed Content Publisher	John Wiley and Sons
Licensed Content Publication	Biopolymers
Licensed Content Title	Mini review: ATP-dependent proteases in bacteria
Licensed Content Author	Franz Narberhaus, Jan Arends, Lisa-Marie Bittner
Licensed Content Date	May 20, 2016
Licensed Content Volume	105
Licensed Content Issue	8
Licensed Content Pages	13
Type of Use	Dissertation/Thesis
Requestor type	University/Academic
Format	Print and electronic
Portion	Figure/table
Number of figures/tables	1
Will you be translating?	No
Title	Deciphering the Mechanism of Action of Armeniaspirol: A Novel Polyketide Gram-positive Antibiotic
Institution name	University of Ottawa
Expected presentation date	Apr 2021
Portions	Figure 3
Requestor Location	University of Ottawa 140 Louis Pasteur Pvt. Marion Hall Ottawa, ON K1N 6N5 Canada Attn: University of Ottawa
Publisher Tax ID	EU826007151
Total	**0.00 CAD**

Permission rights to **Figure 5.1**:

Protein Engineering For Directed Immobilization

Author: Erik Steen Redeker, Duy Tien Ta, David Cortens, et al

Publication: Bioconjugate Chemistry

Publisher: American Chemical Society

Date: Nov 1, 2013

PERMISSION/LICENSE IS GRANTED FOR YOUR ORDER AT NO CHARGE

This type of permission/license, instead of the standard Terms & Conditions, is sent to you because no fee is being charged for your order. Please note the following:

- Permission is granted for your request in both print and electronic formats, and translations.
- If figures and/or tables were requested, they may be adapted or used in part.
- Please print this page for your records and send a copy of it to your publisher/graduate school.
- Appropriate credit for the requested material should be given as follows: "Reprinted (adapted) with permission from (COMPLETE REFERENCE CITATION). Copyright (YEAR) American Chemical Society." Insert appropriate information in place of the capitalized words.
- One-time permission is granted only for the use specified in your request. No additional uses are granted (such as derivative works or other editions). For any other uses, please submit a new request.

If credit is given to another source for the material you requested, permission must be obtained from that source.